



Mata, J., Martins, S., Mattielli, N., Madeira, J., Faria, B., Ramalho, R. S., Silva, P., Moreira, M., Caldeira, R., Rodrigues, J., & Martins, L. (2017). The 2014-15 eruption and the short-term geochemical evolution of the Fogo volcano (Cape Verde): Evidence for small-scale mantle heterogeneity. *Lithos*, 288-289, 91-107.  
<https://doi.org/10.1016/j.lithos.2017.07.001>

Peer reviewed version

License (if available):  
Unspecified

Link to published version (if available):  
[10.1016/j.lithos.2017.07.001](https://doi.org/10.1016/j.lithos.2017.07.001)

[Link to publication record in Explore Bristol Research](#)  
PDF-document

This is the author accepted manuscript (AAM). The final published version (version of record) is available online via ELSEVIER at <http://www.sciencedirect.com/science/article/pii/S0024493717302402?via%3Dihub> . Please refer to any applicable terms of use of the publisher.

## University of Bristol - Explore Bristol Research

### General rights

This document is made available in accordance with publisher policies. Please cite only the published version using the reference above. Full terms of use are available:  
<http://www.bristol.ac.uk/red/research-policy/pure/user-guides/ebr-terms/>

**The 2014-15 eruption and the short-term geochemical evolution of the Fogo volcano (Cape Verde): evidence for small-scale mantle heterogeneity**

J. Mata<sup>1\*</sup>; S. Martins<sup>1</sup>; N. Mattielli<sup>2</sup>; J. Madeira<sup>1</sup>; B. Faria<sup>3</sup>; R.S. Ramalho<sup>1,4,5</sup>; P. Silva<sup>6,1</sup>; M. Moreira<sup>7</sup>; R. Caldeira<sup>8</sup>; M. Moreira<sup>6,1</sup>; J. Rodrigues<sup>9</sup>; L. Martins<sup>1</sup>

- 1- Instituto Dom Luiz, Faculdade de Ciências, Universidade de Lisboa, 1749-016 Lisboa, Portugal.
- 2- Laboratoire G-Time, DGES, Université Libre de Bruxelles, ULB, Av. Roosevelt, 50, CP 160/02, 1050 Brussels, Belgium
- 3- Instituto Nacional de Meteorologia e Geofísica, Mindelo, Cabo Verde
- 4- School of Earth Sciences, University of Bristol, Wills Memorial Building, Queen’s Road, Bristol, BS8 1RJ, UK
- 5- Lamont-Doherty Earth Observatory at Columbia University, Comer Geochemistry Building, 61 Route 9W, P. O. Box 1000, Palisades, NY 10964–8000, USA
- 6- Instituto Politécnico de Lisboa, ISEL/ADF, Lisboa, Portugal
- 7- Institute de Physique du Globe de Paris (France)
- 8- Laboratório Nacional de Energia e Geologia, I.P., 2610-999 Amadora, Portugal.
- 9- Geologist, Cabo Verde

\*- Corresponding author: [jmata@fc.ul.p](mailto:jmata@fc.ul.p)

**Keywords**

2014-15 Fogo Island (Cape Verde) eruption; Ocean island basalts; Mantle heterogeneity; Short-term magmatic variation; Volcano plumbing system

## 92    **1- Introduction**

93    The Earth's mantle is highly heterogeneous as depicted by the composition of oceanic  
94    basalts and particularly by those from oceanic islands (e.g. Hofmann, 2003; White,  
95    2015). Such heterogeneity is considered the result of mixing in different proportions of  
96    the so-called mantle components (Zindler and Hart, 1986; Stracke et al., 2005). The  
97    length scale of mantle heterogeneities sampled by oceanic basalts is highly variable,  
98    sometimes encompassing large regional domains (e.g. DUPAL and SOPITA anomalies;  
99    Hart, 1984; Staudigel et al., 1991; White, 2015), but being also evident at the scale of a  
100   single magmatic province, as reported, for example, for the Azores (e.g. Beier et al.,  
101   2008), Cape Verde (Gerlach et al., 1988; Doucelance et al., 2003) and Galápagos  
102   (Gibson et al., 2012) archipelagos. The same is true at the scale of a single island edifice  
103   (e.g. Barker et al., 2010; Mourão et al., 2012a; Nobre Silva et al., 2013), even when  
104   considering quasi-coeval magmatic products (e.g. Madureira et al., 2011).

105   In this work we evaluate the small-scale heterogeneity of the mantle source feeding a  
106   plume-related intraplate volcano, as well as the short-term geochemical evolution of the  
107   magmas it generated. To this purpose we use as a case study the island of Fogo (Cape  
108   Verde Archipelago), one of the most active oceanic volcanoes in our planet. Indeed,  
109   since the mid-15<sup>th</sup> Century Fogo experienced about 27 eruptions mostly from vents  
110   located within a restricted area ( $\approx 50 \text{ km}^2$ ) of the island's summit depression (Fig. 1).  
111   The latest eruption occurred in 2014-2015 and constitutes the main object of this study.  
112   Their vents are practically coincident or localized less than 2 km away from those of the  
113   two previous eruptions (1995 and 1951, respectively). For this reason, Fogo constitutes  
114   a prime locality to test the existence of small-scale heterogeneities of mantle sources, as  
115   well as to investigate the recent short-term evolution of magmas issued from those  
116   sources. Here we characterize and discuss the geochemistry of the lava flows and  
117   pyroclasts extruded during the initial stages of the eruption (up to December 7, 2014).  
118   Even though we are only considering lavas formed during the first 15 out of 60 days of

eruption, the extracted information allows the demonstration of chemical differences relative to the products erupted in 1951 and 1995.

The preservation of such heterogeneities by magmas is also here discussed emphasizing the role of lithosphere thickness. The mineralogical, geochemical and physical characteristics of a volcano are partially constrained by what happens during magma transit from its source to the surface, i.e. by the nature and dynamics of the associated magma plumbing system (e.g. Longpré et al., 2008; Klügel et al., 2015; Cooper, 2017; Cashman et al., 2017). The Fogo's plumbing system is here assessed using barometric data, which indicates a location of the main magma chamber(s) into the mantle.

Our observations show that magmas erupted in 2014 mark a reversal from the tendency depicted by previous eruptions (Escrig et al., 2005), which exhibited an increasing contribution of a local end-member with relatively radiogenic Sr.

## **2- Cape Verde Geological Setting**

The Cape Verde Archipelago (Eastern Central Atlantic; Fig. 1) lies on top of the largest bathymetric anomaly in the Earth's oceans – the Cape Verde Rise – that coincides with important geoid, heat flow, gravity, and seismic anomalies (e.g. Dash et al., 1976; Courtney and White, 1986; Wilson et al., 2013; Liu and Zhao, 2014). The archipelago, which stand on 120–140 Ma-old seafloor (Williams et al., 1990) is regarded as a hotspot resulting from the impingement of a mantle plume on the quasi-stationary ( $<1 \text{ cm.a}^{-1}$  in the region; Pollitz, 1991; Holm et al., 2008) Nubian plate. These would explain the long-lasting volcanic activity and, at least partially, the age distribution of volcanism and the geometry of both the archipelago and the Cape Verde Rise (Lodge and Helffrich, 2006; Holm et al., 2008; Madeira et al., 2008; Ramalho et al. 2010, Ramalho, 2011). The presence of a mantle plume deeply anchored in the lower mantle is suggested by seismic data (Montelli et al., 2006; Forte et al., 2010; Vinnik et al, 2012; Saki et al., 2015; French and Romanowicz, 2015) and of noble gas studies performed on

carbonatites and alkaline silicate rocks (Christensen et al., 2001; Doucelance et al., 2003; Mata et al., 2010; Mourão et al., 2012b). The oldest exposed hotspot-related volcanism is ~26 Ma (Torres et al., 2010) and at least three islands are considered volcanically active (Santo Antão, Brava and Fogo; see e.g. Madeira et al., 2010; Eisele et al., 2015; Faria and Fonseca, 2014) but only Fogo had post-settlement eruptions. Magmatism in Cape Verde is strongly alkaline, as testified by the occurrence of nephelinitic, melanephelinitic, and melilititic rocks on several islands. It also is well known by its striking geochemical heterogeneity, allowing the isotopic separation of the islands into two groups (Northern and Southern). Lavas from the Southern group have more radiogenic Sr, but unradiogenic Nd and Pb ratios than those from the Northern group, which are also exhibit more unradiogenic He signatures. In addition, magmatic rocks from the Southern group are positioned, on the  $^{208}\text{Pb}/^{204}\text{Pb}$  vs.  $^{206}\text{Pb}/^{204}\text{Pb}$  diagram, above the Northern Hemisphere Reference Line (NHRL; Hart, 1984) whilst lavas from the Northern group tend to plot along the NHRL (e.g. Gerlach et al., 1988; Doucelance et al., 2003; Holm et al., 2006; Kogarko and Asavin, 2007; Martins et al., 2010; Mourão et al. 2012a and references therein). Notable exceptions to this scenario include Brava (the southwesternmost island), which depicts both typical Northern (older sequences) and Southern (younger volcanism) isotope signatures (Mourão et al., 2012a), and the neighbouring Cadamosto seamount, which also presents typical Northern signatures (Barker et al., 2012).

## **2.1 Fogo Volcano**

Fogo is one of the youngest of the Cape Verde Islands and a very prominent oceanic volcano, standing ~7 km above the surrounding seafloor. The island exhibits a slightly asymmetric conical shape, being truncated atop by a summit depression open to the east. This 8 km-wide depression - Chã das Caldeiras - is surrounded on three sides by a almost vertical wall – the Bordeira – up to 1 km tall. Inside the summit depression and

on its eastern side, a 1100 m high strato-volcano – Pico do Fogo – grew up to an elevation of 2829 m (Fig. 1). Fogo volcano is therefore interpreted as a compound volcano, featuring a “somma-vesuvio” association of a younger strato-cone on top of an older, collapsed volcanic edifice (Ribeiro, 1954; Foeken et al., 2009). The opening to the east of the summit depression is interpreted as the result of a massive flank collapse (Day et al., 1999; Brum da Silveira et al., 2006), as attested by a landslide debris deposit extending offshore into the channel between Fogo and Santiago (e.g. Masson et al., 2008), and by field evidence documenting the impact of a megatsunami in the neighbouring island of Santiago (Paris et al., 2011; Ramalho et al., 2015). The present-day Pico do Fogo stands on, and partially fills, the collapse scar, and naturally post-dates the collapse event, which is interpreted to have occurred either at ~117 or at ~73 ka (cf. Eisele et al. 2015 and Ramalho et al. 2015). A older basement is, however, exposed in two shallow valleys near the city of São Filipe, where plutonic calciocarbonatites were dated from 2.5 Ma to 5.1 Ma (Hoernle et al., 2002; Madeira et al., 2005; Foeken et al., 2009). These suggest a > 2 Myr volcanic hiatus in the evolution of Fogo.

Fogo volcano is very active, with 27 eruptive events since 1500 AD (Ribeiro, 1954). The mean recurrence interval between eruptions is 19.8 years, but with individual intervals ranging from 1 to 94 years. Historical eruptions seem to have been confined to Chã das Caldeiras and the eastern slope of the volcano, as it was the case of the recent 1951, 1995 and 2014/2015 events (Fig. 1).

The latest eruption started on November 23, 2014 and continued until February 7, 2015. The eruption occurred on a NE-SW trending 700 m-long fissure located on the SE flank of the previous 1995 cinder cone, an adventitious vent developed on the SW flank of Pico do Fogo (Figs. 2A, 2B e 2D). This eruption started with vigorous “hawaiian” fire-fountain activity, followed by strombolian activity, and later by simultaneous or alternating Hawaiian (Fig. 2C), strombolian and vulcanian (Fig. 2D) eruptive activity

from different craters along a fissural vent, lasting for several days. The eruption also emitted, from the first day, thick a'a lava flows (Fig. 2E; Supplementary Material S1) forming two initial lava lobes. A shorter lobe, 1.7 km-long, progressed southwestwards down to the flank of Cova Tina cone, stalling short of the Bordeira wall in this area. The second, longer lobe advanced 3 km to the northeast in the initial hours of the eruption, crossing the topographic barrier formed by the 1995 lava flows by advancing through the existing road cut. It advanced intermittently towards the village of Portela, causing widespread destruction (Fig. 2F). During the later stages of the eruption, thinner, more fluid, a'a and especially pahoehoe breakouts expanded the flow field to the west and north, the latter descending to the village of Bangaeira, destroying almost completely both villages and reaching a total length of 5.2 km (Fig.1). Overall, the resulting lava flows, with an average thickness of about 9 m, covered an area of 4.8 km<sup>2</sup>, with extruded volumes estimated to correspond to  $\sim 45 \times 10^6$  m<sup>3</sup>, at a mean eruption rate of 6.8 m<sup>3</sup>.s<sup>-1</sup> (Bagnardi et al. 2016; Richter et al. 2016). Lava flow thicknesses as high as 35 m (close to the vent), or 25 m on the lava ponding west of Portela, were described by Richter et al. (2016). See also Cappello et al. (2016) for additional information about the eruption.

### **3- Analytical procedures**

Whole-rock major and trace element concentrations were obtained at Activation Laboratories, Ltd (Ancaster, Ontario, Canada) using the geochemical analytical package 4Lithoresearch (lithium metaborate/tetraborate fusion - ICP and ICP/MS).

Several certified reference materials from USGS (United States Geological Survey), GSJ (Geological Survey of Japan) and CCRMP (Canadian Certificate Reference Material Project) were run to check for accuracy (Supplementary Material S2). Errors associated with the accuracy are  $\leq 4\%$  for major elements and better than 9% for the REE and the most widely used incompatible elements. Reproducibility was generally



227 better than 5% for both major and trace elements. For detailed information regarding  
228 analytical and control procedures consult the Actlabs website ([www.actlabs.com](http://www.actlabs.com)).

229 Mineral analyses were performed on carbon-coated polished thin sections using a JEOL  
230 SUPERPROBE™, model JXA-8200, in wavelength dispersive mode at the  
231 Departamento de Geologia da Faculdade de Ciências da Universidade de Lisboa  
232 (Portugal). Minerals were analysed with an acceleration voltage of 15 kV and a current  
233 of 25 nA, using a 5 µm wide beam for most minerals. Plagioclase and apatite were  
234 analysed using a 7 and 9 µm wide beam, respectively. The analyses performed in each  
235 mineral phase/glass were calibrated using the composition of reference material, with  
236 precisions being better than 2% and ordinarily around 1% (see Supplementary Material  
237 S3-H for specific minerals standards used in each mineral analysis).

238 Isotopic analyses of Pb, Nd, Sr and Hf were performed at the Laboratoire G-Time of the  
239 Université Libre de Bruxelles (ULB, Belgium) on a Nu Plasma I Multi-Collector  
240 Inductively Coupled Plasma Mass Spectrometer (MC-ICP-MS) (@ Nu instruments).

241 Sr analyses were performed in wet mode. In routine, the raw data was normalized to  
242  $^{86}\text{Sr}/^{88}\text{Sr}=0.1194$ , and corrected for mass bias by standard sample bracketing using the  
243 lab's in-house Sr standard solution. The in-house shelf Sr standard was calibrated and  
244 normalized to the certified value of NBS 987 Sr standard (0.710248) reported by Weis  
245 et al. (2006). During our analytical sessions, in-house standard solution was run every  
246 two samples and gave an average value of  $0.710287 \pm 50$  ( $2\sigma$ ) for raw  $^{87}\text{Sr}/^{86}\text{Sr}$  data (21  
247 runs).

248 Nd and Hf were run in dry mode with an Aridus II desolvating system. To monitor the  
249 instrumental mass bias during the analysis sessions, the standard sample bracketing  
250 method was also applied. Standards were systematically run between every two  
251 samples, giving an average value in  $^{143}\text{Nd}/^{144}\text{Nd}$  of  $0.511921 \pm 41$  ( $2\sigma$ , 8 runs) for the  
252 Rennes Nd standard, and  $^{176}\text{Hf}/^{177}\text{Hf}=0.282172 \pm 30$  ( $2\sigma$ , 10 runs) for the JMC 475 Hf  
253 standard. The Nd and Hf isotopic measurements were internally normalised to

$^{146}\text{Nd}/^{144}\text{Nd}=0.7219$  and  $^{179}\text{Hf}/^{177}\text{Hf}=0.7325$ , respectively. All Hf and Nd isotopic data (Table 1) are normalized to the reference values of 0.511961 and 0.282160 as published by Chauvel and Blichert-Toft (2001) and Chauvel et al. (2011). For the Pb isotope analyses, a Tl dopant solution was added for every sample and standard, within a Pb-Tl concentration ratio of  $\pm 5:1$  (for a minimum signal of 100 mV in the axial collector -  $^{204}\text{Pb}$ ).  $^{202}\text{Hg}$  is routinely monitored to correct for the potential isobaric interference of  $^{204}\text{Hg}$  on  $^{204}\text{Pb}$ . Mass discrimination was monitored using  $\ln - \ln$  plots and corrected by the external normalization and the standard sample bracketing technique using the recommended values of Galer and Abouchami (1998) (i.e.  $^{206}\text{Pb}/^{204}\text{Pb}=16.9405\pm 15$ ;  $^{207}\text{Pb}/^{204}\text{Pb}=15.4963\pm 16$ ;  $^{208}\text{Pb}/^{204}\text{Pb}=36.7219\pm 44$ ). The repeated measurements of the NBS981 gave the following values:  $^{206}\text{Pb}/^{204}\text{Pb}=16.9403\pm 8$ ,  $^{207}\text{Pb}/^{204}\text{Pb}=15.4961\pm 10$ ,  $^{208}\text{Pb}/^{204}\text{Pb}=36.7217\pm 31$  ( $2\sigma$ ) for the NBS981 Pb standard (5 runs).

#### 4- Results

The samples used in this study were collected during a field survey undertaken during the course of the last Fogo eruption, between November 27 and December 7, 2014. From all collected samples a sub-set of 14 was selected for petrographic, mineralogical and whole-rock elemental geochemical study (TABLE I), on the basis of its geographical and temporal distribution. Sr, Nd, Hf and Pb isotopes were determined for 8 samples (TABLE II), while the He isotope analysis was performed for one sample. On the Supplementary Material the reader can also find mineral chemistry data (S3) and the whole-rock normative compositions (S4). The composition of interstitial glasses determined by electron microprobe is also presented on Supplementary Material S3-G.

## **4.1. Petrography and mineral chemistry**

On a chemical basis, lava flows and pyroclasts erupted up to December 7 are, sensu lato, tephrites and phonotephrites (see *section* 4.3 and Fig. 3). Some of the most important petrographic characteristics of the studied samples are depicted on Fig. 4 and their mineral chemistry data are displayed on the Supplementary Material S3.

### **4.1.1 Tephrites**

The bulk ( $\approx 85\%$ ) of the eruptive products corresponds to tephrites. The lavas are vesicular and porphyritic with a hypocrySTALLINE groundmass and with phenocrysts amounting up to 10%. Samples are highly vesicular (up to 60% of the rock volume) and the vesicles are irregular in shape and size.

The most abundant phenocryst phase is clinopyroxene. Even though all the clinopyroxene phenocrysts are classified as diopside ( $\text{Wo}_{49}\text{En}_{38}\text{Fs}_{13}$  to  $\text{Wo}_{52}\text{En}_{36}\text{Fs}_{12}$ ) according to IMA recommendations (Supplementary Material S-3A), in most samples two groups must be considered regarding size and composition. One group corresponds to phenocrysts with dimensions up to 2 mm and euhedral shapes. They are characterized by normal zoning patterns, with  $\text{Al}_2\text{O}_3$ , FeO and  $\text{TiO}_2$  increasing and MgO, CaO and Mg# decreasing from core to rim. Opaque mineral inclusions are frequent. The other group of phenocrysts occurs in clusters along with kaersutite, both with dimensions up to 4 mm in length. Clinopyroxene megacrysts in these aggregates usually show complex zoning patterns presenting abnormal compositional variations with increments of  $\text{Al}_2\text{O}_3$ , FeO and  $\text{TiO}_2$  towards the intermediate zone/mantle and then decreasing towards the rim; the opposite occurs with MgO and CaO, suggesting a more complex and multistage crystallization history as compared with the first group. Indeed the increase in MgO/FeO and decrease in  $\text{TiO}_2$  towards the rim is suggestive of a replenishment of the magma chamber where these particular crystals were formed, reflecting an influx of less evolved magmas, thus pointing out to mixing of distinct magma batches. However, both

groups of clinopyroxenes show similar  $Al^{VI}$  values (0.059 to 0) and Al/Ti ratios indicating that megacrysts are cognate, being genetically related with the host lava and with the clinopyroxene phenocrysts. This assertion is also considered valid for kaersutite megacrysts given the chemical evidence for amphibole fractionation (see 5.1).

These kaersutite crystals are Mg- and Ti-rich (MgO = 12.8 – 13.0 wt.%; TiO<sub>2</sub> up to 6.07 wt.%), usually occurring in association with apatite and showing reaction rims where clinopyroxene and rhönite crystals are present, sometimes completely replacing the amphibole (Fig. 4D). Olivine crystals are restricted to inclusions in clinopyroxene phenocrysts, with no signs of resorption, and to the groundmass. In all lava samples the opaque minerals can be considered microphenocrysts, being characterized by euhedral shapes and dimensions up to 1 mm. Most of the occurring oxides can be considered as titanomagnetites, with ulvöspinel component ( $X_{USP}$ ) up to 57, and Cr# ranging from 1.6 to 5.3.

The groundmass is made up of small crystals immersed in a glassy matrix. These comprise plagioclase laths (labradorite, An<sub>56-66</sub>) sometimes with a fluidal arrangement, clinopyroxene elongated crystals (Wo<sub>49</sub>En<sub>37</sub>Fs<sub>14</sub> to Wo<sub>53</sub>En<sub>32</sub>Fs<sub>15</sub>), finely disseminated opaque minerals (titanomagnetites, 58 <  $X_{USP}$  < 67), rare olivine (Fo ≈ 72%), and fluorapatite (1.7 to 2.8 wt.% of F). The electron-microprobe analyses of interstitial glass revealed it to be very rich in alkalis (11.8 to 15.8 wt%, K<sub>2</sub>O+Na<sub>2</sub>O) and poor in MgO (down to 0.66 wt%) having tephriphonolitic and phonolitic (SiO<sub>2</sub> up to 54.15 wt%) compositions (see Fig. 3).

#### **4.1.2 Phonotephrites**

These lavas are vesicular hemicrystalline/hypocrystalline and sparsely porphyritic (phenocrysts up to 3% vol.). The vesicles are elongated reaching up to 10 mm in length and corresponding to 50 to 80% of rock volume. The clinopyroxene phenocrysts are

335 euhedral up to 3 mm in size, frequently showing complex oscillatory zoning patterns  
336 and inclusions of opaque minerals. Despite the striking optical zoning patterns, all the  
337 clinopyroxene phenocrysts are classified as diopside with a short compositional range  
338 ( $\text{Wo}_{49}\text{En}_{35}\text{Fs}_{10}$  to  $\text{Wo}_{53}\text{En}_{40}\text{Fs}_{14}$ ), being very similar to that reported for the tephrites.  
339 Olivine ( $\text{Fo}=80\text{-}84\%$ ) is scarce, being identified only as a core inclusion in a  
340 clinopyroxene phenocryst. Microphenocrysts (up to 1mm) of equant opaque minerals  
341 are classified as titanomagnetites ( $X_{\text{USP}} = 44\text{-}46$ ;  $\text{Cr\#} = 1.15\text{-}5.4$ ). Kaersutite  
342 pseudomorphs are frequent. They consist of aggregates of rhönite and clinopyroxene  
343 elongated crystals, displayed in inward radial arrangements totally or partially replacing  
344 the amphibole. However, in either case, a border of small opaque minerals encloses the  
345 altered/partially altered amphibole crystals. These kaersuites are similar ( $\text{MgO} = 11.9 -$   
346  $12.7 \text{ wt.\%}$ ;  $\text{TiO}_2$  up to  $6.04 \text{ wt.\%}$ ) to those occurring as megacrysts/phenocrysts in  
347 tephritic rocks, and the occurrence of apatite within or in close proximity to the  
348 amphibole is frequent. The groundmass is composed of plagioclase microliths  
349 (labradorite,  $\text{An}_{54\text{-}66}$ ), elongated clinopyroxene crystals (average  $\text{Wo}_{53}\text{En}_{31}\text{Fs}_{16}$ ), opaque  
350 minerals ( $38 < X_{\text{USP}} < 57$ ;  $\text{Cr\#} = 0.67\text{-}1.49$ ), scarce olivine and glass.  
351 In one sample, a cluster of clinopyroxene, opaque crystals, and amphibole is interpreted  
352 as a possible co-magmatic cumulate nodule. This interpretation is based on the large  
353 dimension of the crystals, the sharp contrast between the mineral aggregate and the  
354 surrounding rock matrix, and on its chemical similarity between its minerals and the  
355 rock phenocrysts. The same interpretation is considered for an aggregate of small (0.5  
356 mm in length) plagioclase crystals characterized by anorthite content up to 79 %.  
357 Ultramafic nodules of cumulate origin, mainly composed of olivine, clinopyroxene, and  
358 amphibole, were also reported for this eruption by Caldeira et al. (2015).

## 4.2. Whole rock elemental composition

Major and trace element analyses of the studied rocks are presented in Table I, while normative compositions can be found in Supplementary Material S4.

As all other subaerial lavas in the Cape Verde Islands, Fogo's 2014 volcanic products are alkaline. They plot dominantly in the  $U_1$  field, but also in the  $U_2$  (phonotephrites) field of the TAS diagram (Fig. 3). Rocks plotting inside the  $U_1$  field would be classified, according their CIPW normative composition, either as nephelinites (normative  $ne > 20\%$ ) – the dominant type – or as melanephelinites (normative  $ne < 20\%$ ; normative  $ab < 5\%$ ) according to the subdivision proposed by Le Bas (1989); (see S4). However, as modal plagioclase can be identified in most of the rocks plotting in the  $U_1$  TAS field and for all the samples normative  $ol < 10\%$ , the classification as tephrites is here preferred and used.

The rocks are representative of moderately evolved magmas characterized by  $Mg\#$  ranging from 55.32 to 45.98 and by  $Na_2O/K_2O$  between 1.35 and 1.46. The less evolved rocks ( $Mg\# = 55.32$  to  $51.97$ ) have  $TiO_2$  contents varying from 3.65 to 3.75 wt%,  $P_2O_5$  close to 1 (0.94 to 1.11 wt%),  $CaO/Al_2O_3$  ratios ranging from 0.65 to 0.78 and  $K_2O/TiO_2$  ratios from 0.25 to 0.32.

The 2014 lavas are highly enriched in the most incompatible elements (Fig. 5), which is depicted, for example, by  $(La/Yb)_{cn}$  ratios  $> 20$ , with the most evolved rocks presenting the highest values for this ratio ( $> 23$ ). Primitive mantle normalized incompatible elements patterns (Fig. 5c) show a significant enrichment of Nb and Ta relatively to the light REE and the radiogenic heat producers K, Th and U. Small Hf negative anomalies are also evident, which partially reflects the high Zr/Hf ratios ( $> 49$ ), well above the value of 36 characterizing CI chondrites and the primitive mantle (e.g. Palme and O'Neil, 2003).

The sampled pyroclasts and lava flows are similar in composition, the most significant difference being the sulphur-enriched composition of pyroclasts (120 to 230 ppm;

$\bar{X} = 200$  ppm) as compared to lava flows (60 to 120 ppm;  $\bar{X} = 84$  ppm). This indicates a more effective degassing of lava flows as a consequence of a slower cooling. Most of the characteristics described above are similar to those of lavas erupted during the two precedent eruptions (1995 and 1951), as Fig. 5 shows. Notwithstanding the fact that the samples here studied are only representative of the lava emitted during the first 15 days of the eruption, some differences, however, were noticed: i) the 1995 lavas present a slightly higher compositional range (MgO from 6.86 to 2.40 wt%; Hildner et al., 2011) than the ones from 2014 (MgO from 6.23 to 2.93 wt%); ii) from the three eruptions considered, the 1951 event produced the less evolved lavas (MgO up to 8.24 wt%; Hildner et al., 2012); iii) for the same SiO<sub>2</sub> content, the 1951 lavas tend to be less alkali-rich than the 2014 and 1995 volcanics (Fig. 3); iv) the 2014 and 1995 erupted materials are characterized by small compositional gaps ( $\Delta\text{SiO}_2 = 2.5\%$  and  $3.8\%$ , respectively) in opposition to the described for from the 1951 eruption for which no phonotephrite compositions were reported (see Fig. 1 and references therein); v) for these three eruptions, the most evolved products are the phonotephrites from the 1995 eruption, which also present the highest concentrations in incompatible elements like Nb and Ta. However, the highest concentrations in light REE are found in phonotephrites from the 2014 eruption, which show the highest La/Nb ratios. This higher La/Nb are also observed for the less evolved rocks (MgO > 5 wt%), with 2014 lavas presenting  $\bar{X}$  La/Nb = 0.69, whereas the 1995 and 1951 less evolved rocks show  $\bar{X}$  La/Nb=0.60 (cf. Table 1, Hildner et al., 2011 and Hildner et al., 2012).

#### 4.3. Whole rock isotope composition

The results of Sr, Nd, Hf and Pb isotope analyses are shown on Table II. The lavas erupted in 2014 at Fogo Island present isotope signatures akin to those typical of the Southern islands in the Cape Verde Archipelago. Indeed, in opposition to what is observed for the Northern capeverdean islands (Fig.6), they are characterized by

relatively unradiogenic  $^{206}\text{Pb}/^{204}\text{Pb}$  ratios (up to 19.001) and plot above the Northern Hemisphere Reference Line ( $\Delta 7/4$  from 0.99 to 1.57;  $\Delta 8/4$  from 25.38 to 28.80; see Hart, 1984 for definitions of these parameters). Notwithstanding the fact that their  $^{87}\text{Sr}/^{86}\text{Sr}$  (0.70361 to 0.70369) and  $^{143}\text{Nd}/^{144}\text{Nd}$  (0.51276 to 0.51279) ratios are clearly more and less radiogenic, respectively, than those observed for the Northern islands, the 2014 lavas plot on the second quadrant of the  $^{87}\text{Sr}/^{86}\text{Sr}$  vs.  $^{143}\text{Nd}/^{144}\text{Nd}$  diagram (Fig. 7A). This indicates a provenance from a time-integrated depleted source(s), i.e. which evolved over time with lower Rb/Sr and higher Nd/Sm than those of the BSE (bulk silicate earth) and the CHUR (chondritic uniform reservoir), respectively. Compared to the lavas extruded during the 1951 and 1995 eruptions, the 2014 rocks present more unradiogenic Sr and radiogenic Nd signatures (Fig. 7). The 2014 lavas also exhibit slightly more radiogenic  $^{206}\text{Pb}/^{204}\text{Pb}$  ratios than the most samples from the two previous eruptions, the same being true for  $^{207}\text{Pb}/^{204}\text{Pb}$  ratios (Fig. 6A). Lavas from these 3 eruptions are amongst the Cape Verde rocks with lower  $^{206}\text{Pb}/^{204}\text{Pb}$  ratios. As is typical of the Southern Cape Verde Islands, rocks from these 3 eruptions are characterized by positive  $\Delta 8/4$ , plotting above the NHRL (Fig. 6B).

The 2014 lavas'  $^{176}\text{Hf}/^{177}\text{Hf}$  ratios range from 0.28294 to 0.28296 (Table II). A time-integrated evolution with high Lu/Hf ratios compared to CHUR is shown by positive  $\epsilon\text{Hf}$  values (5.88 to 6.62; Fig. 7B), plotting between the mantle arrays proposed by Vervoort (1999) and Chauvel (2008). These are the first  $^{176}\text{Hf}/^{177}\text{Hf}$  determinations available for Fogo Island, preventing any comparison with previous results. However, noteworthy that the lavas erupted in 2014 plot inside the large field defined in the  $\epsilon\text{Nd}$ - $\epsilon\text{Hf}$  space by the lavas from the neighbouring island of Santiago, which is characterized by significantly higher and lower  $^{176}\text{Hf}/^{177}\text{Hf}$  ratios (see Barker et al., 2009; Martins et al., 2010). Significant correlations between any of these isotope signatures and ratios



involving incompatible trace elements have not been found. This will be discussed later (see 5.3).

The  $^3\text{He}/^4\text{He}$  ratio of a glassy phonotephrite was determined at the Institut de Physique du Globe de Paris (IPGP) using crushing for gas extraction. The obtained value ( $1.11 \pm 0.13$  Ra, where Ra is the present atmospheric ratio of  $1.4 \times 10^{-6}$ ) for a  $^4\text{He}$  concentration of  $2.8 \times 10^{-9}$  cc/g is interpreted as the result of atmospheric contamination during the eruption/consolidation of lava. Consequently, this result will not be considered in the discussion.

## **5. Discussion**

### **5.1 Mantle source composition and magma evolution**

Previous studies, explained the chemical variability of Fogo's lavas by mixing in different proportions of HIMU-like (ancient recycled ocean crust) and EM1-like mantle end-members, diluted by the presence of depleted upper mantle (Gerlach et al., 1988) or by lower mantle material (Doucelance et al., 2003; Escrig et al., 2005) entrained by the upward moving plume.

Although 2014 lavas present low  $^{206}\text{Pb}/^{204}\text{Pb}$  ratios (up to 19.001), clearly below those typical of magmas originated from sources dominated by the HIMU mantle component (e.g. Kawabata et al., 2011), the HIMU fingerprint is shown by trace element patterns (Fig. 5) displaying enrichment in Nb and Ta relative to the LREE and the LILE (e.g. Niu et al., 2012). Additionally, all the analysed rocks are characterized by positive  $\Delta 8/4$  and  $\Delta 7/4$  and plot below the mixing lines between a HIMU type end-member and DMM or lower mantle compositions (Fig. 10), strongly suggesting the contribution of an EM1-type end-member to the 2014 Fogo mantle source(s). Interestingly, the products erupted in 2014 mark a change on the evolutionary trend reported by previous authors for Fogo eruptions (Gerlach et al., 1988; Escrig et al., 2005) which was characterized by an increasing contribution of the enriched component. Indeed, the 2014 lavas have less

radiogenic Sr, but more radiogenic Nd signatures than those from the 1951 and 1995 eruptions.

Fogo's 2014 lavas ( $\text{MgO} \leq 6.4$  wt %,  $\text{Mg\#} \leq 53.2$ ;  $\text{Ni} \leq 42$  ppm) cannot be considered representative of primary magmas. This fact and its chemical variability ( $\text{MgO}$  down to 2.93 wt.%;  $\text{Ni}$  down to 6 ppm) emphasize the role of magma evolution processes to explain the observed compositional range. This is reinforced by the phonolitic composition of the glassy groundmass of some lavas ( $\text{MgO}$  down to 0.66 wt%; total alkalis up to 15.76 wt%; see Supplementary Material S3-G).

The important role of clinopyroxene fractionation is suggested by its occurrence as phenocryst in most samples and by the Sc decrease with increasing concentration of strongly incompatible trace elements such as La (Fig 8A), here used as a proxy of magma evolution index. Fractionation of clinopyroxene must have been preceded by crystallization of olivine as indicated by the occurrence of olivine inclusions in clinopyroxene phenocrysts. The  $\text{Dy/Dy}^*$  ratio, as defined by Davidson et al. (2013), tends to decrease from up to 0.81 in tephrites, down to 0.61 in phonotephrites, a tendency that, according to those authors, can be attributed either to amphibole or to clinopyroxene fractionation. If the importance of clinopyroxene fractionation was already demonstrated, the positive correlation of  $\text{Dy/Dy}^*$  and Nb/U ratios (Fig. 8B) emphasizes the role of amphibole since, at odds with what happens with this mineral, clinopyroxene does not have the capacity to fractionate Nb from U (e.g. Adam and Green, 2006).

The calculated water content of the melt during kaersutite crystallization range from 3.81 to 4.14 wt% ( $\pm 0.78$  wt%) while oxygen fugacity is estimated in the range of 0.92 to 2.3 log units above NNO ( $\pm 0.37$  log units) using the methodology of Ridolfi and Renzulli (2012). The obtained  $f\text{O}_2$  values are comparable to those reported for some other intraplate ocean islands (e.g. Madeira; Mata and Munhá, 2004). These relatively high  $f\text{O}_2$  values are reflected in the composition of pyroxenes for which high  $\text{Fe}^{3+}$

contents were calculated based on the stoichiometry (Supplementary material S3-A), but not in the amphibole (Supplementary material S3-C). This suggests the incorporation of Ti (TiO<sub>2</sub> up to 6.13 wt%) into the octahedral position of kaersutite through the substitution  $^{[VI]}R^{2+} + 2OH^- = ^{[VI]}Ti^{4+} + 2O^{2-}$ , which favours high Fe<sup>2+</sup>/Fe<sup>3+</sup> (Satoh et al., 2004).

As also reported for the previous Fogo's eruption (e.g. Munhá et al., 1997; Hildner et al., 2012) plagioclase did not play a significant role in the evolution of 2014 magmas, as inferred from its rarity among phenocrysts and from the continuous Sr increase (1194 to 1408 ppm) throughout the erupted suite. Judging from the comparatively high Al<sub>2</sub>O<sub>3</sub>, Na<sub>2</sub>O and K<sub>2</sub>O concentrations determined in the glassy phonolitic matrix, plagioclase and alkali feldspar fractionation was also not important for the generation of such evolved compositions. On the other hand, the role of Fe-Ti oxides and apatite fractionation is made evident by the significant decrease on P<sub>2</sub>O<sub>5</sub> (Fig. 8C) and TiO<sub>2</sub> (not shown) concentrations from the most evolved tephrites (SiO<sub>2</sub> < 45.2%) to phonotephrites (SiO<sub>2</sub> > 47.7 wt. %) (see also Table I). The fractionation of these two non-silicate phases, with the consequent significant increase in silica content of magmatic liquids, was probably the cause for the small compositional gap ( $\Delta SiO_2 = 2.5\%$ ) separating those two lithotypes.

Even though the isotope differences precludes the studied rocks to be considered comagmatic with those erupted in 1951 and 1995 (see section 4.4), samples from these three eruptions plot along the same trends in most variation diagrams, suggesting that they share a common magma evolution history (e.g. Fig. 8 A and C). However, Fig. 8B emphasizes, despite similar trends, the lower Nb/U and Dy/Dy\* ratios of the 2014 rocks relatively to the rocks of similar degree of evolution generated during the two previous eruptions.

Indeed, the less evolved 2014 rocks are characterized by lower Nb/U ratios ( $60 \pm 3$ ) than the basanitic/tephritic lavas from the 1995 and 1951 eruptions ( $95 \pm 4$ ; Hildner et

al., 2011; 2012). Given the similar degree of evolution, these differences cannot be explained by fractional crystallization. The 2014 Nb/U ratios fits the typical OIB value (EM lavas excluded) of  $52 \pm 15$  obtained by Hofmann (2003). As shown by this author, either the EM-type mantle components or the continental crust have significantly lower Nb/U ratios. Consequently the higher contribution of an enriched end-member (EM type) for the 1995 and 1951(see above) lavas cannot be invoked as a cause for their higher Nb/U ratios.

Nb/U ratios significantly higher than the typical OIB lavas have also been reported for some Canary lavas by Lundstrom et al. (2003). These authors defended that this can be the reflex of mixing between ascending plume-derived magmas and lithospheric melts with a significant contribution from amphibole present in low-solidus mantle domains. These domains would have been generated by metasomatic (s.l.) processes during previous stages of islands building. We suggest that a similar process may have been responsible for the significantly higher Nb/U and Dy/Dy\* ratios of the 1995 and 1951 lavas. Since their vents, and probably also the ascending magma paths, were almost coincident with those of 2014, we speculate that such low-solidus lithospheric domains were already exhausted and did not contribute significantly for the composition of the subsequent 2014 eruption products.

As observed for the precedent 1995 eruption (Munhá et al., 1997; Silva et al., 1997; Hildner et al., 2011), the initial products erupted in 2014 were more evolved (phonotephrites; SiO<sub>2</sub> up to 47.99 wt.%) than those emitted subsequently (tephrites, s.l.), for which SiO<sub>2</sub> contents as low as 43.03 wt.% were obtained. Considering the composition of the erupted magmas, assuming a complete degassing during eruption (suggested by very low loss on ignition), and using the algorithm of Giordano et al. (2008), the viscosity of the phonotephrites would have been some 10 times higher than that of the less evolved tephrites. This partially explains the evolution of lava flow morphology during the course of the eruption, which exhibited *a'a* characteristics during the initial

eruptive stages, whilst *pāhoehoe* type lavas became more frequent during the subsequent effusion of the less viscous tephritic lava flows.

## **5.2 Thermobarometric evidence for magma reservoirs into the mantle**

Geothermobarometric estimates based on phenocrysts and cognate megacrysts have been considered to be important to constrain the magmatic plumbing system of a volcano, given they can be used to calculate the depths of magma stalling/stagnation at mantle/crustal chambers. Indeed, silicates are characterized by very low intra-crystalline diffusion rates, thus tending to preserve the composition acquired at the moment of crystallization.

We used the clinopyroxene-liquid thermobarometer of Putirka et al. (2003) for which lower uncertainties are foreseen than those reported for methods only using the clinopyroxene composition (Putirka, 2008; see also Geiger et al., 2016 for a review on clinopyroxene thermobarometry). The method is based on jadeite–diopside/hedenbergite exchange equilibria in hydrous conditions, which are shown to have existed at Fogo by the presence of amphibole (see also [above](#) for an estimate of water content in magma). As we used phenocryst cores and whole rock compositions as proxies of the crystal-liquid pairs, the P-T results obtained will be regarded as the conditions prevailing during early stages of clinopyroxene phenocrysts crystallization, assuming that no magma mixing occurred after pyroxene crystallization.

In order to use mineral/liquid thermobarometers it is mandatory to test if the crystal/melt pairs used testify equilibrium conditions. On a first approach a visual screening was made to identify textural evidence for disequilibrium, those showing irregular or reabsorbed shapes were avoided. Furthermore, only core analyses of unzoned or normally zoned phenocrysts were used. No mineral correction was made to the whole-rock composition due to the lack of evidence for significant accumulation ( $\leq 10\%$  of phenocryst phases).

Considering the concerns regarding the efficacy of the Fe-Mg exchange in deciphering  
 situations of pyroxene-melt equilibrium (e.g. Mollo et al., 2013), we used instead the  
 comparison between predicted and measured components in clinopyroxene (diopside-  
 hedenbergite; enstatite-ferrosilite; Ca-Tschermak's) as proposed by Putirka (1999).  
 Following the recommendations of Putirka et al. (2003), only clinopyroxenes whose  
 compositions are within the  $\pm 2\sigma$  level of the predicted ones were used in the  
 thermobarometric calculations. The standard errors of estimation (SEE) of the Putirka et  
 al. (2003) method are 1.7 kbar and 33 °C, while analytical uncertainties, calculated  
 using the relative standard deviation of whole rock and microprobe analyses of  
 reference materials are significantly lower than the uncertainties of the method.  
 The temperatures obtained for pyroxene crystallization range from 1045 to 1063 °C for  
 the phonotephrites and 1102 to 1143 °C for the tephrites. Pyroxene phenocrysts  
 crystallized from phonotephritic magmas at pressures in the range between 560 and 778  
 MPa, whereas the tephrites yield variations between 690 and 890 MPa (Fig. 9).  
 For amphiboles we used the single-phase thermobarometric and chemometric equations  
 proposed by Ridolfi and Renzulli (2012), based on multivariate least-squares regression  
 analyses of a large database of amphibole compositions in alkaline magma systems. For  
 this method the authors claim low uncertainties:  $P \pm 11.5\%$ ,  $T \pm 23.5^\circ\text{C}$ . The application  
 of the thermobarometer shows that the values obtained for kaersutites occurring in  
 phonotephrites and tephrites are similar within error (1032 to 1050°C and 568 to 620  
 MPa; see Fig. 9).  
 The kaersutite occurring in the 2014 Fogo lavas show ubiquitous signs for  
 disequilibrium, presenting evidence for partial (reaction rims) to total  
 (pseudomorphosis) substitution by polycrystalline aggregates of rhönite and  
 clinopyroxene. We interpret the occurrence of rhönite and of the associated  
 clinopyroxene as a consequence of the kaersutite destabilization resulting from magma  
 degassing upon ascent, given the decrease of H<sub>2</sub>O solubility in magmas as pressure

603 drops (e.g. De Angelis et al., 2015). The destabilization of amphibole most probably  
604 occurs at pressures below 100-150 MPa (e.g., Rutherford, 2008) with reaction rims  
605 developing, for hornblende compositions, at pressures from circa 100 MPa down to 40  
606 MPa (Browne and Gardener, 2006).

607 Amphibole reaction rims are often used to estimate magma ascent rate since their  
608 thickness, size and the shape of the replacing mineral phases are all dependent on it  
609 (Chiaradia et al., 2011; Browne and Gardner, 2006). Since the reaction rims observed in  
610 kaersutite crystals from the 2014 lavas are thick ( $> 500$  microns) and complete  
611 pseudomorphosis of mm-sized crystals (up to 4mm) is common, it is valid to assume on  
612 a qualitative basis and based on Browne and Gardener's (2006) experimental data that  
613 the time of exposure of kaersutite to low  $\text{PH}_2\text{O}$  before quenching at the surface was  
614 relatively long ( $> 1$  month). Thus, the occurrence of rhönite and the degree of kaersutite  
615 replacement by rhönite suggest a late and short stagnation/stalling at crustal levels (i.e.  
616 at pressures below 100 MPa;  $< 4.3$  km below the island summit or  $< 1.5$  km below sea  
617 level) after a longer storage at deeper magma chambers.

618 In order to convert the calculated pressures to depths several assumptions has to be  
619 done, the depth of Moho being the one with more impact in the obtained results.

620 Vinnik et al. (2012), proposed that at the Cape Verde archipelago the crust would be  
621 significantly thicker than the normal oceanic crust, extending down to 20-30 km depth.  
622 This was not supported by a later study (Wilson et al., 2013), which placed the Moho at  
623 significantly shallower depths, in agreement with the models of Lodge and Helffrich  
624 (2006), Pim et al. (2008) and Wilson et al. (2010). In this study we adopt 13.5 km as the  
625 depth of Moho beneath the Fogo Island (see Wilson et al., 2010; 2013).

626 Considering a height of 5800 m for the Fogo island edifice ( $\approx 3000$  m below present sea  
627 level), an average density of  $2400 \text{ kg.m}^{-3}$  (Dash et al., 1976) for the island edifice, a  
628 crustal density of  $2800 \text{ kg.m}^{-3}$  inferred from seismic receiver functions (Lodge and  
629 Helffrich, 2006), a mantle density of about  $3200 \text{ kg.m}^{-3}$  at the Fogo region (Pim et al.,

2008), a Moho depth at 13.5 km below sea level (Wilson et al., 2010; 2013) and taking into account the uncertainties of the barometric methods (see above) the crystallization depth of clinopyroxene phenocrysts ranges approximately ( $\pm 5.5$  km) from 17.8 to 28.4 km below Fogo's summit, or 15.0 to 25.6 km below sea level. For amphiboles the same presupposes allow considering their crystallization at depths between 18.2 and 19.9 km ( $\pm 3$  km) below Fogo's summit, or 15.4 to 20.1 km below sea level. Considering the most common estimates for the crustal thickness at the Cape Verde region ( $\approx 12$  to 13.5 km; Lodge and Helffrich, 2006; Pim et al., 2008; Wilson et al., 2010; 2013) the obtained results suggest that the major fractionation events occurred in magma chambers located into the mantle.

Geobarometric studies of the previous two eruptions also revealed pre-eruptive magma storage at shallow mantle depths, followed by a short-period of magma stalling at crustal levels (Munhá et al., 1997; Hildner et al., 2011, 2012). The depths of clinopyroxene equilibration obtained in this study for the 2014 eruption (890 to 560 MPa; see above), although partially overlapping those presented for the historical eruptions by Hildner et al. (2011, 2012) (680 to 460 MPa), extends to higher pressures. However it must be noted that the pressure estimates by those authors refer to the final crystallization level, while our data represents the first crystallization stages of clinopyroxene phenocrysts.

The causes for the development of magma reservoirs within the mantle are still not understood. Changes in buoyancy have been considered as an explanation for magma stagnation during ascent (e.g. Ryan, 1994). However, Jagoutz (2014) emphasized that, ascending magmas can stagnate even when they are less dense than the surrounding rocks. A similar point of view was defended by Menand (2008) who considered that buoyancy is unlikely to be a major control in the emplacement of sills, which can be viewed as precursors of magma reservoirs (Gudmundsson, 2012). Moreover, as shown by Putirka (2017), hydrated magmas with MgO contents similar to those erupted in the



2014 Fogo eruption are less dense than the mantle, or even than the lower crustal rocks, indicating that buoyancy cannot be the explanation for the stagnation of Fogo magmas in the mantle. As proposed by Menand (2008), the presence of rheological anisotropies could be the primary factor determining the depth of magma stalling or stagnation. This can lead to the inference that the thickness of the elastic lithosphere exerts a major control on the depth of magma reservoirs. However, for the Cape Verde Archipelago the elastic thickness is estimated at 30 km (Pim et al., 2008) and our barometric data suggest magma emplacement at shallower depths, invalidating, in this case, such a proposal. Regional flexural stresses produced by the volcanic edifice loading are also thought to strongly influence the plumbing systems by generating a vertical contrast between tensile and compressive stress zones, capable of influencing the depth of magma stalling (see Putirka, 1997 and references therein). We do not have data to evaluate this hypothesis.

Whatever the cause for the development of mantle magma reservoirs, they seem to be common on ocean islands during periods of low magma supply rates (e.g. Longpré et al., 2008; Stroncik et al., 2009; Klügel et al., 2015) as was the case during the latest (this study) and the previous eruptions of Fogo volcano (Munhá et al., 1997; Hildner et al., 2011; 2012).

The scenario here proposed for the ascent of the 2014 Fogo magmas and of its plumbing system receives support from independent data. Indeed, a seismic event on October 4, 2014 (i.e. 50 days before the eruption) with a hypocentre 17 km below sea level (19.8 km below the Fogo summit), was interpreted by Instituto Nacional de Meteorologia e Geofísica (INMG, Cabo Verde) as resulting from the rupture of the roof of a mantle reservoir allowing magma transfer to shallower levels. Also, geodetic modelling of Sentinel-TOPS interferometry by Gonzalez et al. (2015) revealed the lack of deformation at the island-scale during and pre-eruption times, further suggesting the deep location of the main magma reservoirs.

### **5.3 Evidence for small-scale mantle heterogeneity and short-term compositional evolution of Fogo volcano.**

As mentioned above, the Cape Verde Archipelago is known by its remarkable geochemical intra-island heterogeneity (e.g. Gerlach et al., 1988; Doucelance et al., 2003). Significant intra-island time-dependent geochemical variations are also common as shown for most Cape Verde Islands (e.g. Barker et al., 2010; Mourão et al., 2012 a). Intra-island heterogeneities have also been described for presumably coeval rocks, such as the case of the Recent Volcanics of São Vicente Island (Trindade et al., 2003), and also of the Fogo Island where, as shown by Escrig et al. (2005), lavas erupted since 1785 present measurable variability on isotope signatures.

In opposition to incompatible trace-element ratios, which can be fractionated during partial melting and crystal fractionation processes, radiogenic isotope ratios are not changed during such events. They are thus a reliable indicator of source heterogeneity, even though the isotope variability of lavas tends to be smaller than that of the mantle source due to eventual mixing/homogenization processes (e.g. Stracke and Bourdon, 2009).

The 2014 volcanic products have clearly more unradiogenic Pb and Sr ( $^{206}\text{Pb}/^{204}\text{Pb}$  down to 18.972;  $^{87}\text{Sr}/^{86}\text{Sr}$  down to 0.703613) but more radiogenic Nd ( $^{143}\text{Nd}/^{144}\text{Nd}$  up to 0.512789) signatures than the previous two eruptions ( $^{206}\text{Pb}/^{204}\text{Pb}$  up to 19.273;  $^{87}\text{Sr}/^{86}\text{Sr}$  up to 0.70379;  $^{143}\text{Nd}/^{144}\text{Nd}$  down to 0.51272; see also Figs 6 and 7). Considering that the 2014 lavas erupted from vents localized less than 200 and 2000 m of those from the two previous eruptions (1951 and 1995) and that these 3 eruptions occurred within a time lapse of only 63 years, such differences emphasize the presence of small-scale heterogeneities in the mantle sources feeding the volcanism of Fogo Island and the absence of significant magma mingling/homogenization before eruption.

The ability of magmas erupted from a volcano to show the source heterogeneity depends on the degree of partial melting, on the size of magma chambers and on the

time of residence in such reservoirs. The higher the degree of partial melting, the higher is the capability of the extracted magmas to average the composition of a heterogeneous source. As a consequence low degree partial melts reflect better the compositional variability of the source (e.g. Stracke and Bourdon, 2009; Martins et al., 2010). It is accepted that the lithosphere exerts a major control in the final depth and extent of sub-lithospheric mantle melting (e.g. Watson and Mckenzie, 1991; Humphrey and Niu, 2009; Niu et al., 2011), even though the thickness of mature ( $> 70$ Ma) oceanic lithosphere does not surpass  $\approx 90$  km (Niu et al., 2011). The Cape Verde islands stand on a 120-140 My old oceanic crust characterized by significantly high values of admittance (geoid to depth ratio) (Monnerau and Cazennave, 1990). These suggests that lithosphere may extend to depths below the spinel-garnet transition ( $\approx 3$  GPa; Klemme and O'Neil, 2000) in agreement with previous studies for Cape Verde islands (e.g. Gerlach et al., 1998; Barker et al., 2010; Mourão et al., 2012a). Even taking into account that the less evolved 2014 magmas (tephrites) are not characterized by primary or primitive compositions, this percept is endorsed by (Tb/Yb)<sub>n</sub> ratios higher than 2.3, which is significantly above the threshold value of 1.8 proposed by Wang et al. (2002) as a proxy for spinel-garnet facies transition. Indeed it would be necessary to consider a (Tb/Yb)<sub>n</sub> increase higher than 27% during magma evolution – which is not expectable from the commonly accepted D values (e.g. Adam and Green, 2006) – to place the mean melting depths outside the garnet zone. Moreover, 2014 magmas show a Tb/Yb decrease from tephrites for the more evolved phonotephrites.

The thickness of the lithosphere exerts a first-order control on the extent of partial melting (e.g. Humphreys and Niu, 2009). For the present case, a lithosphere some 90 km thick (see above) would have constrained the melting to small extent. Despite the exact extent of melting is difficult to assess given the significantly evolved character of lavas (MgO  $< 6.4$  wt%) and the uncertainty derived from the lack of knowledge about the relative proportion of peridotite and eclogite in the mantle source, the highly SiO<sub>2</sub> -

undersaturated character of the Fogo lavas (2014: normative *ne* up to 23.04 %) and the high TiO<sub>2</sub> contents clearly suggest low percentages of partial melting, with the consequent deficient averaging of the isotopic variability of the source. The above referred lack of correlation between elemental and isotope ratios (see 4.3) also points to low degrees of melting during which a significant elemental fractionation occurs erasing any correlation between incompatible element ratios and isotope ratios (see Stracke and Bourdon, 2009).

After extraction, the degree of melt homogenization will depend on the occurrence of a plumbing system with large magmatic chamber(s), and of long magma residence times within the system, allowing mixing of different batches of melt. Data gathered from several islands suggest that for voluminous magma chambers to form, high magma supply rates are needed; conversely, during evolutionary stages characterized by low magma supply rates a plethora of small and ephemeral magma reservoirs tend to form, many of them within the mantle (see Klügel et al., 2000; 2005; Stroncik et al., 2009 and references therein), and this is also the case for the recent magmatism of Fogo. The evidence for small and ephemeral magma reservoirs beneath Fogo was already proposed for the previous eruptions (Munhá et al., 1997; Hildner et al., 2012). This may be also the case for the 2014 eruption as suggested by the compositional change during the latest two eruptions (from phonotephrites to basanites/tephrites) and, despite the associated methodological errors, by distinct depths of magma chambers where clinopyroxene and kaersutite crystalized, both evidences precluding a large homogenizing reservoir.

## **6. Concluding remarks**

- Magmas erupted from November 23 to December 7, 2014 at Fogo Island (Cape Verde Archipelago) are alkaline, exhibit significantly evolved compositions (Ni < 42 ppm) and are classified as tephrites and phonotephrites. The compositional

range is slightly smaller than that reported for the 1995 eruption, but larger than the displayed by the 1951 eruption, for which no phonotephrites were erupted.

- Similarly to 1995 (Munhá et al., 1997; Silva et al., 1997; Hildner et al., 2011), the eruption of phonotephritic lavas preceded the effusion of the tephritic ones suggesting the existence of a compositional/density zoning inside the pre-eruptive magma chamber or of several magma reservoirs, in agreement with barometric data.
- Geobarometric estimates using clinopyroxene and kaersutite compositions indicate that fractional crystallization mainly occurred in magma chambers located in the mantle (down to  $25.6 \pm 5.5$  km below the sea level), followed by a short residence time ( $< 60$  days) at crustal levels.
- Erupted magmas are characterized by positive  $\epsilon_{\text{Nd}}$ ,  $\epsilon_{\text{Hf}}$ ,  $\Delta 8/4$  and  $\Delta 7/4$ . Their compositions reflect a mantle source where ancient recycled ocean crust and an enriched component (EM1-type) are present. The 2014 lavas have less radiogenic Sr, but more radiogenic Nd compositions, than those from the 1951 and 1995 eruptions, marking a change on the evolutionary trend reported by previous authors for Fogo (Gerlach et al., 1988; Escrig et al., 2005) which was characterized by an increasing contribution of the EM1-type component.
- Although the 2014 eruption vents are almost spatially coincident with those of 1995 and less than 2 km away from the 1951 vents, their lavas are isotopically different from those generated in the previous two eruptions. These differences in magmas erupted on a very limited area and short interval (63 years) reflect the heterogeneity of the mantle source and the lack of averaging/mingling during partial melting and ascent through the plumbing system. For these, the lid effect of the old (120-140 Ma) and thick lithosphere is considered of utmost importance.

- The lower Nb/U ratios of the 2014 rocks as compared with previous eruptions is considered to reflect the lack of significant mixing of ascending plume magmas with lithospheric melts, as opposed to what has been hypothesized for 1995 and 1951 magmas.

## Acknowledgements

We dedicate this paper to the memory of Luís Celestino Silva (1936-2017), a pioneer in the geology of Cape Verde: his knowledge, enthusiasm and kindness marked most of the authors of this work.

This research received financial support from FCT (Fundação para a Ciência e Tecnologia) through projects REGENA (PTDC /GEO-FIQ/3648/2012) and FIRE (PTDC/GEO-GEO/1123/2014), as well as through project UID/GEO/50019/2013 to Instituto Dom Luiz (IDL). R. Ramalho was funded by a FP7-PEOPLE-2011-IOF Marie Curie International Outgoing Fellowship, which is acknowledged. The authors are grateful to Pedro Rodrigues for skilled assistance during electron microprobe analyses. Field work of J. Mata was partially funded by Bernardo Mata. Kayla Iacovino is acknowledged for the permission to use her Excel spreadsheet to calculate magma viscosity (see <http://www.kaylaiacovino.com/tools-for-petrologists/>). Cristina de Ignacio, an anonymous reviewer and the Editor (Nelson Eby) are acknowledged for their constructive comments, corrections and suggestions, which significantly contributed for the quality of this paper.

## References

- Adam, J., Green, T. 2006. Trace element partitioning between mica and amphibole-bearing garnet lherzolite and hydrous basanitic melt: 1. Experimental results and the investigation of controls on partitioning behavior. *Contributions to Mineralogy and Petrology* 152, 1-17.
- Bagnardi, M., González, P.J., Hooper, A. 2016. High-resolution digital elevation model from tri-stereo Pleiades-1 satellite imagery for lava flow volume estimates at Fogo Volcano: Tri-stereo Pleiades DEM of Fogo Volcano. *Geophys. Res. Lett.*, 43, doi:10.1002/2016GL06945

- Barker, A.K., Holm, P.M., Peate, D.W., Baker, J.A. 2009. Geochemical stratigraphy of submarine lavas (3–5 Ma) from the Flamengos Valley, Santiago, southern Cape Verde islands. *Journal of Petrology* 50, 169-193.
- Barker, A.K., Holm, P.M., Peate, D.W., Baker, J.A. 2010. A 5 million year record of compositional variations in mantle sources to magmatism on Santiago, southern Cape Verde archipelago. *Contributions to Mineralogy and Petrology* 160, 133-154.
- Barker, A.K., Troll, V.R., Ellam, R.M., Hansteen, T.H., Harris, C., Stillman, C.J., Andersson, A. 2012. Magmatic evolution of the Cadamosto Seamount, Cape Verde: beyond the spatial extent of EM1. *Contributions to Mineralogy and Petrology* 163, 949 -965.
- Beier, C., Haase, K. M., Abouchami, W., Krienitz, M.-S., Hauff, F. 2008. Magma genesis by rifting of oceanic lithosphere above anomalous mantle: Terceira Rift, Azores. *Geochemistry, Geophysics, Geosystems* 9, Q12013.
- Browne, B.L., Gardner, J.E. 2006. The influence of magma ascent path on the texture, mineralogy, and formation of hornblende reaction rims. *Earth and Planetary Science Letters* 246, 161-176.
- Brum da Silveira, A., Madeira, J., Munhá, J., Mata, J.; Martins, S., Mourão, C., Tassinari, C. 2006. The summit depression of Fogo Island (Cape Verde): caldera and/or flank collapse? Abstracts and Programme of the George P. L. Walker symposium on Advances in Volcanology, Reykolt, Islândia, 23.
- Caldeira, R., Guimarães, F., Mata, J. Silva, P., Moreira, M., Ferreira, P. 2015. Mineral Chemistry of Ultramafic Nodules from Lavas of the Fogo Island 2014 Eruption (Cape Verde). Preliminary results. Livro de Resumos do X Congresso Ibérico de Geoquímica/XVIII Semana de Geoquímica, 51-53, LNEG, Lisboa.
- Cappello, A., G. Ganci, S. Calvari, N. M. Pérez, P. A. Hernández, S. V. Silva, J. Cabral, and C. Del Negro. 2016. Lava flow hazard modeling during the 2014–2015 Fogo eruption, Cape Verde, *Journal of Geophysical Research, Solid Earth* 121, 1-14.
- Chauvel, C., Blichert-Toft, J. 2001. A hafnium isotope and trace element perspective on melting of the depleted mantle. *Earth Planetary Science Letters* 190, 137–151.
- Chauvel, C., Lewin, E., Carpentier, M., Arndt, N., Marini, J.-C. 2008. Role of recycled oceanic basalt and sediment in generating the Hf–Nd mantle array. *Nature Geoscience* 1, 64–67.
- Chauvel, C., Bureau, S., Poggi, C. 2011. Comprehensive chemical and isotopic analyses of basalt and sediment reference materials. *Geostandards and Geoanalytical Research* 35, 125–143.
- Chiaradia, M., Müntener, O., Beate, B. 2011. Enriched basaltic andesites from mid-crustal fractional crystallization, recharge, and assimilation (Pilavo Volcano, Western Cordillera of Ecuador). *Journal of Petrology* 52, 1107-1141.
- Christensen, B., Holm, P., Jambon, A., Wilson, J. 2001. Helium, argon and lead isotopic composition of volcanics from Santo Antão and Fogo, Cape Verde Islands. *Chemical Geology* 178, 127–142.
- Cooper, K.M. 2017. What does a magma reservoir look like? The “crystal’s eye” view. *Elements* 13, 23-28.
- Courtney, R., White, R. 1986. Anomalous heat flow and geoid across the Cape Verde Rise: Evidence for dynamic support from a thermal plume in the mantle. *Geophysical Journal of the Royal Astronomical Society* 87, 815-868.

- Cashman, K.V., Sparks, R.S.J., Blundy, J.D. 2017. Vertically extensive and unstable magmatic systems: A unified view of igneous processes. *Science* 355, eaag3055, 9 pages.
- Dash, B.P., Ball, M.M., King, G.A., Butler, I.W., Rona, P.A. 1976. Geophysical investigation of the Cape Verde archipelago. *Journal of Geophysical Research* 81, 5249-5259.
- Davidson, J., Turner, S., Plank, T. 2013. Dy/Dy\*: Variations Arising from Mantle Sources and Petrogenetic Processes. *Journal of Petrology* 54, 525-537.
- Day, S., Heleno da Silva, S., Fonseca, J. 1999. A past giant lateral collapse and present day instability of Fogo, Cape Verde Islands. *Journal of Volcanology and Geothermal Research* 94, 191-218.
- De Angelis, S.H., Larsen, J., Coombs, Dunn, A., Hayden, L. 2015. Amphibole reaction rims as a record of pre-eruptive magmatic heating: An experimental approach. *Earth and Planetary Science Letters* 426, 235-245
- Doucélance, R., Escrig, S., Moreira, M., Gariépy, C., Kurz, M.D. 2003. Pb-Sr-He isotope and trace element geochemistry of the Cape Verde Archipelago. *Geochimica et Cosmochimica Acta* 67, 3717-3733.
- Eisele, S., Reißig, S., Freundt, A., Kutterolf, S., Nürnberg, D., Wang, K.L., Kwasnitschka, T. 2015. Pleistocene to Holocene offshore tephrostratigraphy of highly explosive eruptions from the southwestern Cape Verde Archipelago. *Marine Geology* 369, 233-250.
- Escrig, S., Doucélance, R., Moreira, M., Allègre, C.J. 2005. Os isotope systematics in Fogo Island: evidence for lower continental crust fragments under the Cape Verde Southern islands. *Chemical Geology* 219, 93-113.
- Faria, B., Fonseca, J. F. B. D. 2014. Investigating volcanic hazard in Cape Verde Islands through geophysical monitoring: network description and first results. *Natural Hazards and Earth System Sciences* 14, 485-499.
- Foeken, J.P.T., Day, S., Stuart, F.M. 2009. Cosmogenic <sup>3</sup>He exposure dating of the Quaternary basalts from Fogo, Cape Verdes: Implications for rift zone and magmatic reorganisation. *Quaternary Geochronology* 4, 37-49.
- Forte, A.M., Quere, S., Moucha, R., Simmons, N.A., Grand, S.P., Mitrovica, J.X., Rowley, D.B. 2010. Joint seismic-geodynamic-mineral physical modelling of African geodynamics: a reconciliation of deep-mantle convection with surface geophysical constraints. *Earth Planetary Science Letters* 295, 329-341.
- French, S.W., Romanowicz, B. 2015. Broad plumes rooted at the base of the earth's mantle beneath major hotspots. *Nature* 525, 95-99.
- Galer, S.J.G., Abouchami, W. 1998. Practical application of lead triple spiking for correction of instrumental mass discrimination. *Mineralogical Magazine* 62 A, 491-492.
- Geiger, H., Barker, A., Troll, V. 2016. Locating the depth of magma supply for volcanic eruptions, insights from Mt. Cameroon. *Scientific Reports* 6, 33629.
- Gerlach, D., Cliff, R., Davies, G., Norry, M., Hodgson, N. 1988. Magma sources of the Cape Verde archipelago: Isotopic and trace element constraints. *Geochimica et Cosmochimica Acta* 52, 2979-2992.
- Gibson, S.A., Geist, D.G., Day, J.A., Dale, C.W. 2012. Short wavelength heterogeneity in the Galápagos plume: Evidence from compositionally diverse basalts on Isla Santiago. *Geochemistry, Geophysics, Geosystems* 13, doi: 10.1029/2012GC004244.



939  
940 Giordano, D., Russell, J. K., Dingwell, D. B. 2008. Viscosity of magmatic liquids: A model.  
941 Earth and Planetary Science Letters, 217, 123-134.

942 González, P. J., M. Bagnardi, A. J. Hooper, Y. Larsen, P. Marinkovic, S. V. Samsonov,  
943 Wright, T. J. 2015. The 2014–2015 eruption of Fogo volcano: Geodetic modeling of Sentinel-1  
944 TOPS interferometry. Geophysical Research Letters 42, 9239–9246.

945 Gudmundsson, A., 2012. Magma chambers: Formation, local stresses, excess pressures, and  
946 compartments: Journal of Volcanology and Geothermal Research 237–238, 19–41.

947 Hart, S.R. 1984. A large-scale isotope anomaly in the Southern Hemisphere mantle. Nature 309,  
948 753-757.

949 Hildner, H., Klügge, A., Hauff, F. 2011. Magma storage and ascent during the 1995 eruption of  
950 Fogo, Cape Verde Archipelago. Contributions to Mineralogy and Petrology 162, 751–772.  
951

952 Hildner, H., Klügge, A., Hansteen, T. 2012. Barometry of lavas from 1951 eruption of Fogo,  
953 Cape Verde Islands: Implications for historic and prehistoric magma plumbing system. Journal  
954 of Volcanology and Geothermal Research 217-218, 73-90.  
955

956 Hoernle, K., Tilton, G., Le Bas, M.J., Duggen, S., Garbe-Schönberg, D. 2002. Geochemistry of  
957 oceanic carbonatites compared with continental carbonatites: mantle recycling of oceanic crustal  
958 carbonate. Contribution to Mineralogy and Petrology 142, 520-542.  
959

960 Hofmann, A.W. 2003. Sampling mantle heterogeneity through oceanic basalts: isotopes and trace  
961 elements, in: Carlson, R. (Ed.), Treatise on geochemistry, vol. 2 - The mantle and core.  
962 Elsevier-Pergamon, Oxford, pp. 61-101.  
963

964 Holm, P.M., Wilson, J.R., Christensen, B.P., Hansen, L., Hansen S.L., Hein, K.M., Mortensen,  
965 A.K., Pedersen, R., Plesner, S., Runge, M.K. 2006. Sampling the Cape Verde mantle plume:  
966 evolution of the melt compositions on Santo Antão, Cape Verde Islands. Journal of Petrology  
967 47, 145-189.  
968

969 Holm, P.M., Grandvuinet, T., Friis, J., Wilson, J.R., Barker, A.K., Plesner, S. 2008. An <sup>40</sup>Ar-  
970 <sup>39</sup>Ar study of the Cape Verde hot spot: Temporal evolution in a semistationary plate  
971 environment. Journal of Geophysical Research 113, B08201.  
972

973 Humphreys, E., Niu, Y. 2009. On the composition of ocean island basalts (OIB): the effects of  
974 lithospheric thickness variation and mantle metasomatism. Lithos 112, 118-136.  
975

976 Iwamori, H., Nakamura, H. 2015. Isotopic heterogeneity of oceanic, arc and continental basalts  
977 and its implications for mantle dynamics. Gondwana Research 27, 1131-1152.  
978

979 Jagoutz O. 2014. Arc crustal differentiation mechanisms. Earth Planetary Science Letters 396,  
980 67–77.  
981

982 Jørgensen, J.Ø., Holm, P.M. 2002. Temporal variation and carbonatite contamination in  
983 primitive ocean island volcanics from S. Vicente, Cape Verde Islands. Chemical Geology 192,  
984 249-267.  
985

986 Kawabata, H., Hanyu, T., Chang, Q., Kimura, J., Nichols, A.R.L., Tatsumi, Y. 2011. The  
987 Petrology and Geochemistry of St. Helena Alkali Basalts: Evaluation of the Oceanic Crust-  
988 recycling Model for HIMU OIB. Journal of Petrology 52, 791-838.  
989

990 Klemme, S., O'Neill, H., 2000. The near solidus transition from garnet lherzolite to spinel  
991 lherzolite. Contributions to Mineralogy and Petrology 138, 237-248.  
992

- Klügel, A., Hoernle, K.A., Schmincke, H-U, White, J.D.L. 2000. The chemically zoned 1949 eruption on La Palma (Canary Islands): Petrologic evolution and magma supply dynamics of a rift-zone eruption. *Journal of Geophysical Research* 105, 5997-6016.
- Klügel, A., Hansteen, T.H., Galipp, K. 2005. Magma storage and underplating beneath Cumbre Vieja volcano, La Palma (Canary Islands). *Earth and Planetary Science Letters* 236, 211-226.
- Klügel, A., Longpré, M-A., Cañada, L. C., Stix, J. 2015. Deep intrusions, lateral magma transport and related uplift at ocean island volcanoes. *Earth and Planetary Science Letters* 431, 140-149.
- Kogarko, L.N., Asavin, A.M. 2007. Regional Features of Primary Alkaline Magmas of the Atlantic Ocean. *Geochemistry International* 45, 841-856.
- Le Bas, M. 1989. Nephelinitic and basanitic rocks. *Journal of Petrology* 30, 1299-1312.
- Le Maitre, R.W., 2002. Igneous rocks. A classification and glossary of terms. Recommendations of the International Union of Geological Sciences Subcommission on the systematics of igneous rocks. Cambridge University Press, Cambridge. 236pp.
- Liu, X., Zhao, D. 2014. Seismic evidence for a mantle plume beneath the Cape Verde hotspot. *International Geology Review* 56, 1213-1225.
- Lodge, A., Helffrich, G. 2006. Depleted swell root beneath the Cape Verde Islands. *Geology* 34, 449-452.
- Longpré, M., Troll, V.R., Hansteen, T.H. 2008. Upper mantle magma storage and transport under a Canarian shield-volcano, Teno, Tenerife (Spain). *Journal of Geophysical Research* 113, doi: 10.1029/2007JB005422.
- Lundstrom, C.C., Hoernle, K., Gill, J. 2003. U-series disequilibria in volcanic rocks from the Canary Islands: Plume versus lithospheric melting. *Geochimica et Cosmochimica Acta* 67, 4153-4177.
- MacDonlad, G.A. 1968. Composition and origin of Hawaiian lavas. *Geological Society of America Memoir* 116, 477-452.
- Madeira, J., Munhá, J., Tassinari, C., Mata, J., Brum, A., Martins, S. 2005. K/Ar ages of carbonatites from the Island of Fogo (Cape Verde). VIII Congresso Ibérico de Geoquímica e XIV Semana de Geoquímica (Portugal).
- Madeira, J., Brum da Silveira, A., Mata, J., Mourão, C., Martins, S. 2008. The role of mass movements on the geomorphologic evolution of ocean islands: examples from Fogo and Brava in the Cape Verde archipelago. *Comunicações Geológicas* 95, 99-112.
- Madeira, J., Mata, J., Mourão, C., Brum da Silveira, A., Martins, S., Ramalho, R., Hoffmann, D.L. 2010. Volcano-stratigraphic and structural evolution of Brava Island (Cape Verde) based on  $^{40}\text{Ar}/^{39}\text{Ar}$ , U-Th and field constraints. *Journal of Volcanology and Geothermal Research* 196, 219-235.
- Madureira, P., Mata, J., Mattielli, N., Queiroz, G., Silva, P. 2011. Mantle source heterogeneity, magma generation and magmatic evolution at Terceira Island (Azores archipelago): Constraints from elemental and isotopic (Sr, Nd, Hf, and Pb) data. *Lithos* 126, 402-418.
- Martins, S., Mata, J., Munhá, J., Mendes, M.H., Maerschalk, C., Caldeira, R., Mattielli, N. 2010. Chemical and mineralogical evidence of the occurrence of mantle metasomatism by carbonate-rich melts in an oceanic environment (Santiago Island, Cape Verde). *Mineralogy and Petrology* 99, 43-65.

- Masson, D.G., Le Bas, T.P., Grevenmeyer, I., Weinrebe, W., 2008. Flank collapse and large-scale landsliding in the Cape Verde Islands, off West Africa. *Geochemistry, Geophysics, Geosystems* 9 (7).
- Mata, J., Munhá, J. 2004. Madeira Island alkaline lava spinels: petrogenetic implications. *Mineralogy and Petrology* 81, 85-111.
- Mata, J., Moreira, M., Doucelance, R., Ader, M., Silva, L.C. 2010. Noble gas and carbon isotopic signatures of Cape Verde oceanic carbonatites: Implications for carbon provenance. *Earth Planetary Science Letters* 291, 70-83.
- McKenzie, D., O'Nions, R.K. 1991. Partial melt distributions from inversion of rare earth element concentrations. *Journal of Petrology* 32, 1021-1091.
- Menand, T. 2008. The mechanics and dynamics of sills in elastic layered media and their implications for the growth of laccoliths. *Earth Planetary Science Letters* 267, 93-99.
- Millet, M.A., Doucelance, R., Schiano, P., David, K., Bosq, C. 2008. Mantle plume heterogeneity versus shallow-level interactions: A case study, the São Nicolau Island, Cape Verde archipelago. *Journal of Volcanology and Geothermal Research* 176, 265-276.
- Mollo, S., Putirka, K., Misiti, V., Soligo, M., Scarlato, P. 2013. A new test for equilibrium based on clinopyroxene-melt pairs: Clues on the solidification temperatures of Etnean alkaline melts at post-eruptive conditions. *Chemical Geology* 352, 92-100.
- Monnereau, M., Cazenave, A. 1990. Depth and geoid anomalies over oceanic hotspot swells: A global survey. *Journal of Geophysical Research (Solid Earth)* 95, 15-429.
- Montelli, R., Nolet, G., Dahlen, F.A., Masters, G. 2006. A catalogue of deep mantle plumes: new results from finite-frequency tomography. *Geochemistry, Geophysics, Geosystems* 7, doi:10.1029/2006GC001248.
- Mourão, C., Mata, J., Doucelance, R., Madeira, J., Millet, M-A., Moreira, M. 2012a. Geochemical temporal evolution of Brava Island magmatism: constraints on the variability of Cape Verde mantle sources and on the carbonatite-silicate magma link. *Chemical Geology* 334, 44-61.
- Mourão, C., Moreira, M., Mata, J., Raquin, A., Madeira, J. 2012b. Primary and secondary processes constraining the noble gas isotopic signatures of carbonatites and silicate rocks from Brava Island: evidence for a lower mantle origin of the Cape Verde plume. *Contributions to Mineralogy and Petrology* 163, 995-1009.
- Munhá, J.M., Mendes, M.H., Palácios, T., Silva, L.C., Torres, P.C., 1997. Petrologia e geoquímica da erupção de 1995 e de outras lavas históricas da ilha do Fogo, Cabo Verde. In: Réffega A et al. (eds). *A Erupção Vulcânica de 1995 na Ilha do Fogo, Cabo Verde*. IICT, Lisboa, 171-186.
- Niu, Y., Wilson, M., Humphreys, E.R., O'Hara, M.J. 2011. The Origin of Intra-plate Ocean Island Basalts (OIB): the Lid Effect and its Geodynamic Implications. *Journal of Petrology* 52, 1443-1468.
- Niu, Y.L., Wilson, M., Humphreys, E.R., O'Hara, M.J. 2012. A trace element perspective on the source of ocean island basalts (OIB) and fate of subducted ocean crust (SOC) and mantle lithosphere (SML). *Episodes* 35, 310-327.

1107 Nobre Silva, I., Weis, D., Scoates, J. 2013. Isotopic systematics of the early Mauna Kea shield  
1108 phase and insight into the deep mantle beneath the Pacific Ocean. *Geochemistry, Geophysics,*  
1109 *Geosystems* 11, Q 09011. doi:10.1029/2010gc003176.  
1110  
1111 Palme, H., O'Neill, H.S.C. 2003. Cosmochemical estimates of mantle compositions. In:  
1112 Carlson, R. (Ed.). *The mantle and core. Treatise on Geochemistry* 2, 1-38.  
1113  
1114 Paris, R., Giachetti, T., Chevalier, J., Guillou, H., Frank, N. 2011. Tsunami deposits in Santiago  
1115 Island (Cape Verde archipelago) as possible evidence of a massive flank failure of Fogo  
1116 volcano. *Sedimentary Geology* 239, 129-145.  
1117  
1118 Pim, J., Peirce, C., Watts, A.B., Grevenmeyer, I., Krabbenhoft, A. 2008. Crustal structure and  
1119 the origin of the Cape Verde Rise. *Earth Planetary Science Letters* 272, 422-428.  
1120  
1121 Pollitz, F. 1991. Two-stage model of African absolute motion during the last 30 million years.  
1122 *Tectonophysics* 194, 91-106.  
1123  
1124 Putirka, K. 1997. Magma transport at Hawaii: Inferences based on igneous thermobarometry.  
1125 *Geology* 25, 69-72.  
1126  
1127 Putirka, K. 1999. Clinopyroxene + liquid equilibria to 100 kbar and 2450 K. *Contributions to*  
1128 *Mineralogy and Petrology* 135, 151-163.  
1129  
1130 Putirka, K.D. 2008. Thermometers and barometers for volcanic systems. *Reviews in*  
1131 *Mineralogy and Geochemistry* 69, 61-120.  
1132  
1133 Putirka, K.D. 2017. Down the crater: where magmas are stored and why they erupt. *Elements*  
1134 13, 11-16.  
1135  
1136 Putirka, K., Mikaelian, H., Ryerson, F., Shaw, H., 2003. New clinopyroxene-liquid  
1137 thermobarometers for mafic, evolved, and volatile-bearing lava compositions, with applications  
1138 to lavas from Tibet and the Snake River Plain, Idaho. *American Mineralogist* 88, 1542-1554.  
1139  
1140 Ramalho, R. 2011. *Building the Cape Verde Islands. Springer Theses*, 207 pp.  
1141  
1142 Ramalho, R., Helffrich, G., Cosca, M., Vance, D., Hoffmann, D., Schmidt, D.N. 2010. Episodic  
1143 swell growth inferred from variable uplift of the Cape Verde hotspot islands. *Nature Geoscience*  
1144 3, 774-777.  
1145  
1146 Ramalho, R., Winckler, G., Madeira, J., Helffrich, G., Hipólito, A., Quartau, R., Adena, K.,  
1147 Schaefer, J. 2015 Hazard potential of volcanic flank collapses raised by new megatsunami  
1148 evidence. *Science Advances* 1, doi: 10.1126/sciadv.1500456.  
1149  
1150 Ribeiro, O. 1954. *A ilha do Fogo e as suas erupções. Junta de Investigações do Ultramar,*  
1151 *Memórias, Série Geográfica I, Lisboa.*  
1152  
1153 Richter, N., Favalli, M., Dalfsen, E.Z., Fornaciai, A., Fernandes, R.M.S., Rodriguez, N.P., Levy,  
1154 J., Victória, S.S., Walter, Th.R. 2016. Lava flow hazard at Fogo Volcano, Cape Verde, before  
1155 and after the 2014-2015 eruption. *Natural Hazards and Earth Systems* 16, 1925-1951.  
1156  
1157 Ridolfi, F., Renzulli, A. 2012. Calcic amphiboles in calc-alkaline and alkaline magmas:  
1158 thermobarometric and chemometric empirical equations valid up to 1130 °C and 2.2 GPa.  
1159 *Contributions to Mineralogy and Petrology* 163, 877-895.  
1160  
1161 Rutherford, M.J. 2008. Magma ascent rates. In: Putirka, K.D. and Tepley, F.J., III (eds)  
1162 *Minerals, Inclusions and Volcanic Processes. Mineralogical Society of America and*  
1163 *Geochemical Society Reviews, in Mineralogy and Geochemistry* 69, 241-271  
1164

- Ryan, M. 1994. Neutral-buoyancy controlled magma transport and storage in mid-ocean ridge magma reservoirs and their sheeted-dike complex: A summary of basic relationships. In: Magmatic Systems. Eds: M. P. Ryan, Chap. 6, Academic, San Diego, California.
- Saki, M., Thomas, C., Nippress, S.E.J., Lessing, S. 2015. Topography of upper mantle seismic discontinuities beneath the North Atlantic: the Azores, Canary and Cape Verde plumes. *Earth and Planetary Science Letters* 409, 193-202.
- Satoh, H., Yamaguchi, Y., Makino, K. 2004. Ti-substitution mechanism in plutonic oxy-kaersutite from the Larvik alkaline complex, Oslo rift, Norway. *Mineralogical Magazine*, Vol. 68, 687-697.
- Silva, L.C., Mendes, M.H., Torres, P.C., Palácios, T., Munhá, J. 1997. Petrografia das Formações Vulcânicas da Erupção de 1995 na Ilha do Fogo, Cabo Verde. In: Réffega, A. et al. (eds.). A Erupção Vulcânica de 1995, na Ilha do Fogo, Cabo Verde. IICT, Lisboa, 164-170.
- Staudigel, H., Park, K.H., Pringle, M., Rubenstone, J.L., Smith, W.H.F., Zindler, A., 1991. The longevity of the South-Pacific isotopic and thermal anomaly. *Earth and Planetary Science Letters* 102, 24-44.
- Stracke, A., Hofmann, A.W., Hart, S.R. 2005. FOZO, HIMU, and the rest of the mantle zoo. *Geochemistry, Geophysics, Geosystems* 6, Q05007, doi:10.1029/2004GC000824.
- Stracke, A., Bourdon, B. 2009. The importance of melt extraction for tracing mantle heterogeneity. *Geochimica et Cosmochimica Acta* 73, 218-238.
- Stroncik, N.A., Klügel A., Hansteen, T. H. 2009. The magmatic plumbing system beneath El Hierro (Canary Islands): Constraints from phenocrysts and naturally quenched basaltic glasses in submarine rocks. *Contributions to Mineralogy and Petrology* 157, 593-607.
- Torres, P.C., Madeira, J., Silva, L.C., Brum da Silveira, A., Serralheiro, A., Mota Gomes, A. 1998. Carta Geológica das Erupções Históricas da Ilha do Fogo (Cabo Verde): revisão e actualização. *Comunicações do Instituto Geológico e Mineiro* 84, A193-196.
- Torres, P., Silva, L.C., Munhá, J., Caldeira, R., Mata, J., Tassinari, C. 2010. Petrology and Geochemistry of lavas from Sal Island: Implications for the variability of the Cape Verde magmatism. *Comunicações Geológicas* 97, 35-62.
- Trindade, M.J., Mata, J., Munhá, J. 2003. Petrogenesis of the Quaternary magmatism from the S. Vicente Island (Cape Verde). *Comunicações do Instituto Geológico e Mineiro* 90, 169-188.
- Vervoort, J., Patchett, P., Blichert-Toft, J., Albarède, F. 1999. Relationships between Lu-Hf and Sm-Nd isotopic systems in the global sedimentary system. *Earth and Planetary Science Letters* 168, 79-99.
- Vinnik, L., Silveira, G., Kiselev, S., Farra, V., Weber, M., Stutzmann, E. 2012. Cape Verde hotspot from the upper crust to the top of the lower mantle. *Earth Planetary Science Letters* 319-320, 259-268.
- Wang, K., Plank, T., Walker J.D., Smith, E.I. 2002. A mantle melting profile across the Basin and Range, SW USA. *Journal of Geophysical Research* 107, ECV 5, 1-21.
- Watson, S., McKenzie, D. 1991. Melt generation by plumes: A study of Hawaiian volcanism. *Journal of Petrology* 32, 501-537.
- Weis, D., Kieffer, B., Maerschalk, C., Barling, J., de Jong, J., Williams, G., Hanano, D., Pretorius, W., Mattielli, N., Scoates, J., Goolaerts, A., Friedman, R., Mahoney, J. 2006. High-precision isotopic characterization of USGS reference materials by TIMS and MC-ICP-MS. *Geochemistry, Geophysics, Geosystems* 7, doi:10.1029/2006GC001283.

1223  
1224 White, W.M. 2015. Isotopes, DUPAL, LLSVPs, and Anekantavada. *Chemical Geology* 419,  
1225 10-28.  
1226  
1227 Williams, C., Hill, I., Young, R., White, R.S. 1990. Fracture zones across the Cape Verde Rise,  
1228 NE Atlantic. *Journal of the Geological Society of London* 147, 851-857.  
1229  
1230 Wilson, D., Peirce, C., Watts, A., Grevemeyer, I., Krabbenhoef, A. 2013. Uplift at lithospheric  
1231 swells-I: Seismic and gravity constraints on the crust and uppermost mantle structure of the  
1232 Cape Verde mid-plate swell. *Geophysical Journal International* 182, 531-550.  
1233  
1234  
1235 Wilson, D., Peirce, C., Watts, A., Grevemeyer, I. 2013. Uplift at lithospheric swells-II: is the  
1236 Cape Verde mid-plate swell supported by a lithosphere of varying mechanical strength?  
1237 *Geophysical Journal International* 193, 798-819.  
1238  
1239 Zindler, A., Hart, S.R. 1986. Chemical geodynamics. *Annual Reviews of Earth Planetary*  
1240 *Sciences* 14, 493-571.  
1241  
1242  
1243  
1244  
1245  
1246  
1247  
1248  
1249  
1250  
1251  
1252  
1253  
1254  
1255  
1256  
1257  
1258  
1259  
1260  
1261  
1262  
1263  
1264  
1265  
1266  
1267  
1268  
1269  
1270  
1271  
1272  
1273  
1274  
1275  
1276

1277     **Captions**

1278     **Fig. 1** – Geological map of the identified historical eruptions in Fogo (modified from  
1279     Torres et al., 1998) superimposed on the digital terrain model of the island. The upper  
1280     inset shows the location of the Island of Fogo in the archipelago of Cape Verde. The  
1281     lower insets correspond to the legend of the geological map and to a structural sketch  
1282     showing the geometry and location of the eruptive fissures of the last three eruptions  
1283     (1951, 1995 and 2014/15), the Bordeira wall (continuous line represents the top; dashed  
1284     line represents the base), and the crater rim of Pico do Fogo.

1285

1286     **Fig 2** – Photos of the 2014/15 Fogo eruption: A- general view looking East of Pico do  
1287     Fogo with the active vents at the base of the cone, the flat region of Chã das Caldeiras  
1288     covered with the 1995 and 2014 lava flows and the south-eastern tip of the Bordeira  
1289     wall; the eruptive column rises 3 km above the vents and is dispersed by south-eastward  
1290     wind at an altitude of approximately 5 km (photo taken on November 29, 2014, at 15:44  
1291     UTC); B- the alignment of active vents, viewed from the south, during a low activity  
1292     phase; the new cone is growing against the southeast flank of the 1995 cone (to the left);  
1293     the lava flow is being fed by the southernmost vent; the lava flow at the base of the cone  
1294     presents a lava channel and several skylights with degassing white columns (photo  
1295     taken on December 2, 2014, at 19:35 UTC); C- night aspect of the central crater  
1296     projecting plastic spatter fragments from the explosion of lava bubbles during an  
1297     hawaiian lava lake phase (photo taken on November 28, 2014, at 20:48 UTC); D- aspect  
1298     of vulcanian activity at the northernmost vent producing ash-laden episodic eruptive  
1299     columns with the wind blowing from the north; the white plume marks the position of  
1300     the effusive south vent (photo taken on November 30, 2014, at 19:24 UTC); E- aspect  
1301     of the surface of the active lava flow seen from the northwest presenting strong thermal  
1302     emission and degassing (photo taken on November 29, 2014, at 15:48 UTC); F- the  
1303     village of Portela invaded by the front of the lava flow 3.5 km away from the effusive

vent (photo taken on December 2, 2014, at 14:39 UTC). For more photos see Supplementary Material S1.

**Fig. 3** - Total alkali-silica (TAS) diagram (Le Maître, 2002) for the 2014 magmatic rocks and interstitial glass occurring in the matrix of the lava samples. The thick line is a compositional divider between alkaline and subalkaline volcanic rocks (MacDonald, 1968). The compositional fields of the 1951 and 1995 are also shown for comparison (data from Doucelance et al., 2003; Escrig et al., 2005; Hildner et al., 2011;). U1, U2, U3 and Ph correspond to the field designations of Le Maitre et al. (2002) (U1: Tephrite/Basanite; U2: Pnotephrite; U3: Tephriphonolite; Ph: Phonolite). See the main text (*Section 4.3*) for a details on the systematics.

**Fig. 4** – Petrographic aspects of the lava flow samples showing the presence of clinopyroxene and kaersutite phenocrysts (A and B) in a hypocrySTALLINE matrix with plagioclase, clinopyroxene and Fe-Ti oxides (A, B, C and D). Note the partial (A and B) or total (D) replacement of kaersutite by rhönite (opaque inosilicate of the aenigmatite group) which is marked by an arrow. Backscattered electron images showing a detailed view of the kaersutite rim replacement (E and F).

**Fig. 5** – Trace element characteristics of the 2014 eruptive products compared with those of the 1951 and 1995 eruptions (see Hildner et al., 2012 and Hildner et al., 2011, respectively). Normalizing values of Palme and O’Neil (2003).

**Fig. 6** - Pb isotopic compositions (A:  $^{206}\text{Pb}/^{204}\text{Pb}$  vs.  $^{207}\text{Pb}/^{204}\text{Pb}$ ; B:  $^{206}\text{Pb}/^{204}\text{Pb}$  vs.  $^{208}\text{Pb}/^{204}\text{Pb}$ ). Data sources: Northern Islands (Santo Antão, São Vicente and São Nicolau: Jørgensen and Holm, 2002; Holm et al., 2006; Millet et al., 2008) and Southern Islands (Fogo and Santiago: Doucelance et al., 2003; Barker et al., 2010;



Martins et al., 2010). The 1951 and 1995 eruptions data are from Escrig et al., 2005. The heavy line represents the Northern Hemisphere Reference Line (NHRL) defined by Hart (1984). Also plotted are the compositions of mantle components (see main text for references).

**Fig. 7** – Sr, Nd (A) and Hf (B) isotope compositions. Data sources: the Santiago Island field was defined using data from Barker et al. (2009) and Martins et al. (2010). See caption of Fig. 6 for further references. No Hf isotope data exist for the 1951 and 1995 eruptions.

**Fig 8** - The role of clinopyroxene, olivine, amphibole and apatite fractionation on the liquid lines of descent for the 2014, 1995 and 1951 eruptions. In 8A and 8B fractional crystallization was modelled using the Rayleigh equation. Partition coefficients used in calculations can be found in the Supplementary Material S5-1 and data relative to the fractional crystallization vectors in the S5-2. Circular ticks represent consecutive increments of 5% crystallization. Crystallization vectors corresponds to  $F=0.7$ .

**Fig. 9** – Temperature and pressure conditions for crystallization of clinopyroxene and amphibole from the 2014 tephritic and phonotephritic rocks.

**Fig.10** - Mixing model between depleted mantle (DMM) and recycled oceanic crust (ROC;  $\approx$  HIMU), and between ROC and EM1 and the lower mantle (LM). Values for these end-members are from Doucelance et al. (2003) (lower mantle), Iwamoro (2015) (EM1, DMM) and Mourão et al. (2012a) (ROC). Given that the 2014 Fogo lavas are characterized by a diluted contribution of ROC (see main text), making difficult its constraint, we considered 1.3 Ga as the age of recycling for mixing calculations, as determined by Mourão et al. (2012a) for the neighbouring Brava Island. Additional line

1358 corresponds to a mixture between recycled oceanic crust and lower mantle material in a  
1359 60:40 proportion, with EM1. Circular marks represent 10% increments. See  
1360 Supplementary Material S5-3 for mixing calculations.  
1361

**The 2014-15 eruption and the short-term geochemical evolution of the  
Fogo volcano (Cape Verde): evidence for small-scale mantle  
heterogeneity**

J. Mata<sup>1\*</sup>; S. Martins<sup>1</sup>; N. Mattioli<sup>2</sup>; J. Madeira<sup>1</sup>; B. Faria<sup>3</sup>; R.S. Ramalho<sup>1,4,5</sup>; P.  
Silva<sup>6,1</sup>; M. Moreira<sup>7</sup>; R. Caldeira<sup>8</sup>; M. Moreira<sup>6,1</sup>; J. Rodrigues<sup>9</sup>; L. Martins<sup>1</sup>

- 1- Instituto Dom Luiz, Faculdade de Ciências, Universidade de Lisboa, 1749-016 Lisboa, Portugal.
- 2- Laboratoire G-Time, DGES, Université Libre de Bruxelles, ULB, Av. Roosevelt, 50, CP 160/02, 1050 Brussels, Belgium
- 3- Instituto Nacional de Meteorologia e Geofísica, Mindelo, Cabo Verde
- 4- School of Earth Sciences, University of Bristol, Wills Memorial Building, Queen's Road, Bristol, BS8 1RJ, UK
- 5- Lamont-Doherty Earth Observatory at Columbia University, Comer Geochemistry Building, 61 Route 9W, P. O. Box 1000, Palisades, NY 10964–8000, USA
- 6- Instituto Politécnico de Lisboa, ISEL/ADF, Lisboa, Portugal
- 7- Institute de Physique du Globe de Paris (France)
- 8- Laboratório Nacional de Energia e Geologia, I.P., 2610-999 Amadora, Portugal.
- 9- Geologist, Cabo Verde

\*- Corresponding author: [jmata@fc.ul.p](mailto:jmata@fc.ul.p)

46  
47  
48  
49  
50  
51  
52  
53  
54  
55  
56  
57  
58  
59  
60  
61  
62  
63  
64  
65  
66  
67  
68  
69  
70  
71  
72  
73  
74  
75  
76  
77  
78  
79  
80  
81  
82  
83  
84  
85  
86  
87  
88  
89  
90  
91

|

**Keywords**

2014-15 Fogo Island (Cape Verde) eruption; Ocean island basalts; Mantle heterogeneity; Short-term magmatic variation; Volcano plumbing system

## 1- Introduction

The Earth's mantle is highly heterogeneous as depicted by the composition of oceanic basalts and particularly by those from oceanic islands (e.g. Hofmann, 2003; White, 2015). Such heterogeneity is considered the result of mixing in different proportions of the so-called mantle components (Zindler and Hart, 1986; Stracke et al., 2005). The length scale of mantle heterogeneities sampled by oceanic basalts is highly variable, sometimes encompassing large regional domains (e.g. DUPAL and SOPITA anomalies; Hart, 1984; Staudigel et al., 1991; White, 2015), but being also evident at the scale of a single magmatic province, as reported, for example, for the Azores (e.g. Beier et al., 2008), Cape Verde (Gerlach et al., 1988; Doucelance et al., 2003) and Galápagos (Gibson et al., 2012) archipelagos. The same is true at the scale of a single island edifice (e.g. Barker et al., 2010; Mourão et al., 2012a; Nobre Silva et al., 2013), even when considering quasi-coeval magmatic products (e.g. Madureira et al., 2011).

In this work we evaluate the small-scale heterogeneity of the mantle source feeding a plume-related intraplate volcano, as well as the short-term geochemical evolution of the magmas it generated. To this purpose we use as a case study the island of Fogo (Cape Verde Archipelago), one of the most active oceanic volcanoes in our planet. Indeed, since the mid-15<sup>th</sup> Century Fogo experienced about 27 eruptions mostly from vents located within a ~~restricted~~ restricted area ( $\approx 50 \text{ km}^2$ ) of the ~~edifice's~~ island's summit depression (Fig. 1). The latest eruption occurred in 2014-2015 and constitutes the main object of this study. Their vents are practically coincident ~~(1995)~~ or localized less than 2 km away ~~(1951)~~ from those of the ~~2014-15 eruption~~ two previous eruptions (1995 and 1951, respectively). For this reason, Fogo constitutes a prime locality to test the existence of small-scale heterogeneities of mantle sources, as well as to investigate the recent short-term evolution of magmas issued from those sources. Here we characterize and discuss the geochemistry of the lava flows and pyroclasts extruded during the initial

119 stages of the eruption (up to December 7, 2014). Even though we are only considering  
120 lavas formed during the first 15 out of 60 days of eruption, the extracted information  
121 allows the demonstration of chemical differences relative to the products erupted in  
122 1951 and 1995.

123 The preservation of such heterogeneities by magmas is also here discussed emphasizing  
124 the role of lithosphere thickness. The mineralogical, geochemical and physical  
125 characteristics of a volcano are partially constrained by what happens during magma  
126 transit from its source to the surface, i.e. by the nature and dynamics of the associated  
127 magma plumbing system (e.g. Longpré et al., 2008; Klügel et al., 2015; Cooper, 2017;  
128 Cashman et al., 2017). The Fogo's plumbing system is here assessed using barometric  
129 data, which indicates a location of the main magma chamber(s) into the mantle.

130 Our observations show that magmas erupted in 2014-~~erupted~~ mark a reversal from the  
131 tendency depicted by previous eruptions (Escrig et al., 2005), which exhibited an  
132 increasing contribution of a ~~radiogenic-Sr~~-local end-member with relatively radiogenic  
133 Sr.

## 135 2- Cape Verde Geological Setting

136 The Cape Verde Archipelago (Eastern Central Atlantic; Fig. 1) lies on top of the largest  
137 bathymetric anomaly in the Earth's oceans – the Cape Verde Rise – that coincides with  
138 important geoid, heat flow, gravity, and seismic anomalies (e.g. Dash et al., 1976;  
139 Courtney and White, 1986; Wilson et al., 2013; Liu and Zhao, 2014). The  
140 ~~islands~~archipelago, which stand on 120–140 Ma-old seafloor (Williams et al., 1990)  
141 ~~are~~is regarded as ~~the result of a~~ hotspot-~~volcanism~~ resulting from the impingement of a  
142 mantle plume on the quasi-stationary ( $<1 \text{ cm.a}^{-1}$  in the region; Pollitz, 1991; Holm et al.,  
143 2008) Nubian plate. These would explain the long-lasting volcanic activity and, at least  
144 partially, the age distribution of volcanism and the geometry of both the archipelago and  
145 the Cape Verde Rise (Lodge and Helffrich, 2006; Holm et al., 2008; Madeira et al.,

2008; Ramalho et al. 2010, Ramalho, 2011). The presence of a mantle plume deeply anchored in the lower mantle is ~~also~~ suggested by seismic data (Montelli et al., 2006; Forte et al., 2010; Vinnik et al, 2012; Saki et al., 2015; French and Romanowicz, 2015) and of noble gas studies performed on ~~carbonatitic~~carbonatites and alkaline silicate rocks (Christensen et al., 2001; Doucelance et al., 2003; Mata et al., 2010; Mourão et al., 2012b). The oldest exposed hotspot-related volcanism is ~26 Ma (Torres et al., 2010) and at least three islands are considered volcanically active (Santo Antão, Brava and Fogo; see e.g. Madeira et al., 2010; Eisele et al., 2015; Faria and Fonseca, 2014) but only Fogo had post-settlement eruptions.

Magmatism in Cape Verde is strongly alkaline, as testified by the occurrence of nephelinitic, melanephelinitic, and melilititic rocks on several islands. It also is well known by its striking geochemical heterogeneity, allowing the isotopic separation of the islands into two groups, ~~a~~ (Northern and a-Southern-). Lavas from the Southern group have more radiogenic Sr, but unradiogenic Nd and Pb ratios than those from the Northern group, which are also exhibit more unradiogenic He signatures. In addition, magmatic rocks from the Southern group are positioned, on the  $^{208}\text{Pb}/^{204}\text{Pb}$  vs.  $^{206}\text{Pb}/^{204}\text{Pb}$  diagram, above the Northern Hemisphere Reference Line (NHRL; Hart, 1984) whilst lavas from the Northern group tend to plot along the NHRL (e.g. Gerlach et al., 1988; Doucelance et al., 2003; Holm et al., 2006; Kogarko and Asavin, 2007; Martins et al., 2010; Mourão et al. 2012a and references therein). Notable exceptions to this scenario include Brava (the southwesternmost island), which depicts both typical Northern (older sequences) and Southern (younger volcanism) isotope signatures (Mourão et al., 2012a), and the neighbouring Cadamosto seamount, which also presents typical Northern signatures (Barker et al., 2012).

## 2.1 Fogo Volcano

172 Fogo is one of the youngest of the Cape Verde Islands and a very prominent oceanic  
173 volcano, standing ~7 km above the surrounding seafloor. The island exhibits a slightly  
174 asymmetric conical shape, being truncated atop by a summit depression open to the  
175 east. This 8 km-wide depression - Chã das Caldeiras - is surrounded on three sides by a  
176 almost vertical wall – the Bordeira – up to 1 km tall. Inside the summit depression and  
177 on its eastern side, a 1100 m high strato-volcano – Pico do Fogo – grew up to an  
178 elevation of 2829 m (Fig. 1). Fogo volcano is therefore interpreted as a compound  
179 volcano, featuring a “somma-vesuvio” association of a younger strato-cone on top of an  
180 older, collapsed volcanic edifice (Ribeiro, 1954; ~~Machado and Assunção, 1965~~; Foeken  
181 et al., 2009). The opening to the east of the summit depression is interpreted as the  
182 result of a massive flank collapse (Day et al., 1999; Brum da Silveira et al., 2006), as  
183 attested by a landslide debris deposit extending offshore into the channel between Fogo  
184 and Santiago (e.g. Masson et al., 2008), and by field evidence documenting the impact  
185 of a megatsunami in the neighbouring island of Santiago (Paris et al., 2011; Ramalho et  
186 al., 2015). The present-day Pico do Fogo stands on, and partially fills, the collapse scar,  
187 and naturally post-dates the collapse event, which is interpreted to have occurred either  
188 at ~117 or at ~73 ka (cf. Eisele et al. 2015 and Ramalho et al. 2015). A older basement  
189 is, however, exposed in two shallow valleys near the city of São Filipe, where plutonic  
190 calciocarbonatites were dated from 2.5 Ma to 5.1 Ma (Hoernle et al., 2002; Madeira et  
191 al., 2005; Foeken et al., 2009). These suggest a > 2 Myr volcanic hiatus in the evolution  
192 of Fogo.

193 Fogo volcano is very active, with 27 eruptive events since 1500 AD (Ribeiro, 1954).  
194 The mean recurrence interval between eruptions is 19.8 years, but with individual  
195 intervals ranging from 1 to 94 years. Historical eruptions seem to have been confined to  
196 Chã das Caldeiras and the eastern slope of the volcano, as it was the case of the recent  
197 1951, 1995 and 2014/2015 events (Fig. 1).



The latest eruption started on November 23, 2014 and continued until February 7, 2015. The eruption occurred on a NE-SW trending 700 m-long fissure located on the SE flank of the previous 1995 cinder cone, an adventitious vent developed on the SW flank of Pico do Fogo (Figs. ~~2C~~[2A](#), [2B](#) e 2D). This eruption started with vigorous “hawaiian” fire-fountain activity, followed by strombolian activity, and later by simultaneous or alternating ~~hawaiian~~[Hawaiian \(Fig. 2C\)](#), strombolian and vulcanian [\(Fig. 2D\)](#) eruptive activity from different craters along a fissural vent, lasting for several days. The eruption also emitted, from the first day, thick a’ā lava flows (Fig. 2E; Supplementary Material S1) forming two initial lava lobes. A shorter lobe, 1.7 km-long, progressed southwestwards down to the flank of Cova Tina cone, stalling short of the Bordeira wall in this area. The second, longer lobe advanced 3 km to the northeast in the initial hours of the eruption, crossing the topographic barrier formed by the 1995 lava flows by advancing through the existing road cut. It advanced intermittently towards the village of Portela, causing widespread destruction (Fig. 2F). During the later stages of the eruption, thinner, more fluid, a’ā and especially pahoehoe breakouts expanded the flow field to the west and north, the latter descending to the village of Bangaeira, destroying almost completely both villages and reaching a total length of 5.2 km (Fig.1). Overall, the resulting lava flows, with an average thickness of about 9 m, covered an area of 4.8 km<sup>2</sup>, with extruded volumes estimated to correspond to  $\sim 45 \times 10^6 \text{ m}^3$  ~~(Richter et al. 2016;~~[, at a mean eruption rate of  \$6.8 \text{ m}^3 \cdot \text{s}^{-1}\$  \(Bagnardi et al. 2016; Richter et al. 2016\)](#). Lava flow thicknesses as high as 35 m (close to the vent), or 25 m on the lava ponding west of Portela, were described by Richter et al. (2016). See also Cappello et al. (2016) for additional information about the eruption.

### 3- Analytical procedures

223 Whole-rock major and trace element concentrations were obtained at Activation  
224 Laboratories, Ltd (Ancaster, Ontario, Canada) using the geochemical analytical package  
225 4Lithoresearch (lithium metaborate/tetraborate fusion - ICP and ICP/MS).  
226 Several certified reference materials from USGS (United States Geological Survey),  
227 GSJ (Geological Survey of Japan) and CCRMP (Canadian Certificate Reference  
228 Material Project) were run to check for accuracy (Supplementary Material S2). Errors  
229 associated with the accuracy are  $\leq 4\%$  for major elements and better than 9% for the  
230 REE and the most widely used incompatible elements. Reproducibility was generally  
231 better than 5% for both major and trace elements. ~~Four blanks were also analysed.~~ For  
232 detailed information regarding analytical and control procedures consult the Actlabs  
233 website (www.actlabs.com).  
234 Mineral analyses were performed on carbon-coated polished thin sections using a JEOL  
235 SUPERPROBE™, model JXA-8200, in wavelength dispersive mode at the  
236 Departamento de Geologia da Faculdade de Ciências da Universidade de Lisboa  
237 (Portugal). Minerals were analysed with an acceleration voltage of 15 kV and a current  
238 of 25 nA, using a 5  $\mu\text{m}$  wide beam for most minerals. Plagioclase and apatite were  
239 analysed using a 7 and 9  $\mu\text{m}$  wide beam, respectively. The analyses performed in each  
240 mineral phase/glass were calibrated using the composition of reference material, with  
241 precisions being better than 2% and ordinarily around 1% (see Supplementary Material  
242 S3-H for specific minerals standards used in each mineral analysis).  
243 Isotopic analyses of Pb, Nd, Sr and Hf were performed at the Laboratoire G-Time of the  
244 Université Libre de Bruxelles (ULB, Belgium) on a Nu Plasma I Multi-Collector  
245 Inductively Coupled Plasma Mass Spectrometer (MC-ICP-MS) (@ Nu instruments).  
246 Sr analyses were performed in wet mode. In routine, the raw data was normalized to  
247  $^{86}\text{Sr}/^{88}\text{Sr}=0.1194$ , and corrected for mass bias by standard sample bracketing using the  
248 lab's in-house Sr standard solution. The in-house shelf Sr standard was calibrated and  
249 normalized to the certified value of NBS 987 Sr standard (0.710248) reported by Weis

et al. (2006). During our analytical sessions, in-house standard solution was run every two samples and gave an average value of  $0.710287 \pm 50$  ( $2\sigma$ ) for raw  $^{87}\text{Sr}/^{86}\text{Sr}$  data (21 runs).

Nd and Hf were run in dry mode with an Aridus II desolvating system. To monitor the instrumental mass bias during the analysis sessions, the standard sample bracketing method was also applied. Standards were systematically run between every two samples, giving an average value in  $^{143}\text{Nd}/^{144}\text{Nd}$  of  $0.511921 \pm 41$  ( $2\sigma$ , 8 runs) for the Rennes Nd standard, and  $^{176}\text{Hf}/^{177}\text{Hf}=0.282172 \pm 30$  ( $2\sigma$ , 10 runs) for the JMC 475 Hf standard. The Nd and Hf isotopic measurements were internally normalised to  $^{146}\text{Nd}/^{144}\text{Nd}=0.7219$  and  $^{179}\text{Hf}/^{177}\text{Hf}=0.7325$ , respectively. All Hf and Nd isotopic data (Table 1) are normalized to the reference values of 0.511961 and 0.282160 as published by Chauvel and Blichert-Toft (2001) and Chauvel et al. (2011).

For the Pb isotope analyses, a Tl dopant solution was added for every sample and standard, within a Pb-Tl concentration ratio of  $\pm 5:1$  (for a minimum signal of 100 mV in the axial collector -  $^{204}\text{Pb}$ ).  $^{202}\text{Hg}$  is routinely monitored to correct for the potential isobaric interference of  $^{204}\text{Hg}$  on  $^{204}\text{Pb}$ . Mass discrimination was monitored using  $\ln - \ln$  plots and corrected by the external normalization and the standard sample bracketing technique using the recommended values of Galer and Abouchami (1998) (i.e.  $^{206}\text{Pb}/^{204}\text{Pb}=16.9405\pm 15$ ;  $^{207}\text{Pb}/^{204}\text{Pb}=15.4963\pm 16$ ;  $^{208}\text{Pb}/^{204}\text{Pb}=36.7219\pm 44$ ). The repeated measurements of the NBS981 gave the following values:  $^{206}\text{Pb}/^{204}\text{Pb}=16.9403\pm 8$ ,  $^{207}\text{Pb}/^{204}\text{Pb}=15.4961\pm 10$ ,  $^{208}\text{Pb}/^{204}\text{Pb}=36.7217\pm 31$  ( $2\sigma$ ) for the NBS981 Pb standard (5 runs).

272

#### 273 4- Results

274 The samples used in this study were collected during a field survey undertaken during  
275 the course of the last Fogo eruption, between November 27 and December 7, 2014.  
276 From all collected samples a sub-set of 14 was selected for petrographic, mineralogical

and whole-rock elemental geochemical study (TABLE I), on the basis of its geographical and temporal distribution. Sr, Nd, Hf and Pb isotopes were determined for 8 samples (TABLE II), while the He isotope analysis was performed for one sample. On the Supplementary Material the reader can also find mineral chemistry data (S3) and the whole-rock normative compositions (S4). The composition of interstitial glasses determined by electron microprobe is also presented on Supplementary Material S3-G.

#### 4.1. Petrography and mineral chemistry

On a chemical basis, lava flows and pyroclasts erupted up to December 7 are, sensu lato, tephrites and phonotephrites (see *section* 4.3 and Fig. 3). Some of the most important petrographic characteristics of the studied samples are depicted on Fig. 4 and their mineral chemistry data are displayed on the Supplementary Material S3.

##### 4.1.1 Tephrites

The bulk ( $\approx 85\%$ ) of the eruptive products corresponds to tephrites. The lavas are vesicular and porphyritic with a hypocrySTALLINE groundmass and with phenocrysts amounting up to 10%. Samples are highly vesicular (up to 60% of the rock volume) and the vesicles are irregular in shape and size.

The most abundant phenocryst phase is clinopyroxene. Even though all the clinopyroxene phenocrysts are classified as diopside ( $\text{Wo}_{49}\text{En}_{38}\text{Fs}_{13}$  to  $\text{Wo}_{52}\text{En}_{36}\text{Fs}_{12}$ ) according to IMA recommendations (Supplementary Material S-3A), in most samples two groups must be considered regarding size and composition. One group corresponds to phenocrysts with dimensions up to 2 mm and euhedral shapes. They are characterized by normal zoning patterns, with  $\text{Al}_2\text{O}_3$ , FeO and  $\text{TiO}_2$  increasing and MgO, CaO and Mg# decreasing from core to rim. Opaque mineral inclusions are frequent. The other

Formatted: List Paragraph

Formatted: Font: Not Bold

group of phenocrysts occurs in clusters along with kaersutite, both with dimensions up to 4 mm in length. Clinopyroxene megacrysts in these aggregates usually show complex zoning patterns presenting abnormal compositional variations with increments of  $\text{Al}_2\text{O}_3$ , FeO and  $\text{TiO}_2$  towards the intermediate zone/mantle and then decreasing towards the rim; the opposite occurs with MgO and CaO, suggesting a more complex and multistage crystallization history as compared with the first group. Indeed the increase in MgO/FeO and decrease in  $\text{TiO}_2$  towards the rim is suggestive of a replenishment of the magma chamber where these particular crystals were formed, reflecting an influx of less evolved magmas, thus pointing out to mixing of distinct magma batches. However, both groups of clinopyroxenes show similar  $\text{Al}^{\text{VI}}$  values (0.059 to 0) and Al/Ti ratios indicating that megacrysts are cognate, being genetically related with the host lava and with the clinopyroxene phenocrysts. This assertion is also considered valid for kaersutite megacrysts given the chemical evidence for amphibole fractionation (see 5.1).

These kaersutite crystals are Mg- and Ti-rich (MgO = 12.8 – 13.0 wt.%;  $\text{TiO}_2$  up to 6.07 wt.%), usually occurring in association with apatite and showing reaction rims where clinopyroxene and rhönite crystals are present, sometimes completely replacing the amphibole ~~and forming pseudomorphs~~ (Fig. 4D). Olivine crystals are restricted to inclusions in clinopyroxene phenocrysts, with no signs of resorption, and to the groundmass.

In all lava samples the opaque minerals can be considered microphenocrysts, being characterized by euhedral shapes and dimensions up to 1 mm. Most of the occurring oxides can be considered as titanomagnetites, with ulvöspinel component ( $X_{\text{USP}}$ ) up to 57, ~~but with low and Cr# (ranging from 1.6 to 5.3).~~

The groundmass is made up of small crystals immersed in a glassy matrix. These comprise plagioclase laths (labradorite,  $\text{An}_{56-66}$ ) sometimes with a fluidal arrangement, clinopyroxene elongated crystals ( $\text{Wo}_{49}\text{En}_{37}\text{Fs}_{14}$  to  $\text{Wo}_{53}\text{En}_{32}\text{Fs}_{15}$ ), finely disseminated

331 opaque minerals (titanomagnetites,  $58 < X_{\text{USP}} < 67$ ), rare olivine ( $\text{Fo} \approx 72\%$ ), and  
332 fluorapatite (1.7 to 2.8 wt.% of F). The electron-microprobe analyses of interstitial glass  
333 revealed it to be very rich in alkalis (11.8 to 15.8 wt%,  $\text{K}_2\text{O}+\text{Na}_2\text{O}$ ) and poor in  $\text{MgO}$   
334 (down to 0.66 wt%) having tephriphonolitic and phonolitic ( $\text{SiO}_2$  up to 54.15 wt%)  
335 compositions (see Fig. 3).

336

#### 337 **4.1.2 Phonotephrites**

338 These lavas are vesicular hemicrystalline/hypocrystalline and sparsely porphyritic  
339 (phenocrysts up to 3% vol.). The vesicles are elongated reaching up to 10 mm in length  
340 and corresponding to 50 to 80% of rock volume. The clinopyroxene phenocrysts are  
341 euhedral up to 3 mm in size, frequently showing complex oscillatory zoning patterns  
342 and inclusions of opaque minerals. Despite the striking optical zoning patterns, all the  
343 clinopyroxene phenocrysts are classified as diopside with a short compositional range  
344 ( $\text{Wo}_{49}\text{En}_{35}\text{Fs}_{10}$  to  $\text{Wo}_{53}\text{En}_{40}\text{Fs}_{14}$ ), being very similar to that reported for the tephrites.  
345 Olivine ( $\text{Fo}=80\text{-}84\%$ ) is scarce, being identified only as a core inclusion in a  
346 clinopyroxene phenocryst. Microphenocrysts (up to 1mm) of equant opaque minerals  
347 are classified as titanomagnetites ( $X_{\text{USP}}=44\text{-}46$ ;  $\text{Cr\#}=1.15\text{-}5.4$ ).

348 Kaersutite pseudomorphs are frequent. They consist of aggregates of rhönite and  
349 clinopyroxene elongated crystals, displayed in inward radial arrangements totally or  
350 partially replacing the amphibole. However, in either case, a border of small opaque  
351 minerals encloses the altered/partially altered amphibole crystals. These kaersuites are  
352 similar ( $\text{MgO} = 11.9 - 12.7$  wt.%:  $\text{TiO}_2$  up to 6.04 wt.%) to those occurring as  
353 megacrysts/phenocrysts in tephritic rocks, and the occurrence of apatite within or in  
354 close proximity to the amphibole is frequent.

355 The groundmass is composed of plagioclase microliths (labradorite,  $\text{An}_{54\text{-}66}$ ), elongated  
356 clinopyroxene crystals (average  $\text{Wo}_{53}\text{En}_{31}\text{Fs}_{16}$ ), opaque minerals ( $38 < X_{\text{USP}} < 57$ ;  $\text{Cr\#} =$   
357 0.67-1.49), scarce olivine and glass.

In one sample, a cluster of clinopyroxene, opaque crystals, ~~an opaque mineral~~, and amphibole is interpreted as a possible co-magmatic cumulate nodule. This interpretation is based on the large dimension of the crystals, the sharp contrast between the mineral aggregate and the surrounding rock matrix, and on its chemical similarity between its minerals and the rock phenocrysts. The same interpretation is considered for an aggregate of small (0.5 mm in length) plagioclase crystals characterized by anorthite content up to 79 %. Ultramafic nodules of cumulate origin, mainly composed of olivine, clinopyroxene, and amphibole, were also reported for this eruption by Caldeira et al. (2015).

#### 4.2. Whole rock elemental composition

Major and trace element analyses of the studied rocks are presented in Table I, while normative compositions can be found in Supplementary Material S4.

As all other subaerial lavas in the Cape Verde Islands, Fogo's 2014 volcanic products are alkaline. They plot dominantly in the  $U_1$  field, but also in the  $U_2$  (phonotephrites) field of the TAS diagram (Fig. 3). Rocks plotting inside the  $U_1$  field would be classified, according their CIPW normative composition, either as nephelinites (normative  $ne > 20\%$ ) – the dominant type – or as melanephelinites (normative  $ne < 20\%$ , ~~but~~ normative  $ab < 5\%$ ) according to the subdivision proposed by Le Bas ( 1989); (see ~~S-4~~ S4). However, as modal plagioclase can be identified in most of the rocks plotting in the  $U_1$  TAS field and for all the samples normative  $ol < 10\%$ , the classification as tephrites is here preferred and used.

The rocks are representative of moderately evolved magmas characterized by Mg# ranging from 55.32 ~~and to~~ 45.98 and by  $Na_2O/K_2O$  between 1.35 and 1.46. The less evolved rocks (Mg# = 55.32 to 51.97) have  $TiO_2$  contents varying from 3.65 to 3.75

385 wt%,  $P_2O_5$  close to 1 (0.94 to 1.11 wt%),  $CaO/Al_2O_3$  ratios ranging from 0.65 to 0.78  
386 and  $K_2O/TiO_2$  ratios from 0.25 to 0.32.

387 The 2014 lavas are highly enriched in the most incompatible elements (Fig. 5), which is  
388 depicted, for example, by  $(La/Yb)_{cn}$  ratios  $> 20$ , with the most evolved rocks presenting  
389 the highest values for this ratio ( $> 23$ ). Primitive mantle normalized incompatible  
390 elements patterns (Fig. 5c) show a significant enrichment of Nb and Ta relatively to the  
391 light REE and the radiogenic heat producers K, Th and U. Small Hf negative anomalies  
392 are also evident, which partially reflects the high Zr/Hf ratios ( $>49$ ), well above the  
393 value of 36 characterizing CI chondrites and the primitive mantle (e.g. Palme and  
394 O'Neil, 2003).

395 The sampled pyroclasts and lava flows are similar in composition, the most significant  
396 difference being the sulphur-enriched composition of pyroclasts (120 to 230 ppm;  
397  $\bar{X} = 200$  ppm) as compared to lava flows (60 to 120 ppm;  $\bar{X} = 84$  ppm). This  
398 indicates a more effective degassing of lava flows as a consequence of a slower cooling.

399 ~~Concerning elemental compositions, most~~Most of the characteristics described above  
400 are similar to those of lavas erupted during the two precedent eruptions (1995 and  
401 1951), as Fig. 5 shows. Notwithstanding the fact that the samples here studied are only  
402 representative of the lava emitted during the first 15 days of the eruption, some  
403 differences, however, were noticed: i) the 1995 lavas present a slightly higher  
404 compositional range (MgO from 6.86 to 2.40 wt%; Hildner et al., 2011) than the ones  
405 from 2014 (MgO from 6.23 to 2.93 wt%); ii) from the three eruptions considered, the  
406 1951 event produced the less evolved lavas (MgO up to 8.24 wt%; Hildner et al., 2012);  
407 iii) for the same  $SiO_2$  content, the 1951 lavas tend to be less alkali-rich than the 2014  
408 and 1995 volcanics (Fig. 3); ~~iv~~iv) the 2014 and 1995 erupted materials are  
409 characterized by small compositional gaps ( $\Delta SiO_2 = 2.5\%$  and  $3.8\%$ , respectively) in  
410 opposition to the described for from the 1951 eruption for which no phonotephrite  
411 compositions were reported (see Fig. 1 and references therein); v) for these three



eruptions, the most evolved products are the phonotephrites from the 1995 eruption, which also present the highest concentrations in incompatible elements like Nb and Ta. However, the highest concentrations in light REE are found in phonotephrites from the 2014 eruption, which show the highest La/Nb ratios. This ~~is~~higher La/Nb are also observed for the less evolved rocks ( $\text{MgO} > 5 \text{ wt\%}$ ), with 2014 lavas presenting  $\bar{X} \text{ La/Nb} = 0.69$ , whereas the 1995 and 1951 less evolved rocks show  $\bar{X} \text{ La/Nb} = 0.60$  (cf. Table 1, Hildner et al., 2011 and Hildner et al., 2012).

### 4.3. Whole rock isotope composition

The results of Sr, Nd, Hf and Pb isotope analyses are shown on Table II. The lavas erupted in 2014 at Fogo Island present isotope signatures akin to those typical of the Southern islands in the Cape Verde Archipelago. Indeed, in opposition to what is observed for the Northern capeverdean islands (Fig.6), they are characterized by relatively unradiogenic  $^{206}\text{Pb}/^{204}\text{Pb}$  ratios (up to 19.001) and plot above the Northern Hemisphere Reference Line ( $\Delta 7/4$  from 0.99 to 1.57;  $\Delta 8/4$  from 25.38 to 28.80; see Hart, 1984 for definitions of these parameters). Notwithstanding the fact that their  $^{87}\text{Sr}/^{86}\text{Sr}$  (0.70361 to 0.70369) and  $^{143}\text{Nd}/^{144}\text{Nd}$  (0.51276 to 0.51279) ratios are clearly more and less radiogenic, respectively, than those observed for the Northern islands, the 2014 lavas plot on the second quadrant of the  $^{87}\text{Sr}/^{86}\text{Sr}$  vs.  $^{143}\text{Nd}/^{144}\text{Nd}$  diagram (Fig. 7A). This indicates a provenance from a time-integrated depleted source(s), i.e. ~~which evolved over time with lower Rb/Sr and higher Nd/Sm than those of the CHUR (chondritic uniform reservoir).~~ which evolved over time with lower Rb/Sr and higher Nd/Sm than those of the BSE (bulk silicate earth) and the CHUR (chondritic uniform reservoir), respectively. Compared to the lavas extruded during the 1951 and 1995 eruptions, the 2014 rocks present more unradiogenic Sr and radiogenic Nd signatures (Fig. 7). The 2014 lavas also exhibit slightly more radiogenic  $^{206}\text{Pb}/^{204}\text{Pb}$  ratios than the most samples from the

two previous eruptions, the same being true for  $^{207}\text{Pb}/^{204}\text{Pb}$  ratios (Fig. 6A). Lavas from these 3 eruptions are amongst the Cape Verde rocks with lower  $^{206}\text{Pb}/^{204}\text{Pb}$  ratios. As is typical of the Southern Cape Verde Islands, rocks from these 3 eruptions are characterized by positive  $\Delta 8/4$ , plotting above the NHRL (Fig. 6B).

The 2014 lavas'  $^{176}\text{Hf}/^{177}\text{Hf}$  ratios range from 0.28294 to 0.28296 (Table II). A time-integrated evolution with high Lu/Hf ratios compared to CHUR is shown by positive  $\epsilon\text{Hf}$  values (5.88 to 6.62; Fig. 7B), plotting between the mantle arrays proposed by Vervoort (1999) and Chauvel (2008). These are the first  $^{176}\text{Hf}/^{177}\text{Hf}$  determinations available for Fogo Island, preventing any comparison with previous results. However, noteworthy that the lavas erupted in 2014 plot inside the large field defined in the  $\epsilon\text{Nd}$ - $\epsilon\text{Hf}$  space by the lavas from the neighbouring island of Santiago, which is characterized by significantly higher and lower  $^{176}\text{Hf}/^{177}\text{Hf}$  ratios (see Barker et al., 2009; Martins et al., 2010). Significant correlations between any of these isotope signatures and ratios involving incompatible trace elements have not been found. This will be discussed later (see 5.3).

The  $^3\text{He}/^4\text{He}$  ratio of a glassy phonotephrite was determined at the Institut de Physique du Globe de Paris (IPGP) using crushing for gas extraction. The obtained value ( $1.11 \pm 0.13 \text{ Ra}$ , where Ra is the present atmospheric ratio of  $1.4 \times 10^{-6}$ ) for a  $^4\text{He}$  concentration of  $2.8 \times 10^{-9} \text{ cc/g}$  is interpreted as the result of atmospheric contamination during the eruption/consolidation of lava. Consequently, this result will not be considered in the discussion.

~~Compared to the lavas extruded during the 1951 and 1995 eruptions, the 2014 rocks present more unradiogenic Sr and radiogenic Nd signatures (Fig. 7). The 2014 lavas also exhibit slightly more radiogenic  $^{206}\text{Pb}/^{204}\text{Pb}$  ratios than the most samples from the two previous eruptions, the same being true for  $^{207}\text{Pb}/^{204}\text{Pb}$  ratios (Fig. 6A). Lavas from these 3 eruptions are amongst the Cape Verde rocks with lower  $^{206}\text{Pb}/^{204}\text{Pb}$  ratios. As is~~

~~typical of the Southern Cape Verde Islands, rocks from these 3 eruptions are characterized by positive  $\Delta 8/4$ , plotting above the NHRL (Fig. 6B).~~

## 5. Discussion

### 5.1 Magma Mantle source composition and magma evolution

Previous studies, explained the chemical variability of Fogo's lavas by mixing in different proportions of HIMU-like (ancient recycled ocean crust) and EM1-like mantle end-members, diluted by the presence of depleted upper mantle (Gerlach et al., 1988) or by lower mantle material (Doucelance et al., 2003; Escrig et al., 2005) entrained by the upward moving plume.

Although 2014 lavas present low  $^{206}\text{Pb}/^{204}\text{Pb}$  ratios (up to 19.001), clearly below those typical of magmas originated from sources dominated by the HIMU mantle component (e.g. Kawabata et al., 2011), the HIMU fingerprint is shown by trace element patterns (Fig. 5) displaying enrichment in Nb and Ta relative to the LREE and the LILE (e.g. Niu et al., 2012). Additionally, all the analysed rocks are characterized by positive  $\Delta 8/4$  and  $\Delta 7/4$  and plot below the mixing lines between a HIMU type end-member and DMM or lower mantle compositions (Fig. 10), strongly suggesting the contribution of an EM1-type end-member to the 2014 Fogo mantle source(s). Interestingly, the products erupted in 2014 mark a change on the evolutionary trend reported by previous authors for Fogo eruptions (Gerlach et al., 1988; Escrig et al., 2005) which was characterized by an increasing contribution of the enriched component. Indeed, the 2014 lavas have less radiogenic Sr, but more radiogenic Nd signatures than those from the 1951 and 1995 eruptions.

Fogo's 2014 lavas ( $\text{MgO} \leq 6.4$  wt %,  $\text{Mg\#} \leq 53.2$ ;  $\text{Ni} \leq 42$  ppm) cannot be considered representative of primary magmas. This fact and its chemical variability ( $\text{MgO}$  down to 2.93 wt.%;  $\text{Ni}$  down to 6 ppm) emphasize the role of magma evolution processes to explain the observed compositional range. This is reinforced by the phonolitic

Formatted: English (United States)

Formatted: English (United States)

composition of the glassy groundmass of some lavas (MgO down to 0.66 wt%; total alkalis up to 15.76 wt%; see Supplementary Material S3-G).

The important role of clinopyroxene fractionation is suggested by its occurrence as phenocryst in most samples and by the Sc decrease with increasing concentration of strongly incompatible trace elements such as La (Fig 8A), here used as a proxy of magma evolution index. Fractionation of clinopyroxene must have been preceded by crystallization of olivine as indicated by the occurrence of olivine inclusions in clinopyroxene phenocrysts.

~~However, the smooth decrease of Ni during magma evolution (not shown), indicates that olivine role must have been restricted to previous stages of fractionation for which there were no magmas erupted.~~

~~With continuing magma evolution~~The Dy/Dy<sup>\*,\*</sup> ratio, as defined by Davidson et al. (2013), tends to decrease from up to 0.81 in tephrites, down to 0.61 in phonotephrites, a tendency that, according to those authors, can be attributed either to amphibole or to clinopyroxene fractionation. If the importance of clinopyroxene fractionation was already demonstrated, the positive correlation of Dy/Dy<sup>\*</sup> and Nb/U ratios (Fig. 8B) emphasizes the role of amphibole since, at odds with what happens with this mineral, clinopyroxene does not have the capacity to fractionate Nb from U (e.g. Adam and Green, 2006; ~~see also <https://earthref.org/KDD/>~~).

The calculated water content of the melt during kaersutite crystallization range from 3.81 to 4.14 wt% (± 0.78 wt%) while oxygen fugacity is estimated in the range of 0.92 to 2.3 log units above NNO (± 0.37 log units) using the methodology of Ridolfi and Renzulli (2012). The obtained fO<sub>2</sub> values are comparable to those reported for some other intraplate ocean islands (e.g. [Madeira; Mata and Munhá, 2004](#)). These relatively high fO<sub>2</sub> values are reflected in the composition of pyroxenes for which high Fe<sup>3+</sup> contents were calculates based on the stoichiometry (Supplementary material S3-A), but not in the amphibole (Supplementary material S3-C). This suggests the incorporation of Ti (TiO<sub>2</sub> up to 6.13 wt%) into the octahedral position of kaersutite through the

substitution  $^{[VI]}R^{2+} + 2OH^- = ^{[VI]}Ti^{4+} + 2O^{2-}$ , which favours high  $Fe^{2+}/Fe^{3+}$  (Satoh et al., 2004).

As also reported for the previous Fogo's eruption (e.g. Munhá et al., 1997; Hildner et al., 2012) plagioclase did not play a significant role in the evolution of 2014 magmas, as inferred from its rarity among phenocrysts and from the continuous Sr increase (1194 to 1408 ppm) throughout the erupted suite. ~~However, judging~~ Judging from the comparatively ~~low CaO~~ high  $Al_2O_3$ ,  $Na_2O$  and  $Al_2O_3/K_2O$  concentrations determined in the glassy phonolitic matrix, plagioclase and alkali feldspar fractionation ~~must have been~~ was also not important for the generation of such evolved compositions. On the other hand, the role of Fe-Ti oxides and apatite fractionation is made evident by the significant decrease on  $P_2O_5$  (Fig. 8C) and  $TiO_2$  (not shown) concentrations from the most evolved tephrites ( $SiO_2 < 45.2\%$ ) to phonotephrites ( $SiO_2 > 47.7$  wt. %) (see also

Table I), ~~which form two groups separated by a compositional gap ( $\Delta SiO_2 = 2.5\%$ ).~~ The ~~generation of this gap is beyond the scope of this paper. However, we note that the gap is immediately preceded by the inflexion on the liquid line of descent of  $P_2O_5$  (Fig. 8C) and  $TiO_2$  (not shown). Considering this, we interpret that small gap as the result of crystal fractionation of these two non-silicate phases (Fe-Ti oxides, apatite), with the consequent significant increase in silica content of magmatic liquids. Similar, but more important gap ( $\Delta SiO_2 = 3.8\%$ ) characterize the 1995 lavas (see Hildner et al., 2011), but not the rocks from the 1951 eruption, was probably the cause for which no phonotephrite compositions were reported (see Fig. 1 and Fig. 8C and references therein).~~ the small compositional gap ( $\Delta SiO_2 = 2.5\%$ ) separating those two lithotypes.

Even though the isotope differences precludes the studied rocks to be considered ~~eo-~~ magmatic ~~comagmatic~~ with those erupted in 1951 and 1995 (see section 4.4), samples from these three eruptions plot along the same trends in most variation diagrams, suggesting that they share a common magma evolution history (e.g. Fig. 8 A and C).

However, Fig. 8B emphasizes, despite similar trends, the lower Nb/U and Dy/Dy\*

Formatted: Font color: Text 1

Formatted: Font color: Text 1

ratios of the 2014 rocks relatively to the rocks of similar degree of evolution generated during the two previous eruptions. ~~Despite these differences, even for these ratios, they exhibit the same trends with magma evolution.~~

~~The Nb/U of~~Indeed, the less evolved 2014 lavas ~~ranges between 48 and 65, with tephrites being rocks are~~ characterized by lower Nb/U ratios of  $(60 \pm 3)$  ~~( $60 \pm 3$ )~~ than the basanitic/tephritic lavas from the 1995 and 1951 ~~lavas have Nb/U ratios ranging from 70 to 100~~ eruptions ( $95 \pm 4$  ~~for basanites/tephrites~~). Considering such significant differences ~~between lavas with~~; Hildner et al., 2011; 2012). Given the similar ~~degrees~~degree of evolution, ~~primary/primitive~~ magmas of the 2014 lavas had to these differences cannot be explained by fractional crystallization. The 2014 Nb/U ratios fits the typical OIB value (EM lavas excluded) of  $52 \pm 15$  obtained by Hofmann (2003).

~~distinct from those erupted in~~ As shown by this author, either the EM-type mantle components or the continental crust have significantly lower Nb/U ratios. Consequently the higher contribution of an enriched end-member (EM type) for the 1995 and 1951 (see 5.2 above) lavas cannot be invoked as a cause for a discussion). their higher Nb/U ratios.

Nb/U ratios significantly higher than the typical OIB lavas have also been reported for some Canary lavas by Lundstrom et al. (2003). These authors defended that this can be the reflex of mixing between ascending plume-derived magmas and lithospheric melts with a significant contribution from amphibole present in low-solidus mantle domains. These domains would have been generated by metasomatic (s.l.) processes during previous stages of islands building. We suggest that a similar process may have been responsible for the significantly higher Nb/U and Dy/Dy\* ratios of the 1995 and 1951 lavas. Since their vents, and probably also the ascending magma paths, were almost coincident with those of 2014, we speculate that such low-solidus lithospheric domains were already exhausted and did not contribute significantly for the composition of the subsequent 2014 eruption products.

As observed for the precedent 1995 eruption (Munhá et al., 1997; Silva et al., 1997; Hildner et al., 2011), the initial products erupted in 2014 were more evolved (phonotephrites; SiO<sub>2</sub> up to 47.99 wt.%) than those emitted subsequently (tephrites, s.l.), for which SiO<sub>2</sub> contents as low as 43.03 wt.% were obtained. Considering the composition of the erupted magmas, assuming a complete degassing during eruption (suggested by very low loss on ignition), and using the algorithm of Giordano et al. (2008), the viscosity of the phonotephrites would have been some 10 times higher than that of the less evolved tephrites. This partially explains the evolution of lava flow morphology during the course of the eruption, which exhibited *a'a* characteristics during the initial eruptive stages, whilst *pāhoehoe* type lavas became more frequent during the subsequent effusion of the less viscous tephritic lava flows.

Formatted: Pattern: Clear (White)

Formatted: Font: Not Bold, Font color: Text 1, Pattern: Clear (White)

#### **5.1.12 Thermobarometric evidence for magma reservoirs into the mantle**

~~Phenocrysts and cognate megacrysts are considered to grow slowly as a consequence of low magmatic cooling rates. This indicates stagnant or quasi-stagnant conditions at some stage during the process of magma transfer from the mantle source(s) to the surface, such as those characterizing magma stalling/stagnation at mantle/crustal chambers.~~ Geothermobarometric estimates based on ~~such type of crystals can thus phenocrysts and cognate megacrysts have been considered to~~ be important to constrain the magmatic plumbing system of a volcano, ~~given they can be used to calculate the depths of magma stalling/stagnation at mantle/crustal chambers.~~ Indeed, silicates are characterized by very ~~slow~~low intra-crystalline diffusion rates, thus tending to preserve the composition acquired at the moment of crystallization.

We used the clinopyroxene-liquid thermobarometer of Putirka et al. (2003) for which lower uncertainties are foreseen than those reported for methods only using the clinopyroxene composition (Putirka, 2008); ~~see also Geiger et al., 2016 for a review on clinopyroxene thermobarometry).~~ The method is based on jadeite–

600 diopside/hedenbergite exchange equilibria in hydrous conditions, which are shown to  
 601 have existed at Fogo by the presence of amphibole (see also ~~below~~<sup>above</sup> for an estimate  
 602 of water content in magma). As we used phenocryst cores and whole rock compositions  
 603 as proxies of the crystal-liquid pairs, the P-T results obtained will be regarded as the  
 604 conditions prevailing during early stages of clinopyroxene phenocrysts crystallization,  
 605 assuming that no magma mixing occurred after pyroxene crystallization.  
 606 In order to use mineral/liquid thermobarometers it is mandatory to test if the  
 607 crystal/melt pairs used testify equilibrium conditions. On a first approach a visual  
 608 screening was made to identify textural evidence for disequilibrium, those showing  
 609 irregular or reabsorbed shapes were avoided. Furthermore, only core analyses of un-  
 610 zoned or normally zoned phenocrysts were used. No mineral correction was made to  
 611 the whole-rock composition due to the lack of evidence for significant accumulation ( $\leq$   
 612 10 % of phenocryst ~~phase~~<sup>phases</sup>).  
 613 Considering the concerns regarding the efficacy of the Fe-Mg exchange in deciphering  
 614 situations of pyroxene-melt equilibrium (e.g. Mollo et al., 2013), we used instead the  
 615 comparison between predicted and measured components in clinopyroxene (diopside-  
 616 hedenbergite; enstatite-ferrosilite; Ca-Tschermak's) as proposed by Putirka (1999).  
 617 Following the recommendations of Putirka et al. (2003), only clinopyroxenes whose  
 618 compositions are within the  $\pm 2\sigma$  level of the predicted ones were used in the  
 619 thermobarometric calculations. The standard errors of estimation (SEE) of the Putirka et  
 620 al. (2003) method are 1.7 kbar and 33 °C, while analytical uncertainties, calculated  
 621 using the relative standard deviation of whole rock and microprobe analyses of  
 622 reference materials are significantly lower than the uncertainties of the method.  
 623 The temperatures obtained for pyroxene crystallization range from 1045 to 1063 °C for  
 624 the phonotephrites and 1102 to 1143 °C for the tephrites. ~~Concerning pressure~~  
 625 estimates, Pyroxene phenocrysts crystallized from phonotephritic magmas at pressures



in the phonotephrites are characterized by a range between 560 and 778 MPa, whereas the tephrites yield variations between 690 and 890 MPa (Fig. 9).

~~The calculated pressures can be converted to depth estimates considering a height of 5800 m for the Fogo island edifice (~ 3000 m below present sea level), an average density of  $2400 \text{ kg m}^{-3}$  (Dash et al., 1976) for the island edifice, a crustal density of  $2800 \text{ kg m}^{-3}$  inferred from seismic receiver functions (Lodge and Helffrich, 2006), a mantle density of about  $3200 \text{ kg m}^{-3}$  at the Fogo region (Pim et al., 2008), and a Moho depth at 12 km below sea level (Pim et al., 2008). Taking into account these values and the referred uncertainties, the crystallization depth of clinopyroxene phenocrysts ranges approximately from 14.8 to 36.4 km below Fogo's summit, or 12 to 33.6 km below sea level.~~

For amphiboles we used the single-phase thermobarometric and chemometric equations proposed by Ridolfi and Renzulli (2012), based on multivariate least-squares regression analyses of a large database of amphibole compositions in alkaline magma systems. For this method the authors claim low uncertainties:  $P \pm 11.5\%$ ,  $T \pm 23.5^\circ\text{C}$ ,  ~~$\text{ANNO} \pm 0.37$  log units and  $\text{H}_2\text{O}_{\text{melt}} \pm 0.78 \text{ wt}\%$ .~~ The application of the thermobarometer shows that the values obtained for kaersutites occurring in phonotephrites and tephrites are similar within error (1032 to 1050°C and 568 to 620 MPa; see Fig. 9), ~~which, considering the method uncertainties, would correspond to depths ranging from ~16 to 21.8 km below sea level. The calculated melt water content during kaersutite crystallization is very similar for both lithotypes, ranging from 3.81 to 4.14 wt%. Oxygen fugacity estimates show a range of 0.92 to 2.3 log units above NNO. The obtained  $f\text{O}_2$  values are comparable to those reported for some andesitic lavas in convergent tectonic settings (e.g. Chiaradia et al., 2011), but also for other intraplate ocean islands (e.g. 9). Madeira, Mata and Munhá, 2004).~~ These relatively high  $f\text{O}_2$  values may have resulted from the  ~~$\text{H}_2\text{O}$ -rich composition of magmas (see above), which allowed the crystallization of amphibole. Indeed, the liberation of free oxygen and the consequent increase of magma~~

~~fO<sub>2</sub> are thought to be a consequence of amphibole crystallization (Frost and Lindsley, 1991; Chiaradia et al., 2011).~~

The kaersutite occurring in the 2014 Fogo lavas show ubiquitous signs for disequilibrium, presenting evidence for partial (reaction rims) to total (pseudomorphosis) substitution by polycrystalline aggregates of rhönite and clinopyroxene. We interpret the occurrence of rhönite and of the associated clinopyroxene as a consequence of the kaersutite destabilization resulting from magma degassing upon ascent, given the decrease of H<sub>2</sub>O solubility in magmas as pressure drops (e.g. De Angelis et al., 2015). The destabilization of amphibole most probably occurs at pressures below 100-150 MPa (e.g., Rutherford, 2008) with reaction rims developing, for hornblende compositions, at pressures from circa 100 MPa down to 40 MPa (Browne and Gardener, 2006).

Amphibole reaction rims are often used to estimate magma ascent rate since their thickness, size and the shape of the replacing mineral phases are all dependent on it (Chiaradia et al., 2011; Browne and Gardner, 2006). Since the reaction rims observed in kaersutite crystals from the 2014 lavas are thick (> 500 microns) and complete pseudomorphosis of mm-sized crystals (up to 4mm) is common, it is valid to assume on a qualitative basis and based on Browne and Gardener's (2006) experimental data that the time of exposure of kaersutite to low P<sub>H<sub>2</sub>O</sub> before quenching at the surface was

relatively long ~~(several months).~~ (> 1 month). Thus, the occurrence of rhönite and the degree of kaersutite replacement by rhönite suggest a late and short stagnation/stalling at crustal levels (i.e. at pressures below 100 MPa; < 4.3 km below the island summit or < 1.5 km below sea level) after a longer storage at deeper magma chambers.

~~The pressure constraints emerging from this study, based on phenocrysts occurring in relatively evolved magmas (Ni < 42 ppm), indicate that magma evolution processes involving clinopyroxene and amphibole fractionation occurred approximately at depths of 14.8 to 36.4 km below the island's summit, or ~12 to ~33.6 km below sea level.~~

680 ~~Considering a sub-Fogo Moho depth of 12 km below sea level (Pim et al., 2008), these~~  
681 ~~data indicates that magmas stagnated and evolved at mantle depths. On the other hand,~~  
682 ~~this depths range suggests that Fogo is underlain by a complex plumbing system~~  
683 ~~characterized by several magma chambers at distinct depths where clinopyroxene and~~  
684 ~~kaersutite crystallized.~~

685 ~~Additionally, the occurrence of rhönite and the degree of kaersutite replacement by~~  
686 ~~rhönite suggest a later (shorter and less significant) stagnation/stalling at crustal levels~~  
687 ~~(i.e. at pressures below 100 MPa; < 4.3 km below the island summit or < 1.5 km below~~  
688 ~~sea level). Even considering the uncertainties associated to the barometric data, it can be~~  
689 ~~concluded that the magma chambers where the major magma fractionation events~~  
690 ~~occurred were located in the mantle.~~

691 ~~The scenario here proposed for the ascent of the 2014 Fogo magmas is in agreement~~  
692 ~~with seismic data. In order to convert the calculated pressures to depths several~~  
693 ~~assumptions has to be done, the depth of Moho being the one with more impact in the~~  
694 ~~obtained results.~~

695 ~~Vinnik et al. (2012), proposed that at the Cape Verde archipelago the crust would be~~  
696 ~~significantly thicker than the normal oceanic crust, extending down to 20-30 km depth.~~  
697 ~~This was not supported by a later study (Wilson et al., 2013), which placed the Moho at~~  
698 ~~significantly shallower depths, in agreement with the models of Lodge and Helffrich~~  
699 ~~(2006), Pim et al. (2008) and Wilson et al. (2010). In this study we adopt 13.5 km as the~~  
700 ~~depth of Moho beneath the Fogo Island (see Wilson et al., 2010; 2013).~~

701 ~~Considering a height of 5800 m for the Fogo island edifice ( $\approx 3000$  m below present sea~~  
702 ~~level), an average density of  $2400 \text{ kg.m}^{-3}$  (Dash et al., 1976) for the island edifice, a~~  
703 ~~crustal density of  $2800 \text{ kg.m}^{-3}$  inferred from seismic receiver functions (Lodge and~~  
704 ~~Helffrich, 2006), a mantle density of about  $3200 \text{ kg.m}^{-3}$  at the Fogo region (Pim et al.,~~  
705 ~~2008), a Moho depth at 13.5 km below sea level (Wilson et al., 2010; 2013) and taking~~  
706 ~~into account the uncertainties of the barometric methods (see above) the crystallization~~

depth of clinopyroxene phenocrysts ranges approximately ( $\pm 5.5$  km) from 17.8 to 28.4 km below Fogo's summit, or 15.0 to 25.6 km below sea level. For amphiboles the same presupposes allow considering their crystallization at depths between 18.2 and 19.9 km ( $\pm 3$  km) below Fogo's summit, or 15.4 to 20.1 km below sea level. Considering the most common estimates for the crustal thickness at the Cape Verde region ( $\approx 12$  to 13.5 km; Lodge and Helffrich, 2006; Pim et al., 2008; Wilson et al., 2010; 2013) the obtained results suggest that the major fractionation events occurred in magma chambers located into the mantle.

~~Indeed, a seismic event on October 4, 2014 (i.e. 50 days before the eruption) with a hypocentre 17 km below sea level (19.8 km below the Fogo summit), was interpreted by Instituto Nacional de Meteorologia e Geofisica (INMG, Cabo Verde) as resulting from the rupture of the roof of a mantle reservoir allowing magma transfer to shallower levels. Also, geodetic modelling of Sentinel TOPS interferometry by Gonzalez et al. (2015) revealed the lack of deformation at the island scale during and pre-eruption times, further suggesting the deep location of the main magma reservoirs.~~

Geobarometric studies of the previous two eruptions also revealed pre-eruptive magma storage at shallow mantle depths, followed by a short-period of magma stalling at crustal levels (Munhá et al., 1997; Hildner et al., 2011, 2012). The depths of clinopyroxene equilibration obtained in this study for the 2014 eruption (890 to 560 MPa; see above), although partially overlapping those presented for the historical eruptions by Hildner et al. (2011, 2012) (680 to 460 MPa), extends to higher pressures. However it must be noted that the pressure estimates by those authors refer to the final crystallization level, while our data represents ~~the~~ the first crystallization stages of clinopyroxene phenocrysts.

The causes for the development of magma reservoirs within the mantle are still not understood. Changes in buoyancy have been considered as an explanation for magma stagnation during ascent (e.g. Ryan, 1994). However, Jagoutz (2014) emphasized that,

~~at continental arcs, melts ascending magmas can stagnate even when they~~ are less dense  
than the surrounding rocks ~~and that its emplacement is not controlled by the existence~~  
~~of a neutral buoyancy level~~. A similar point of view was defended by Menand (2008)  
who considered that buoyancy is unlikely to be a major control in the emplacement of  
sills, which can be viewed as precursors of magma reservoirs (Gudmundsson, 2012).  
Moreover, as shown by Putirka (2017), hydrated magmas with MgO contents similar to  
those erupted in the 2014 Fogo eruption are less dense than the mantle, or even than the  
lower crustal rocks, indicating that buoyancy cannot be the explanation for the  
stagnation of Fogo magmas in the mantle. As proposed by Menand (2008), the presence  
of ~~rheology~~rheological anisotropies could be the primary factor determining the depth  
of magma stalling or stagnation. This can lead to the inference that the thickness of the  
elastic lithosphere exerts a major control on the depth of magma reservoirs. However,  
for the Cape Verde Archipelago the elastic thickness is estimated at 30 km (Pim et al.,  
2008) and our barometric data suggest magma emplacement at shallower depths,  
invalidating, in this case, such a proposal. Regional flexural stresses produced by the  
volcanic edifice loading are also thought to strongly influence the plumbing systems by  
generating a vertical contrast between tensile and compressive stress zones, capable of  
influencing the depth of magma stalling (see Putirka, 1997 and references therein). We  
do not have data to evaluate this hypothesis.

Whatever the cause for the development of mantle magma reservoirs, they seem to be  
common on ocean islands during periods of low magma supply rates (e.g. Longpré et  
al., 2008; Stroncik et al., 2009; Klügel et al., 2015) as was the case during the latest (this  
study) and the previous eruptions of Fogo volcano (Munhá et al., 1997; Hildner et al.,  
2011; 2012).

## **5.2 Mantle source**

~~In agreement with the location of Fogo Island, all its lavas and, particularly, the~~  
~~products erupted in 2014, are chemically akin to those characterizing the Southern~~  
~~Islands of the Cape Verde Archipelago. This is true for all the isotope systems used, as~~  
~~shown above (Fig. 6 and 7). Previous studies (see below), explained the chemical~~  
~~variability of Fogo's lavas by mixing in different proportions of two recycled end-~~  
~~members with characteristics similar to those of the HIMU (ancient recycled ocean~~  
~~crust) and EM1 mantle components. These end members would have been diluted by~~  
~~the presence of depleted upper mantle entrained by the upward moving plume (Gerlach~~  
~~et al., 1988). The scenario here proposed for the ascent of the 2014 Fogo magmas and of~~  
~~its plumbing system receives support from independent data, lower mantle material~~  
~~(Doucencane et al., 2003; Eserig et al., 2005), as also proposed by Mourão et al. (2012a)~~  
~~for the neighbouring Brava Island.~~

~~The 2014 erupted lavas do not show extreme isotope compositions when compared the~~  
~~other Southern Cape Verde Islands, or even with other Fogo rocks (Fig. 6 and 7). This~~  
~~makes it difficult to determine the end members contributing to its source, also~~  
~~hindering a strong contribution for the discussion of the end members of the mantle~~  
~~underlying Cape Verde. Nonetheless, some remarks have to be done:~~

~~Although the low  $^{206}\text{Pb}/^{204}\text{Pb}$  ratios (up to 19.001) are clearly below those presented by~~  
~~lavas originated from sources dominated by HIMU (recycled ocean crust) (e.g. Indeed,~~  
~~a seismic event on October 4, 2014 (i.e. 50 days before the eruption) with a hypocentre~~  
~~17 km below sea level (19.8 km below the Fogo summit), was interpreted by Instituto~~  
~~Nacional de Meteorologia e Geofísica (INMG, Cabo Verde) as resulting from the~~  
~~rupture of the roof of a mantle reservoir allowing magma transfer to shallower levels.~~  
~~Also, geodetic modelling of Sentinel-TOPS interferometry by Gonzalez et al. (2015)~~  
~~revealed the lack of deformation at the island-scale during and pre-eruption times,~~  
~~further suggesting the deep location of the main magma reservoirs.~~

~~Kawabata et al., 2011), the HIMU fingerprint is shown by trace element patterns (Fig. 5) displaying enrichment in Nb (and Ta) relative to the LREE and the LILE (e.g. Niu et al., 2012).~~

~~All the analysed rocks are characterized by positive  $\Delta 8/4$  and  $\Delta 7/4$  and plot below the mixing lines between a HIMU type end member and DMM or lower mantle compositions on the  $^{206}\text{Pb}/^{204}\text{Pb}$  vs.  $^{143}\text{Nd}/^{144}\text{Nd}$  diagram (Fig. 10), strongly suggesting the contribution of an enriched end member to the 2014 Fogo mantle source(s).~~

~~The products erupted in 2014 mark a change on the evolutionary trend reported by previous authors for Fogo eruptions (Gerlach et al., 1988; Eserig et al., 2005) which was characterized by an increasing contribution of the enriched component. Indeed, the 2014 lavas have less radiogenic Sr, but more radiogenic Nd signatures when compared with those from the 1951 and 1995 eruptions.~~

For Fogo Island, Eserig et al., (2005), based on radiogenic Os signatures (up to 0.1369), proposed the incorporation of lower continental crust materials present in Fogo lithosphere during the ascent and differentiation of plume-derived magmas. We note that, for the studied 2014 rocks there is no positive correlation between  $^{87}\text{Sr}/^{86}\text{Sr}$  ratios and  $\text{SiO}_2$  contents (not shown), which is at odds with what would be expectable from processes of simultaneous assimilation and fractional crystallization (e.g. EC-AFC from Bohrson and Spera, 2001) involving a typical basic/ultrabasic alkaline magma and lower continental crust materials. This could eventually be explained admitting that magmas continued to evolve after the end of the assimilation process, as proposed by Eserig et al. (2005) to explain, for the previous eruptions, the lack of correlation between  $^{187}\text{Os}/^{186}\text{Os}$  ratios and differentiation indices. However, in such a model the correlation between  $\text{SiO}_2$  and  $^{87}\text{Sr}/^{86}\text{Sr}$  would only be lost for the most evolved rocks, which is clearly not the case. Taking these into account we consider more plausible that

the mixing of the enriched continental lithosphere (s.l.) with plume material occurred in the mantle before melting.

As shown before (see 5.1) the less evolved 2014 rocks are characterized by Nb/U ratios of  $60 \pm 3$ , while for basanitic/tephritic lavas from the 1995 and 1951 eruptions a mean value of  $95 \pm 4$  has been assigned (Hildner et al., 2011; 2012). These differences cannot be explained by fractional crystallization (see 5.1). The 2014 Nb/U ratios fits the typical OIB value (EM lavas excluded) of  $52 \pm 15$  obtained by Hofmann (2003). We demonstrated above that the contribution of a local enriched end member is less significant for the 2014 lavas than for those of the two previous eruptions. However, as shown by Hofmann (2003), either the EM-type mantle components or the continental crust have low Nb/U ratios. Consequently the higher contribution of an enriched end member for the 1995 and 1951 lavas cannot be invoked as a cause for their higher Nb/U ratios.

Nb/U ratios significantly higher than the typical OIB lavas have also been reported for some Canarian lavas by Lundstrom et al. (2003). These authors defended that this can be the reflex of mixing between ascending plume derived magmas and lithospheric melts with a significant contribution of amphibole present in low solidus mantle domains. These domains would have been generated by metasomatic (s.l.) processes during previous stages of islands building. We defend that a similar process may have been responsible for the higher Nb/U and Dy/Dy\* ratios of the 1995 and 1951 lavas. Since their vents, and probably also the ascending magma paths, were almost coincident with those of 2014 we speculate that such low solidus lithospheric domains were already exhausted and did not contribute significantly for the composition of the subsequent 2014 eruption products.

### 5.3 Evidence for small-scale mantle heterogeneity and short-term compositional evolution of Fogo volcano.



As mentioned above, the Cape Verde Archipelago is known by its remarkable geochemical intra-island heterogeneity. ~~With few exceptions, Cape Verde alkaline rocks form two groups with distinct elemental and isotopic signatures, according to their geographical location (Northern vs. Southern Islands; (e.g. Gerlach et al., 1988; Doucelance et al., 2003). Intra~~Significant intra-island ~~heterogeneities~~time-dependent geochemical variations are also common as shown for most Cape Verde Islands ~~and particularly for the neighbouring islands of Santiago (e.g. Barker et al., 2010) and Brava (Mourão et al., 2012 a) where significant time dependent geochemical variations were described.~~ Intra-island spatial heterogeneities have also been described for presumably coeval rocks. ~~This, such~~ is the case of ~~lavas from~~ the Recent Volcanics of São Vicente Island ~~whose major element compositions suggest magma extraction at variable depths, and also present significantly different incompatible trace element ratios (Trindade et al., 2003). This is), and also of~~ the ~~case of~~ Fogo Island where, as shown by Escrig et al. (2005), lavas erupted since 1785 present measurable variability on isotope signatures. ~~The 2014-15 and the 1995 eruptive fissures are separated by less than 200 m, and less than 2000 m from the 1951 vents, thus offering the opportunity to further constrain mantle heterogeneity beneath Cape Verde and particularly in Fogo Island.~~ It is well known that ratios involving elements characterized by highly incompatible behaviour ( $D \ll 1$ ) ~~tend~~In opposition to reflect mantle source values when the extent of partial melting is higher than about 5%. However, the behaviour of such elements can be significantly different during melting of peridotite or pyroxenite. ~~This is true, for example, for incompatible trace element ratios involving Ba or for the La/Nb ratio, which tend to be lower or equal to the pyroxenite source ratios can be fractionated during partial melting and higher or equal to the peridotite source ratios (Stracke and Bourdon, 2009). In addition we have shown that the studied rocks are significantly evolved (Ni < 42 ppm) and that amphibole, one of the crystallized phases, is capable of~~

~~fractionating elemental ratios involving Nb. In contrast, as crystal fractionation~~  
~~processes,~~ radiogenic isotope ratios are not changed during ~~meltingsuch~~ events ~~they~~.  
~~They~~ are ~~consideredthus~~ a ~~more~~ reliable indicator of source heterogeneity, even though  
the isotope variability of lavas ~~tendtends~~ to be smaller than that of the mantle source due  
to eventual mixing/homogenization processes (e.g. Stracke and Bourdon, 2009).  
The 2014 volcanic products have clearly more unradiogenic Pb and Sr ( $^{206}\text{Pb}/^{204}\text{Pb}$   
down to 18.972;  $^{87}\text{Sr}/^{86}\text{Sr}$  down to 0.703613) but more radiogenic Nd ( $^{143}\text{Nd}/^{144}\text{Nd}$  up to  
0.512789) signatures than the previous two eruptions ( $^{206}\text{Pb}/^{204}\text{Pb}$  up to 19.273;  $^{87}\text{Sr}/^{86}\text{Sr}$   
up to 0.70379;  $^{143}\text{Nd}/^{144}\text{Nd}$  down to 0.51272; see also Figs 6 and 7). ~~Such differences,~~  
~~observed in volcanic products erupted during a time span of just 63 years from vents so~~  
~~closely located (200 to < 2000 m)~~ Considering that the 2014 lavas erupted from vents  
localized less than 200 and 2000 m of those from the two previous eruptions (1951 and  
1995) and that these 3 eruptions occurred within a time lapse of only 63 years, such  
differences emphasize the presence of small-scale heterogeneities in the mantle sources  
feeding the volcanism of Fogo Island and the absence of significant magma  
mingling/homogenization before eruption.  
The ability of magmas erupted from a volcano to show the source heterogeneity  
depends on the degree of partial melting, on the size of magma chambers and on the  
time of residence in such reservoirs. The higher the degree of partial melting, the higher  
is the capability of the extracted magmas to average the composition of a heterogeneous  
source. As a consequence low degree partial melts reflect better the compositional  
variability of the source. ~~This was shown, for example, by (e.g. Stracke and Bourdon,~~  
~~2009; Martins et al. (., 2010) for the neighbouring Santiago Island, who evidenced an~~  
~~increasing variability of the  $^{143}\text{Nd}/^{144}\text{Nd}$  ratios with decreasing degrees of partial~~  
~~melting.~~  
~~).~~ It is ~~consideredaccepted~~ that the lithosphere exerts a major control in the final depth  
and extent of sub-lithospheric mantle melting ~~and, consequently, also on the extent and~~

~~mean pressure of melting (e.g. (e.g. Watson and Mckenzie, 1991; Humphrey and Niu,~~  
~~2009; Niu et al., 2011), even though the thickness of mature (> 70Ma) oceanic~~  
~~lithosphere does not surpass ≈90 km (Niu et al., 2011). The Cape Verde islands stand on~~  
~~a 120-140 My old oceanic crust characterized by significantly high values of admittance~~  
~~(geoid to depth ratio) (Monnerau and Cazennave, 1990). ThisThese suggests that~~  
~~lithosphere may extend to depths below the spinel-garnet transition, considered to occur~~  
~~at depths corresponding to ~ (≈3 GPa (e.g.; Klemme and O'Neil, 2000). Consequently,~~  
~~the depth of melting would have been totally or partially confined to the mantle garnet~~  
~~zone.) in agreement with previous studies for Cape Verde islands (e.g. Gerlach et al.,~~  
~~1998; Barker et al., 2010; Mourão et al., 2012a).~~ Even taking into account that the less  
 evolved 2014 magmas (tephrites) are not characterized by primary or primitive  
 compositions, this percept is endorsed by (Tb/Yb)<sub>n</sub> ratios higher than 2.3, which is  
 significantly above the threshold value of 1.8 proposed by Wang et al. (2002) as a proxy  
 for spinel-garnet facies transition. Indeed it would be necessary to consider a (Tb/Yb)<sub>n</sub>  
 increase higher than 27% during magma evolution – which is not expectable from the  
 commonly accepted D values (~~see for example <https://earthref.org/KDD/>~~ e.g. Adam and  
 Green, 2006) – to place the mean melting depths outside the garnet zone. ~~This and~~  
~~Moreover, 2014 magmas show a Tb/Yb decrease from tephrites for the highly SiO<sub>2</sub>–~~  
~~undersaturated character of the Fogo lavas (2014: normative *ne* up to 23.04 %) point out~~  
~~to low degree of partial melting events with the consequent deficient averaging of the~~  
~~isotopic variability of the source; more evolved phonotephrites.~~  
 The thickness of the lithosphere exerts a first-order control on the extent of partial  
 melting (e.g. Humphreys and Niu, 2009). For the present case, a lithosphere some 90  
 km thick (see above) would have constrained the melting to small extent. Despite the  
 exact extent of melting is difficult to assess given the significantly evolved character of  
 lavas (MgO < 6.4 wt%) and the uncertainty derived from the lack of knowledge about  
 the relative proportion of peridotite and eclogite in the mantle source, the highly SiO<sub>2</sub> -

undersaturated character of the Fogo lavas (2014: normative *ne* up to 23.04 %) and the high TiO<sub>2</sub> contents clearly suggest low percentages of partial melting, with the consequent deficient averaging of the isotopic variability of the source. The above referred lack of correlation between elemental and isotope ratios (see 4.3) also points to low degrees of melting during which a significant elemental fractionation occurs erasing any correlation between incompatible element ratios and isotope ratios (see Stracke and Bourdon, 2009).

After extraction, the degree of melt homogenization will depend on the occurrence of a plumbing system with large magmatic chamber(s), and of long magma residence times within the system, allowing mixing of different batches of melt. Data gathered from several islands suggest that for voluminous magma chambers to form, high magma supply rates are needed; conversely, during evolutionary stages characterized by low magma supply rates a plethora of small and ephemeral magma reservoirs tend to form, many of them within the mantle (see Klügel et al., 2000; 2005; Stroncik et al., 2009 and references therein), and this is also the case for the recent magmatism of Fogo. The evidence for small and ephemeral magma reservoirs beneath Fogo was already proposed for the previous eruptions (Munhá et al., 1997; Hildner et al., 2012). This may be also the case for the 2014 eruption as suggested by the compositional change during the latest two eruptions (from phonotephrites to basanites/tephrites) and, despite the associated methodological errors, by distinct depths of magma chambers where clinopyroxene and kaersutite crystalized, both evidences precluding a large homogenizing reservoir.

~~Thus, the isotopic heterogeneity depicted by the lavas erupted during the three last eruptions at Fogo Island (1951, 1995 and 2014) can be considered as the result of source heterogeneities and the presence of a thick lithosphere that, by restraining the extent of partial melting to low degrees—and consequently limiting magma supply to low rates—inhibited both significant averaging of source composition and the~~

~~subsequent mixing/homogenization during ascent to the surface. It must be emphasized that, to some degree, melt aggregation and magma mixing must have occurred (see for example the reverse zoning in some clinopyroxenes), and thus the isotopic heterogeneity of the erupted materials is considered to be smaller than that of the mantle source.~~

~~Another consequence of the low degrees of partial melting in Cape Verde is the referred lack of correlation between elemental and isotope ratios (see 4.3). Indeed, during such melting events an elemental fractionation occurs erasing any correlation between incompatible element ratios and isotope ratios characterizing the mantle source (see Stracke and Bourdon, 2009).~~

## 6. Concluding remarks

- Magmas erupted from November 23 to December 7, 2014 at Fogo Island (Cape Verde Archipelago) are alkaline, exhibit significantly evolved compositions (Ni < 42 ppm) and are classified as tephrites and phonotephrites. The compositional range is slightly smaller than that reported for the 1995 eruption, but larger than the displayed by the 1951 eruption, for which no phonotephrites were erupted.
- Similarly to 1995 (Munhá et al., 1997; Silva et al., 1997; Hildner et al., 2011), the eruption of phonotephritic lavas preceded the effusion of the tephritic ones ~~pointing to~~suggesting the existence of a compositional/density zoning inside the pre-eruptive magma chamber or of several magma reservoirs, in agreement with barometric data.
- Geobarometric estimates using clinopyroxene and kaersutite compositions indicate that fractional crystallization mainly occurred in magma chambers located in the mantle (~~≈ 12~~(down to 3425.6 ± 5.5 km below the sea level), followed by a short residence time (< 60 days) at crustal levels.

Formatted: Font: Bold

973 ~~•~~ Erupted magmas are characterized by positive  $\epsilon\text{Nd}$ ,  $\epsilon\text{Hf}$ ,  $\Delta 8/4$  and  $\Delta 7/4$ . Their  
974 compositions reflect a mantle source where ancient recycled ocean crust and an  
975 enriched component (EM1-type) are present. The 2014 lavas have less  
976 radiogenic Sr, but more radiogenic Nd compositions, ~~when compared with~~ than  
977 those from the 1951 and 1995 eruptions, marking a change on the evolutionary  
978 trend reported by previous authors for Fogo (Gerlach et al., 1988; Escrig et al.,  
979 2005) which was characterized by an increasing contribution of the  
980 ~~enriched~~ EM1-type component.

- 981 • Although the 2014 eruption vents are almost spatially coincident with those of  
982 1995 and less than 2 km away from the 1951 vents, their lavas are isotopically  
983 different from those generated in the previous two eruptions. These differences  
984 in magmas erupted on a very limited area and short interval (63 years) reflect the  
985 heterogeneity of the mantle source and the lack of averaging/mingling during  
986 partial melting and ascent through the plumbing system. For these, the lid effect  
987 of the old (120-140 Ma) and thick lithosphere is considered of utmost  
988 importance.
- 989 • The lower Nb/U ratios of the 2014 rocks as compared with previous eruptions is  
990 considered to reflect the lack of significant mixing of ascending plume magmas  
991 with lithospheric melts, as opposed to what has been hypothesized for 1995 and  
992 1951 magmas.

993 ~~• It is inferred that the lid effect of an old (120-140 Ma) and thick lithosphere,~~  
994 ~~imposing low melting degrees, limited the averaging of source compositions. In~~  
995 ~~turn, low melting degrees induced low magma ascent rates, a condition not~~  
996 ~~favourable to the generation of voluminous magma chambers where isotopically~~  
997 ~~distinct magma batches issued from heterogeneous sources could pond and mix~~

Formatted: Font: Verdana, 10 pt

Formatted: Bulleted + Level: 1 +  
Aligned at: 0.63 cm + Indent at: 1.27  
cm

Formatted: Font: Verdana, 10 pt

Formatted: Font: Verdana, 10 pt

Formatted: Font: Verdana, 10 pt

~~with each other, producing homogeneous compositions over significant periods  
of time.~~

## **Acknowledgements**

We dedicate this paper to the memory of Luís Celestino Silva (1936-2017), a pioneer in the geology of Cape Verde: his knowledge, enthusiasm and kindness marked most of the authors of this work.

This research received financial support from FCT (Fundação para a Ciência e Tecnologia) through projects REGENA (PTDC /GEO-FIQ/3648/2012) and FIRE (PTDC/GEO-GEO/1123/2014), as well as through project UID/GEO/50019/2013 to Instituto Dom Luiz (IDL). R. Ramalho was funded by a FP7-PEOPLE-2011-IOF Marie Curie International Outgoing Fellowship, which is acknowledged. The authors are grateful to Pedro Rodrigues for skilled assistance during electron microprobe analyses. Field work of J. Mata was partially funded by Bernardo Mata. Kayla Iacovino is acknowledged for the permission to use her Excel spreadsheet to calculate magma viscosity (see <http://www.kaylaiacovino.com/tools-for-petrologists/>). Cristina de Ignacio, an anonymous reviewer and the Editor (Nelson Eby) are acknowledged for their constructive comments, corrections and suggestions, which significantly contributed for the quality of this paper.

## **References**

- Adam, J., Green, T. 2006. Trace element partitioning between mica and amphibole-bearing garnet lherzolite and hydrous basaltic melt: 1. Experimental results and the investigation of controls on partitioning behavior. *Contributions to Mineralogy and Petrology* 152, 1-17.
- ~~Aignertorres, M., Blundy, J., Ulmer, P., Pettke, T. 2007. Laser Ablation ICPMS study of trace element partitioning between plagioclase and basaltic melts: an experimental approach. *Contributions to Mineralogy and Petrology* 153, 647-667.~~
- ~~Bagnardi, M., González, P.J., Hooper, A. 2016. High-resolution digital elevation model from tri-stereo Pleiades-1 satellite imagery for lava flow volume estimates at Fogo Volcano: Tri-stereo Pleiades DEM of Fogo Volcano. *Geophys. Res. Lett.* 43, doi:10.1002/2016GL06945~~

- 1031 |  
1032 |  
1033 |  
1034 |  
1035 |  
1036 |  
1037 |  
1038 |  
1039 |  
1040 |  
1041 |  
1042 |  
1043 |  
1044 |  
1045 |  
1046 |  
1047 |  
1048 |  
1049 |  
1050 |  
1051 |  
1052 |  
1053 |  
1054 |  
1055 |  
1056 |  
1057 |  
1058 |  
1059 |  
1060 |  
1061 |  
1062 |  
1063 |  
1064 |  
1065 |  
1066 |  
1067 |  
1068 |  
1069 |  
1070 |  
1071 |  
1072 |  
1073 |  
1074 |  
1075 |  
1076 |  
1077 |  
1078 |  
1079 |  
1080 |  
1081 |  
1082 |  
1083 |  
1084 |  
1085 |  
1086 |
- ▲  
Barker, A.K., Holm, P.M., Peate, D.W., Baker, J.A. 2009. Geochemical stratigraphy of submarine lavas (3–5 Ma) from the Flamengos Valley, Santiago, southern Cape Verde islands. *Journal of Petrology* 50, 169-193.
- Barker, A.K., Holm, P.M., Peate, D.W., Baker, J.A. 2010. A 5 million year record of compositional variations in mantle sources to magmatism on Santiago, southern Cape Verde archipelago. *Contributions to Mineralogy and Petrology* 160, 133-154.
- Barker, A.K., Troll, V.R., Ellam, R.M., Hansteen, T.H., Harris, C., Stillman, C.J., Andersson, A. 2012. Magmatic evolution of the Cadamosto Seamount, Cape Verde: beyond the spatial extent of EM1. *Contributions to Mineralogy and Petrology* 163, 949 -965.
- ~~Beattie, P. 1994. Systematics and energetics of trace element partitioning between olivine and silicate melts: Implications for the nature of mineral/melt partitioning. *Chemical Geology* 117, 57-71.~~
- Beier, C., Haase, K. M., Abouchami, W., Krienitz, M.-S., Hauff, F. 2008. Magma genesis by rifting of oceanic lithosphere above anomalous mantle: Terceira Rift, Azores. *Geochemistry, Geophysics, Geosystems* 9, Q12013.
- ~~Bohrson, Wendy A., Spera, Frank J. 2001. Energy Constrained Open System Magmatic Processes II: Application of Energy Constrained Assimilation Fractional Crystallization (EC-AFC) Model to Magmatic Systems. *Journal of Petrology* 42, 1019-1041.~~
- ~~Bottazzi, P., M. Tiepolo, R. Vannucci, A. Zanetti, S. Foley, R. Brumm, Oberti, R. 1999. Distinct site preference for heavy and light REE and the prediction of  $D_{\text{REE}}^{\text{Amph}}$ . *Contributions to Mineralogy and Petrology* 137, 36-45.~~
- Browne, B.L., Gardner, J.E. 2006. The influence of magma ascent path on the texture, mineralogy, and formation of hornblende reaction rims. *Earth and Planetary Science Letters* 246, 161-176.
- Brum da Silveira, A., Madeira, J., Munhá, J., Mata, J.; Martins, S., Mourão, C., Tassinari, C. 2006. The summit depression of Fogo Island (Cape Verde): caldera and/or flank collapse? Abstracts and Programme of the George P. L. Walker symposium on Advances in Volcanology, Reykolt, Islândia, 23.
- Caldeira, R., Guimarães, F., Mata, J. Silva, P., Moreira, M., Ferreira, P. 2015. Mineral Chemistry of Ultramafic Nodules from Lavas of the Fogo Island 2014 Eruption (Cape Verde). Preliminary results. Livro de Resumos do X Congresso Ibérico de Geoquímica/XVIII Semana de Geoquímica, 51-53, LNEG, Lisboa.
- Cappello, A., G. Ganci, S. Calvari, N. M. Pérez, P. A. Hernández, S. V. Silva, J. Cabral, and C. Del Negro. 2016. Lava flow hazard modeling during the 2014–2015 Fogo eruption, Cape Verde, *Journal of Geophysical Research, Solid Earth* 121, 1-14.
- Chauvel, C., Blichert-Toft, J. 2001. A hafnium isotope and trace element perspective on melting of the depleted mantle. *Earth Planetary Science Letters* 190, 137–151.
- Chauvel, C., Lewin, E., Carpentier, M., Arndt, N., Marini, J.-C. 2008. Role of recycled oceanic basalt and sediment in generating the Hf–Nd mantle array. *Nature Geoscience* 1, 64–67.
- Chauvel, C., Bureau, S., Poggi, C. 2011. Comprehensive chemical and isotopic analyses of basalt and sediment reference materials. *Geostandards and Geoanalytical Research* 35, 125–143.

**Formatted:** Font color: Custom Color( RGB(34,34,34)), English (United States), Kern at 18 pt

**Formatted:** Level 1, Pattern: Clear (White)



- 1087 Chiaradia, M., Müntener, O., Beate, B. 2011. Enriched basaltic andesites from mid-crustal  
1088 fractional crystallization, recharge, and assimilation (Pilavo Volcano, Western Cordillera of  
1089 Ecuador). *Journal of Petrology* 52, 1107-1141.
- 1090  
1091 Christensen, B., Holm, P., Jambon, A., Wilson, J. 2001. Helium, argon and lead isotopic  
1092 composition of volcanics from Santo Antão and Fogo, Cape Verde Islands. *Chemical Geology*  
1093 178, 127-142.
- 1094  
1095 Cooper, K.M. 2017. What does a magma reservoir look like? The “crystal’s eye” view.  
1096 *Elements* 13, 23-28.
- 1097  
1098 Courtney, R., White, R. 1986. Anomalous heat flow and geoid across the Cape Verde Rise:  
1099 Evidence for dynamic support from a thermal plume in the mantle. *Geophysical Journal of the*  
1100 *Royal Astronomical Society* 87, 815-868.
- 1101  
1102 Cashman, K.V., Sparks, R.S.J., Blundy, J.D. 2017. Vertically extensive and unstable magmatic  
1103 systems: A unified view of igneous processes. *Science* 355, eaag3055, 9 pages.
- 1104  
1105 Dash, B.P., Ball, M.M., King, G.A., Butler, I.W., Rona, P.A. 1976. Geophysical investigation of  
1106 the Cape Verde archipelago. *Journal of Geophysical Research* 81, 5249-5259.
- 1107  
1108 Davidson, J., Turner, S., Plank, T. 2013. Dy/Dy\*: Variations Arising from Mantle Sources and  
1109 Petrogenetic Processes. *Journal of Petrology* 54, 525-537.
- 1110  
1111 | Day, S., Heleno da Silva, S., Fonseca, J. 1999. A past giant lateral collapse and present day  
1112 instability of Fogo, Cape Verde Islands. *Journal of Volcanology and Geothermal Research* 94,  
1113 191-218.
- 1114  
1115 De Angelis, S.H., Larsen, J., Coombs, Dunn, A., Hayden, L. 2015. Amphibole reaction rims as  
1116 a record of pre-eruptive magmatic heating: An experimental approach. *Earth and Planetary*  
1117 *Science Letters* 426, 235-245
- 1118  
1119 Doucelance, R., Escrig, S., Moreira, M., Gariépy, C., Kurz, M.D. 2003. Pb-Sr-He isotope and  
1120 trace element geochemistry of the Cape Verde Archipelago. *Geochimica et Cosmochimica*  
1121 *Acta* 67, 3717-3733.
- 1122  
1123 Eisele, S., Reißig, S., Freundt, A., Kutterolf, S., Nürnberg, D., Wang, K.L., Kwasnitschka, T.  
1124 2015. Pleistocene to Holocene offshore tephrostratigraphy of highly explosive eruptions from  
1125 the southwestern Cape Verde Archipelago. *Marine Geology* 369, 233-250.
- 1126  
1127 Escrig, S., Doucelance, R., Moreira, M., Allègre, C.J. 2005. Os isotope systematics in Fogo  
1128 Island: evidence for lower continental crust fragments under the Cape Verde Southern islands.  
1129 *Chemical Geology* 219, 93-113.
- 1130  
1131 | Faria, B., Fonseca, J. F. B. D. 2014. Investigating volcanic hazard in Cape Verde Islands  
1132 through geophysical monitoring: network description and first results. *Natural Hazards and*  
1133 *Earth System Sciences* 14, 485-499.
- 1134  
1135 Foeken, J.P.T., Day, S., Stuart, F.M. 2009. Cosmogenic <sup>3</sup>He exposure dating of the Quaternary  
1136 basalts from Fogo, Cape Verdes: Implications for rift zone and magmatic reorganisation.  
1137 *Quaternary Geochronology* 4, 37-49.
- 1138  
1139 Forte, A.M., Quere, S., Moucha, R., Simmons, N.A., Grand, S.P., Mitrovica, J.X., Rowley, D.B.  
1140 2010. Joint seismic-geodynamic-mineral physical modelling of African geodynamics: a  
1141 reconciliation of deep-mantle convection with surface geophysical constraints. *Earth Planetary*  
1142 *Science Letters* 295, 329-341.
- 1143

Formatted: Portuguese (Portugal)

Formatted: Portuguese (Portugal)

1144 French, S.W., Romanowicz, B. 2015. Broad plumes rooted at the base of the earth's mantle  
 1145 beneath major hotspots. *Nature* 525, 95-99.  
 1146  
 1147 ~~Frost, B.R., Lindsley, D.H. 1991. Occurrence of iron titanium oxides in igneous rocks. In:~~  
 1148 ~~Lindsley, D.H. (ed.) *Oxide Minerals. Mineralogical Society of America, Reviews in Mineralogy*~~  
 1149 ~~25, 433-468.~~  
 1150  
 1151 Galer, S.J.G., Abouchami, W. 1998. Pratical application of lead triple spiking for correction of  
 1152 instrumental mass discrimination. *Mineralogical Magazine* 62 A, 491-492.  
 1153  
 1154 Geiger, H., Barker, A., Troll, V. 2016. Locating the depth of magma supply for volcanic  
 1155 eruptions, insights from Mt. Cameroon. *Scientific Reports* 6, 33629.  
 1156  
 1157 Gerlach, D., Cliff, R., Davies, G., Norry, M., Hodgson, N. 1988. Magma sources of the Cape  
 1158 Verde archipelago: Isotopic and trace element constraints. *Geochimica et Cosmochimica Acta*  
 1159 52, 2979-2992.  
 1160  
 1161 Gibson, S.A., Geist, D.G., Day, J.A., Dale, C.W. 2012. Short wavelength heterogeneity in the  
 1162 Galápagos plume: Evidence from compositionally diverse basalts on Isla Santiago.  
 1163 *Geochemistry, Geophysics, Geosystems* 13, doi: 10.1029/2012GC004244.  
 1164  
 1165 Giordano, D., Russell, J. K., Dingwell, D. B. 2008. Viscosity of magmatic liquids: A model.  
 1166 *Earth and Planetary Science Letters*, 217, 123-134.  
 1167  
 1168 González, P. J., M. Bagnardi, A. J. Hooper, Y. Larsen, P. Marinkovic, S. V. Samsonov,  
 1169 Wright, T. J. 2015. The 2014–2015 eruption of Fogo volcano: Geodetic modeling of Sentinel-1  
 TOPS interferometry. *Geophysical Research Letters* 42, 9239–9246.  
 1170  
 1171 Gudmundsson, A., 2012. Magma chambers: Formation, local stresses, excess pressures, and  
 compartments: *Journal of Volcanology and Geothermal Research* 237–238, 19–41.  
 1172  
 1173 Hart, S.R. 1984. A large-scale isotope anomaly in the Southern Hemisphere mantle. *Nature* 309,  
 753-757.  
 1174  
 1175 Hildner, H., Klügge, A., Hauff, F. 2011. Magma storage and ascent during the 1995 eruption of  
 Fogo, Cape Verde Archipelago. *Contributions to Mineralogy and Petrology* 162, 751–772.  
 1176  
 1177 Hildner, H., Klügge, A., Hansteen, T. 2012. Barometry of lavas from 1951 eruption of Fogo,  
 1178 Cape Verde Islands: Implications for historic and prehistoric magma plumbing system. *Journal*  
 1179 *of Volcanology and Geothermal Research* 217-218, 73-90.  
 1180  
 1181 Hoernle, K., Tilton, G., Le Bas, M.J., Duggen, S., Garbe-Schönberg, D. 2002. Geochemistry of  
 1182 oceanic carbonatites compared with continental carbonatites: mantle recycling of oceanic crustal  
 1183 carbonate. *Contribution to Mineralogy and Petrology* 142, 520-542.  
 1184  
 1185 Hofmann, A.W. 2003. Sampling mantle heterogeneity trough oceanic basalts: isotopes and trace  
 1186 elements, in: Carlson, R. (Ed.), *Treatise on geochemistry*, vol. 2 - The mantle and core.  
 1187 Elsevier-Pergamon, Oxford, pp. 61-101.  
 1188  
 1189 Holm, P.M., Wilson, J.R., Christensen, B.P., Hansen, L., Hansen S.L., Hein, K.M., Mortensen,  
 1190 A.K., Pedersen, R., Plesner, S., Runge, M.K. 2006. Sampling the Cape Verde mantle plume:  
 1191 evolution of the melt compositions on Santo Antão, Cape Verde Islands. *Journal of Petrology*  
 1192 47, 145-189.  
 1193  
 1194 Holm, P.M., Grandvuinet, T., Friis, J., Wilson, J.R., Barker, A.K., Plesner, S. 2008. An <sup>40</sup>Ar-  
 1195 <sup>39</sup>Ar study of the Cape Verde hot spot: Temporal evolution in a semistationary plate  
 1196 environment. *Journal of Geophysical Research* 113, B08201.  
 1197

- 1198 Humphreys, E., Niu, Y. 2009. On the composition of ocean island basalts (OIB): the effects of  
1199 lithospheric thickness variation and mantle metasomatism. *Lithos* 112, 118-136.  
1200
- 1201 Iwamori, H., Nakamura, H. 2015. Isotopic heterogeneity of oceanic, arc and continental basalts  
1202 and its implications for mantle dynamics. *Gondwana Research* 27, 1131-1152.  
1203
- 1204 Jagoutz O. 2014. Arc crustal differentiation mechanisms. *Earth Planetary Science Letters* 396,  
1205 67–77.  
1206
- 1207 Jørgensen, J.Ø., Holm, P.M. 2002. Temporal variation and carbonatite contamination in  
1208 primitive ocean island volcanics from S. Vicente, Cape Verde Islands. *Chemical Geology* 192,  
1209 249-267.  
1210
- 1211 Kawabata, H., Hanyu, T., Chang, Q., Kimura, J., Nichols, A.R.L., Tatsumi, Y. 2011. The  
1212 Petrology and Geochemistry of St. Helena Alkali Basalts: Evaluation of the Oceanic Crust-  
1213 recycling Model for HIMU OIB. *Journal of Petrology* 52, 791-838.  
1214
- 1215 Klemme, S., O'Neill, H., 2000. The near solidus transition from garnet lherzolite to spinel  
1216 lherzolite. *Contributions to Mineralogy and Petrology* 138, 237-248.  
1217
- 1218 Klügel, A., Hoernle, K.A., Schmincke, H-U, White, J.D.L. 2000. The chemically zoned 1949  
1219 eruption on La Palma (Canary Islands): Petrologic evolution and magma supply dynamics of a  
1220 rift-zone eruption. *Journal of Geophysical Research* 105, 5997-6016.  
1221
- 1222 Klügel, A., Hansteen, T.H., Galipp, K. 2005. Magma storage and underplating beneath Cumbre  
1223 Vieja volcano, La Palma (Canary Islands). *Earth and Planetary Science Letters* 236, 211-226.  
1224
- 1225 Klügel, A., Longpré, M-A., Cañada, L. C., Stix, J. 2015. Deep intrusions, lateral magma  
1226 transport and related uplift at ocean island volcanoes. *Earth and Planetary Science Letters* 431,  
1227 140-149.  
1228
- 1229 Kogarko, L.N., Asavin, A.M. 2007. Regional Features of Primary Alkaline Magmas of the  
1230 Atlantic Ocean. *Geochemistry International* 45, 841-856.  
1231
- 1232 Le Bas, M. 1989. Nephelinitic and basanitic rocks. *Journal of Petrology* 30, 1299-1312.  
1233
- 1234 ~~Le Bas, T.P., Masson, D.G., Holtom, R.T., Grevemeyer, I. 2007. Slope failures of the flanks of~~  
1235 ~~the southern Cape Verde Islands. Submarine Mass Movements and Their Consequences, 337–~~  
1236 ~~345. V. Lykousis, D. Sakellariou and J. Locat (eds.), Springer.~~  
1237
- 1238 Le Maitre, R.W., 2002. Igneous rocks. A classification and glossary of terms.  
1239 Recommendations of the International Union of Geological Sciences Subcommittee on the  
1240 systematics of igneous rocks. Cambridge University Press, Cambridge. 236pp.  
1241
- 1242 Liu, X., Zhao, D. 2014. Seismic evidence for a mantle plume beneath the Cape Verde hotspot.  
1243 *International Geology Review* 56, 1213-1225.  
1244
- 1245 Lodge, A., Helffrich, G. 2006. Depleted swell root beneath the Cape Verde Islands. *Geology* 34,  
1246 449-452.  
1247
- 1248 Longpré, M., Troll, V.R., Hansteen, T.H. 2008. Upper mantle magma storage and transport  
1249 under a Canarian shield-volcano, Teno, Tenerife (Spain). *Journal of Geophysical Research* 113,  
1250 doi: 10.1029/2007JB005422.  
1251
- 1252 Lundstrom, C.C., Hoernle, K., Gill, J. 2003. U-series disequilibria in volcanic rocks from the  
1253 Canary Islands: Plume versus lithospheric melting: *Geochimica et Cosmochimica Acta* 67,  
1254 4153–4177.  
1255

Formatted: List Paragraph

1256 MacDonlad, G.A. 1968. Composition and origin of Hawaiian lavas. Geological Society of  
1257 America Memoir 116, 477-452.  
1258

1259 Madeira, J., Munhá, J., Tassinari, C., Mata, J., Brum, A., Martins, S. 2005. K/Ar ages of  
1260 carbonatites from the Island of Fogo (Cape Verde). VIII Congresso Ibérico de Geoquímica e  
1261 XIV Semana de Geoquímica (Portugal).  
1262

1263 Madeira, J., Brum da Silveira, A., Mata, J., Mourão, C., Martins, S. 2008. The role of mass  
1264 movements on the geomorphologic evolution of ocean islands: examples from Fogo and Brava  
1265 in the Cape Verde archipelago. *Comunicações Geológicas* 95, 99-112.  
1266

1267 Madeira, J., Mata, J., Mourão, C., Brum da Silveira, A., Martins, S., Ramalho, R., Hoffmann,  
1268 D.L. 2010. Volcano-stratigraphic and structural evolution of Brava Island (Cape Verde) based  
1269 on  $^{40}\text{Ar}/^{39}\text{Ar}$ , U–Th and field constraints. *Journal of Volcanology and Geothermal Research* 196,  
1270 219-235.  
1271

1272 Madureira, P., Mata, J., Mattielli, N., Queiroz, G., Silva, P. 2011. Mantle source heterogeneity,  
1273 magma generation and magmatic evolution at Terceira Island (Azores archipelago): Constraints  
1274 from elemental and isotopic (Sr, Nd, Hf, and Pb) data. *Lithos* 126, 402-418.  
1275

1276 Martins, S., Mata, J., Munhá, J., Mendes, M.H., Maerschalk, C., Caldeira, R., Mattielli, N.  
1277 2010. Chemical and mineralogical evidence of the occurrence of mantle metasomatism by  
1278 carbonate-rich melts in an oceanic environment (Santiago Island, Cape Verde). *Mineralogy and*  
1279 *Petrology* 99, 43-65.  
1280

1281 [Masson, D.G., Le Bas, T.P., Grevenmeyer, I., Weinrebe, W., 2008. Flank collapse and large-](#)  
1282 [scale landsliding in the Cape Verde Islands, off West Africa. \*Geochemistry, Geophysics,\*](#)  
1283 [Geosystems 9 \(7\).](#)  
1284

1285 Mata, J., Munhá, J. 2004. Madeira Island alkaline lava spinels: petrogenetic implications.  
1286 *Mineralogy and Petrology* 81, 85-111.  
1287

1288 Mata, J., Moreira, M., Doucelance, R., Ader, M., Silva, L.C. 2010. Noble gas and carbon  
1289 isotopic signatures of Cape Verde oceanic carbonatites: Implications for carbon provenance.  
1290 *Earth Planetary Science Letters* 291, 70-83.  
1291

1292 McKenzie, D., O'Nions, R.K. 1991. Partial melt distributions from inversion of rare earth  
1293 element concentrations. *Journal of Petrology* 32, 1021-1091.  
1294

1295 Menand, T. 2008. The mechanics and dynamics of sills in elastic layered media and their  
1296 implications for the growth of laccoliths. *Earth Planetary Science Letters* 267, 93-99.  
1297

1298 Millet, M.A., Doucelance, R., Schiano, P., David, K., Bosq, C. 2008. Mantle plume  
1299 heterogeneity versus shallow-level interactions: A case study, the São Nicolau Island, Cape  
1300 Verde archipelago. *Journal of Volcanology and Geothermal Research* 176, 265-276.  
1301

1302 Mollo, S., Putirka, K., Misiti, V., Soligo, M., Scarlato, P. 2013. A new test for equilibrium  
1303 based on clinopyroxene-melt pairs: Clues on the solidification temperatures of Etnean alkaline  
1304 melts at post-eruptive conditions. *Chemical Geology* 352, 92-100.  
1305

1306 Monnereau, M., Cazenave, A. 1990. Depth and geoid anomalies over oceanic hotspot swells: A  
1307 global survey. *Journal of Geophysical Research (Solid Earth)* 95, 15-429.  
1308

1309 Montelli, R., Nolet, G., Dahlen, F.A., Masters, G. 2006. A catalogue of deep mantle plumes:  
1310 new results from finite-frequency tomography. *Geochemistry, Geophysics, Geosystems* 7,  
1311 doi:10.1029/2006GC001248.  
1312

1313 Mourão, C., Mata, J., Doucelance, R., Madeira, J., Millet, M-A., Moreira, M. 2012a.  
1314 Geochemical temporal evolution of Brava Island magmatism: constraints on the variability of  
1315 Cape Verde mantle sources and on the carbonatite-silicate magma link. *Chemical Geology* 334,  
1316 44-61.

1317  
1318 Mourão, C., Moreira, M., Mata, J., Raquin, A., Madeira, J. 2012b. Primary and secondary  
1319 processes constraining the noble gas isotopic signatures of carbonatites and silicate rocks from  
1320 Brava Island: evidence for a lower mantle origin of the Cape Verde plume. *Contributions to*  
1321 *Mineralogy and Petrology* 163, 995-1009.

1322  
1323 Munhá, J.M., Mendes, M.H., Palácios, T., Silva, L.C., Torres, P.C., 1997. Petrologia e  
1324 geoquímica da erupção de 1995 e de outras lavas históricas da ilha do Fogo, Cabo Verde. In:  
1325 Réffega A et al. (eds). *A Erupção Vulcânica de 1995 na Ilha do Fogo, Cabo Verde*. IICT,  
1326 Lisboa, 171-186.

1327  
1328 Niu, Y., Wilson, M., Humphreys, E.R., O'Hara, M.J. 2011. The Origin of Intra-plate Ocean  
1329 Island Basalts (OIB): the Lid Effect and its Geodynamic Implications. *Journal of Petrology* 52,  
1330 1443-1468.

1331  
1332 Niu, Y.L., Wilson, M., Humphreys, E.R., O'Hara, M.J. 2012. A trace element perspective on the  
1333 source of ocean island basalts (OIB) and fate of subducted ocean crust (SOC) and mantle  
1334 lithosphere (SML). *Episodes* 35, 310-327.

1335  
1336 Nobre Silva, I., Weis, D., Scoates, J. 2013. Isotopic systematics of the early Mauna Kea shield  
1337 phase and insight into the deep mantle beneath the Pacific Ocean. *Geochemistry, Geophysics,*  
1338 *Geosystems* 11, Q 09011. doi:10.1029/2010gc003176.

1339  
1340 Palme, H., O'Neill, H.S.C. 2003. Cosmochemical estimates of mantle compositions. In:  
1341 Carlson, R. (Ed.). *The mantle and core. Treatise on Geochemistry* 2, 1-38.

1342  
1343 Paris, R., Giachetti, T., Chevalier, J., Guillou, H., Frank, N. 2011. Tsunami deposits in Santiago  
1344 Island (Cape Verde archipelago) as possible evidence of a massive flank failure of Fogo  
1345 volcano. *Sedimentary Geology* 239, 129-145.

1346  
1347 ~~Paster, T.P., Schauwecker, D.S., Haskin, L.A. 1974. The behavior of some trace elements during~~  
1348 ~~solidification of the Skaergaard layered series. *Geochimica et Cosmochimica Acta* 38, 1549-~~  
1349 ~~1577.~~

1350  
1351 Pim, J., Peirce, C., Watts, A.B., Grevemeyer, I., Krabbenhoft, A. 2008. Crustal structure and  
1352 the origin of the Cape Verde Rise. *Earth Planetary Science Letters* 272, 422-428.

1353  
1354 Pollitz, F. 1991. Two-stage model of African absolute motion during the last 30 million years.  
1355 *Tectonophysics* 194, 91-106.

1356  
1357 Putirka, K. 1997. Magma transport at Hawaii: Inferences based on igneous thermobarometry.  
1358 *Geology* 25, 69-72.

1359  
1360 Putirka, K. 1999. Clinopyroxene + liquid equilibria to 100 kbar and 2450 K. *Contributions to*  
1361 *Mineralogy and Petrology* 135, 151-163.

1362  
1363 Putirka, K.D. 2008. Thermometers and barometers for volcanic systems. *Reviews in*  
1364 *Mineralogy and Geochemistry* 69, 61-120.

1365  
1366 Putirka, K.D. 2017. Down the crater: where magmas are stored and why they erupt. *Elements*  
1367 13, 11-16.

1368

- 1369 Putirka, K., Mikaelian, H., Ryerson, F., Shaw, H., 2003. New clinopyroxene-liquid  
1370 thermobarometers for mafic, evolved, and volatile-bearing lava compositions, with applications  
1371 to lavas from Tibet and the Snake River Plain, Idaho. *American Mineralogist* 88, 1542-1554.  
1372
- 1373 Ramalho, R. 2011. Building the Cape Verde Islands. Springer Theses, 207 pp.  
1374
- 1375 Ramalho, R., Helffrich, G., Cosca, M., Vance, D., Hoffmann, D., Schmidt, D.N. 2010. Episodic  
1376 swell growth inferred from variable uplift of the Cape Verde hotspot islands. *Nature Geoscience*  
1377 3, 774-777.  
1378
- 1379 Ramalho, R., Winckler, G., Madeira, J., Helffrich, G., Hipólito, A., Quartau, R., Adena, K.,  
1380 Schaefer, J. 2015 Hazard potential of volcanic flank collapses raised by new megatsunami  
1381 evidence. *Science Advances* 1, doi: 10.1126/sciadv.1500456.  
1382
- 1383 Ribeiro, O. 1954. A ilha do Fogo e as suas erupções. Junta de Investigações do Ultramar,  
1384 Memórias, Série Geográfica I, Lisboa.  
1385
- 1386 Richter, N., Favalli, M., Dalfsen, E.Z., Fornaciai, A., Fernandes, R.M.S., Rodriguez, N.P., Levy,  
1387 J., Victória, S.S., Walter, Th.R. 2016. Lava flow hazard at Fogo Volcano, Cape Verde, before  
1388 and after the 2014-2015 eruption. *Natural Hazards and Earth Systems* 16, 1925-1951.  
1389
- 1390 Ridolfi, F., Renzulli, A. 2012. Calcic amphiboles in calc-alkaline and alkaline magmas:  
1391 thermobarometric and chemometric empirical equations valid up to 1130 °C and 2.2 GPa.  
1392 *Contributions to Mineralogy and Petrology* 163, 877-895.  
1393
- 1394 Rutherford, M.J. 2008. Magma ascent rates. In: Putirka, K.D. and Tepley, F.J., III (eds)  
1395 Minerals, Inclusions and Volcanic Processes. Mineralogical Society of America and  
1396 Geochemical Society Reviews, in *Mineralogy and Geochemistry* 69, 241-271  
1397
- 1398 Ryan, M. 1994. Neutral-buoyancy controlled magma transport and storage in mid-ocean ridge  
1399 magma reservoirs and their sheeted-dike complex: A summary of basic relationships. In:  
1400 Magmatic Systems. Eds: M. P. Ryan, Chap. 6, Academic, San Diego, California.  
1401
- 1402 Saki, M., Thomas, C., Nippress, S.E.J., Lessing, S. 2015. Topography of upper mantle seismic  
1403 discontinuities beneath the North Atlantic: the Azores, Canary and Cape Verde plumes. *Earth*  
1404 *and Planetary Science Letters* 409, 193-202.
- 1405 Satoh, H., Yamaguchi, Y., Makino, K. 2004. Ti-substitution mechanism in plutonic oxy-  
1406 kaersutite from the Larvik alkaline complex, Oslo rift, Norway. *Mineralogical Magazine*, Vol.  
1407 68, 687-697.  
1408
- 1409 ▲ Silva, L.C., Mendes, M.H., Torres, P.C., Palácios, T., Munhá, J. 1997. Petrografia das  
1410 Formações Vulcânicas da Erupção de 1995 na Ilha do Fogo, Cabo Verde. In: Réffega, A. et al.  
1411 (eds.). *A Erupção Vulcânica de 1995, na Ilha do Fogo, Cabo Verde*. IICT, Lisboa, 164-170.  
1412
- 1413 Staudigel, H., Park, K.H., Pringle, M., Rubenstone, J.L., Smith, W.H.F., Zindler, A., 1991. The  
1414 longevity of the South-Pacific isotopic and thermal anomaly. *Earth and Planetary Science*  
1415 *Letters* 102, 24-44.  
1416
- 1417 Stracke, A., Hofmann, A.W., Hart, S.R. 2005. FOZO, HIMU, and the rest of the mantle zoo.  
1418 *Geochemistry, Geophysics, Geosystems* 6, Q05007, doi:10.1029/2004GC000824.  
1419
- 1420 Stracke, A., Bourdon, B. 2009. The importance of melt extraction for tracing mantle  
1421 heterogeneity. *Geochimica et Cosmochimica Acta* 73, 218-238.  
1422
- 1423 Stronck, N.A., Klügel A., Hansteen, T. H. 2009. The magmatic plumbing system beneath El  
1424 Hierro (Canary Islands): Constraints from phenocrysts and naturally quenched basaltic glasses  
1425 in submarine rocks. *Contributions to Mineralogy and Petrology* 157, 593-607.  
1426

Formatted: Portuguese (Portugal)

Formatted: English (United States)



1427 Torres, P.C., Madeira, J., Silva, L.C., Brum da Silveira, A., Serralheiro, A., Mota Gomes, A.  
 1428 1998. Carta Geológica das Erupções Históricas da Ilha do Fogo (Cabo Verde): revisão e  
 1429 actualização. Comunicações do Instituto Geológico e Mineiro 84, A193-196.  
 1430  
 1431 Torres, P., Silva, L.C., Munhá, J., Caldeira, R., Mata, J., Tassinari, C. 2010. Petrology and  
 1432 Geochemistry of lavas from Sal Island: Implications for the variability of the Cape Verde  
 1433 magmatism. Comunicações Geológicas 97, 35-62.  
 1434  
 1435 | ▲ Trindade, M.J., Mata, J., Munhá, J. 2003. Petrogenesis of the Quaternary magmatism from the  
 1436 S. Vicente Island (Cape Verde). Comunicações do Instituto Geológico e Mineiro 90, 169-188.  
 1437  
 1438 | ▲ Vervoort, J., Patchett, P., Blichert-Toft, J., Albarède, F. 1999. Relationships between Lu-Hf and  
 1439 Sm-Nd isotopic systems in the global sedimentary system. Earth and Planetary Science Letters  
 1440 168, 79-99.  
 1441 | ▲  
 1442 Vinnik, L., Silveira, G., Kiselev, S., Farra, V., Weber, M., Stutzmann, E. 2012. Cape Verde  
 1443 hotspot from the upper crust to the top of the lower mantle. Earth Planetary Science Letters 319-  
 1444 320, 259-268.  
 1445  
 1446 Wang, K., Plank, T., Walker J.D., Smith, E.I. 2002. A mantle melting profile across the Basin  
 1447 and Range, SW USA. Journal of Geophysical Research 107, ECV 5, 1-21.  
 1448  
 1449 Watson, S., McKenzie, D. 1991. Melt generation by plumes: A study of Hawaiian volcanism.  
 1450 Journal of Petrology 32, 501-537.  
 1451  
 1452 Weis, D., Kieffer, B., Maerschalk, C., Barling, J., de Jong, J., Williams, G., Hanano, D.,  
 1453 Pretorius, W., Mattielli, N., Scoates, J., Goolaerts, A., Friedman, R., Mahoney, J. 2006. High-  
 1454 precision isotopic characterization of USGS reference materials by TIMS and MC-ICP-MS.  
 1455 Geochemistry, Geophysics, Geosystems 7, doi:10.1029/2006GC001283.  
 1456  
 1457 White, W.M. 2015. Isotopes, DUPAL, LLSVPs, and Anekantavada. Chemical Geology 419,  
 1458 10-28.  
 1459  
 1460 Williams, C., Hill, I., Young, R., White, R.S. 1990. Fracture zones across the Cape Verde Rise,  
 1461 NE Atlantic. Journal of the Geological Society of London 147, 851-857.  
 1462  
 1463 | Wilson, D., Peirce, C., Watts, A., Grevemeyer, I., Krabbenhoef, A. 2013. Uplift at lithospheric  
 1464 swells-I: Seismic and gravity constraints on the crust and uppermost mantle structure of the  
 1465 Cape Verde mid-plate swell. Geophysical Journal International 182, 531-550.  
 1466  
 1467 | Wilson, D., Peirce, C., Watts, A., Grevemeyer, I. 2013. Uplift at lithospheric swells-II: is the  
 1468 Cape Verde mid-plate swell supported by a lithosphere of varying mechanical strength?  
 1469 Geophysical Journal International 193, 798-819.  
 1470  
 1471 Zindler, A., Hart, S.R. 1986. Chemical geodynamics. Annual Reviews of Earth Planetary  
 1472 Sciences 14, 493-571.  
 1473  
 1474  
 1475  
 1476  
 1477  
 1478 | ▲  
 1479  
 1480  
 1481  
 1482  
 1483

Formatted: Portuguese (Portugal)

Formatted: English (United States)

Formatted: Portuguese (Portugal)

Formatted: Font: Verdana, 10 pt, Font color: Auto

Formatted: Line spacing: Multiple 1.15 li

1484  
1485  
1486  
1487  
1488  
1489  
1490  
1491  
1492  
1493  
1494  
1495  
1496  
1497  
1498  
1499  
1500  
1501  
1502  
1503  
1504  
1505  
1506  
1507  
1508  
1509  
1510

#### Captions

1511 **Fig. 1** – Geological map of the identified historical eruptions in Fogo (modified from  
1512 Torres et al., 1998) superimposed on the digital terrain model of the island. The upper  
1513 inset shows the location of the Island of Fogo in the archipelago of Cape Verde. The  
1514 lower insets correspond to the legend of the geological map and to a structural sketch  
1515 showing the geometry and location of the eruptive fissures of the last three eruptions  
1516 (1951, 1995 and 2014/15), the Bordeira wall (continuous line represents the top; dashed  
1517 line represents the base), and the crater rim of Pico do Fogo.

1518

1519 **Fig 2** – Photos of the 2014/15 Fogo eruption: A- general view looking East of Pico do  
1520 Fogo with the active vents at the base of the cone, the flat region of Chã das Caldeiras  
1521 covered with the 1995 and 2014 lava flows and the south-eastern tip of the Bordeira  
1522 wall; the eruptive column rises 3 km above the vents and is dispersed by south-eastward



wind at an altitude of approximately 5 km (photo taken on November 29, 2014, at 15:44 UTC); B- the alignment of active vents, viewed from the south, during a low activity phase; the new cone is growing against the southeast flank of the 1995 cone (to the left); the lava flow is being fed by the southernmost vent; the lava flow at the base of the cone presents a lava channel and several skylights with degassing white columns (photo taken on December 2, 2014, at 19:35 UTC); C- night aspect of the central crater projecting plastic spatter fragments from the explosion of lava bubbles during an hawaiian lava lake phase (photo taken on November 28, 2014, at 20:48 UTC); D- aspect of vulcanian activity at the northernmost vent producing ash-laden episodic eruptive columns with the wind blowing from the north; the white plume marks the position of the effusive south vent (photo taken on November 30, 2014, at 19:24 UTC); E- aspect of the surface of the active lava flow seen from the northwest presenting strong thermal emission and degassing (photo taken on November 29, 2014, at 15:48 UTC); F- the village of Portela invaded by the front of the lava flow 3.5 km away from the effusive vent (photo taken on December 2, 2014, at 14:39 UTC). For more photos see Supplementary Material S1.

**Fig. 3** - Total alkali-silica (TAS) diagram (Le Maître, 2002) for the 2014 magmatic rocks and interstitial glass occurring in the matrix of the lava samples. The thick line is a compositional divider between alkaline and subalkaline volcanic rocks (MacDonald, 1968). The compositional fields of the 1951 and 1995 are also shown for comparison (data from Doucelance et al., 2003; Escrig et al., 2005; Hildner et al., 2011;). U1, U2, U3 and Ph correspond to the field designations of Le Maitre et al. ~~(2002). For complete rock systematics of the 2014 rocks see Section 4.3).~~(2002) (U1: Tephrite/Basanite; U2: Pnotephrite; U3: Tephriphonolite; Ph: Phonolite). See the main text (Section 4.3) for a details on the systematics.

**Fig. 4** – Petrographic aspects of the lava flow samples showing the presence of clinopyroxene and kaersutite phenocrysts (A and B) in a hypocrystalline matrix with plagioclase, clinopyroxene and Fe-Ti oxides (A, B, C and D). Note the partial (A and B) or total (D) replacement of kaersutite by rhönite (opaque inosilicate of the aenigmatite group) which is marked by an arrow. Backscattered electron images showing a detailed view of the kaersutite rim replacement (E and F).

**Fig. 5** – Trace element characteristics of the 2014 eruptive products compared with those of the 1951 and 1995 eruptions (see Hildner et al., 2012 and Hildner et al., 2011, respectively). Normalizing values of Palme and O'Neil (2003).

**Fig. 6** - Pb isotopic compositions (A:  $^{206}\text{Pb}/^{204}\text{Pb}$  vs.  $^{207}\text{Pb}/^{204}\text{Pb}$ ; B:  $^{206}\text{Pb}/^{204}\text{Pb}$  vs.  $^{208}\text{Pb}/^{204}\text{Pb}$ ). Data sources: Northern Islands (Santo Antão, São Vicente and São Nicolau: Jørgensen and Holm, 2002; Holm et al., 2006; Millet et al., 2008) and Southern Islands (Fogo and Santiago: Doucelance et al., 2003; Barker et al., 2010; Martins et al., 2010). The 1951 and 1995 eruptions data are from Escrig et al., 2005. The heavy line represents the Northern Hemisphere Reference Line (NHRL) defined by Hart (1984). Also plotted are the compositions of mantle components (see main text for references).

**Fig. 7** – Sr, Nd (A) and Hf (B) isotope compositions. Data sources: the Santiago Island field was defined using data from Barker et al. (2009) and Martins et al. (2010). See caption of Fig. 6 for further references. No Hf isotope data exist for the 1951 and 1995 eruptions.

**Fig 8** - The role of clinopyroxene, olivine, amphibole and apatite fractionation on the liquid lines of descent for the 2014, 1995 and 1951 eruptions. In 8A and 8B fractional

crystallization was modelled using the Rayleigh equation. Partition coefficients ~~are from~~  
~~Aignertorres et al. (2007), Adam used in calculations can be find in the Supplementary~~  
~~Material S5-1 and Green (2006), Bottazzi et al. (1999), Beattie (1994), McKenzie and~~  
~~O'Nions (1991) and Paster et al. (1974)-data relative to the fractional crystallization~~  
~~vectors in the S5-2.~~ Circular ticks represent consecutive increments of 5%  
crystallization. Crystallization vectors corresponds to  $F=0.7$ . ~~Note that despite similar~~  
~~liquid lines of descent the 2014 rocks are characterized by lower Nb/U ratios than their~~  
~~1995 and 1951 counterparts.~~

**Fig. 9 – T vs. P diagram** Temperature and pressure conditions for crystallization of  
clinopyroxene and amphibole from the 2014 tephritic and phonotephritic rocks ~~from the~~  
~~2014 eruption.~~

**Fig.10 -** Mixing model between depleted mantle (DMM) and recycled oceanic crust  
(ROC;  $\approx$  HIMU), and between ROC and EM1 and the lower mantle (LM). Values for  
these end-members are from Doucelance et al. (2003) (lower mantle), Iwamoro (2015)  
(EM1, DMM) and Mourão et al. ~~(2012) (ROC).~~  
~~(2012a) (ROC).~~ Given that the 2014 Fogo lavas are characterized by a diluted  
contribution of ROC (see main text), making difficult its constraint, we considered 1.3  
Ga as the age of recycling for mixing calculations, as determined by Mourão et al.  
~~(2012a) for the neighbouring Brava Island.~~ Additional line corresponds to a mixture  
between recycled oceanic crust and lower mantle material in a 60:40 proportion, with  
EM1. Circular marks represent 10% increments. See Supplementary Material S5-3 for  
mixing calculations.

Formatted: Font color: Auto

[Click here to download high resolution image](#)

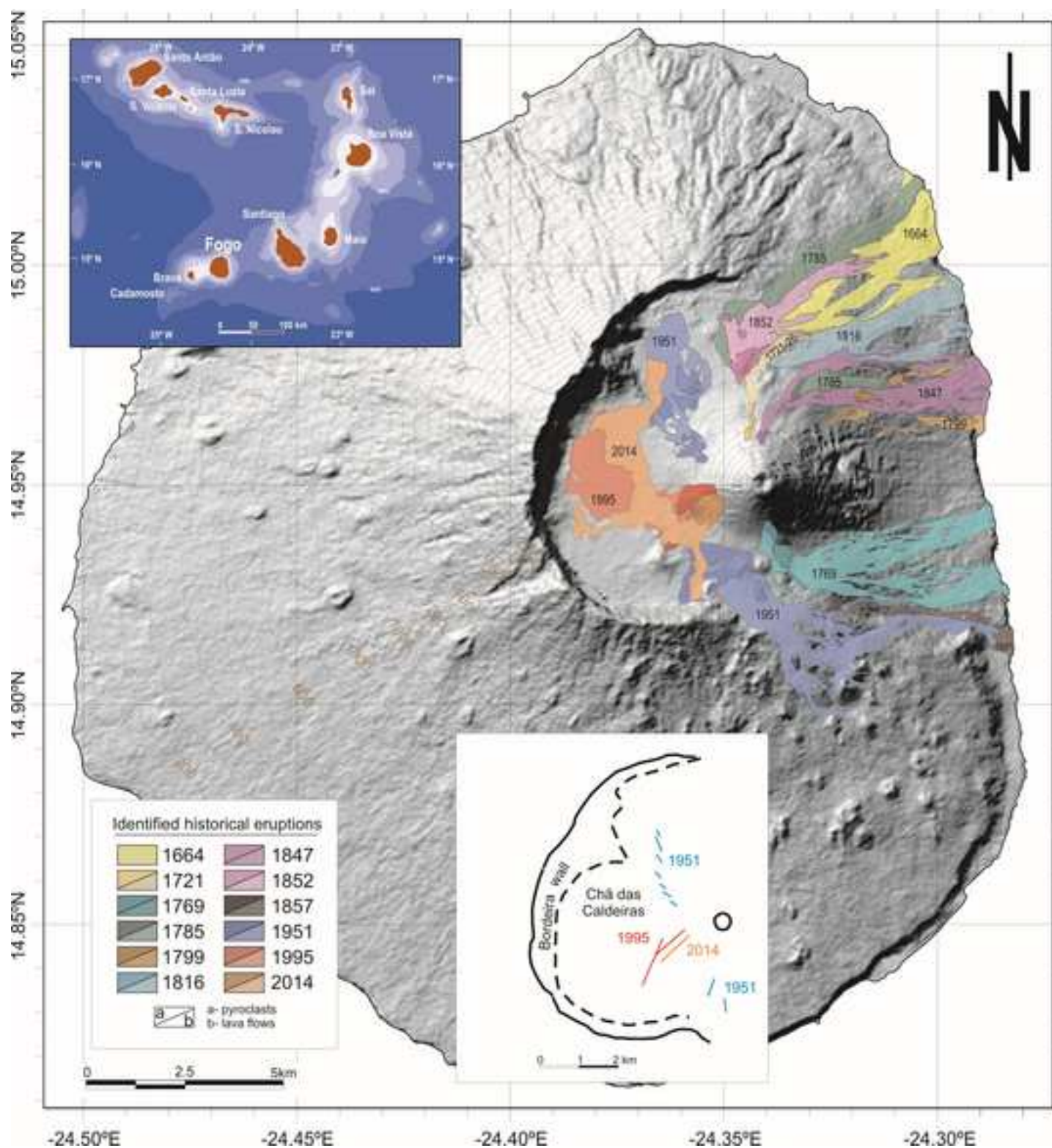




Figure 2



Figure 2 B&W

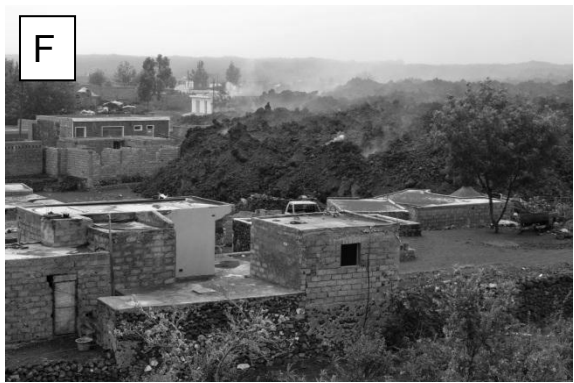
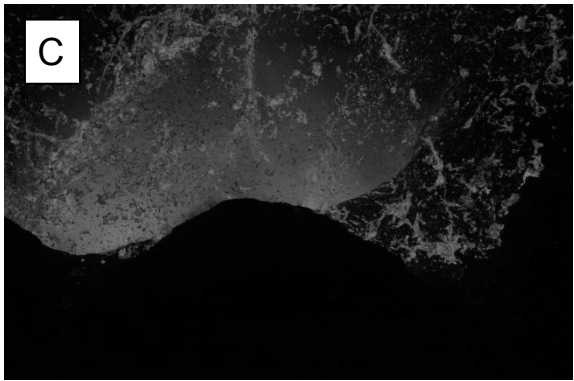


Figure 3  
[Click here to download high resolution image](#)

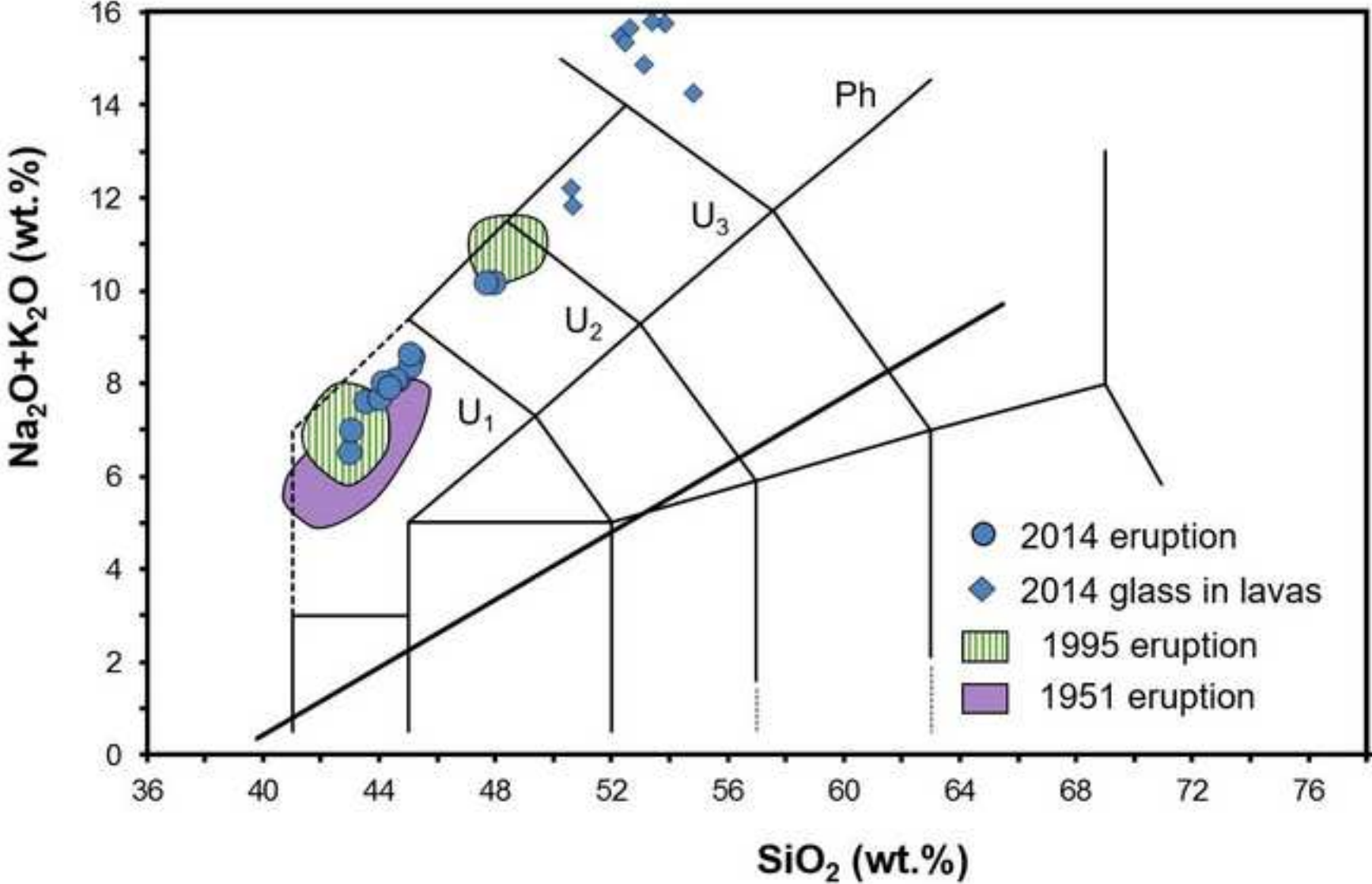


Figure 3 B&W  
[Click here to download high resolution image](#)

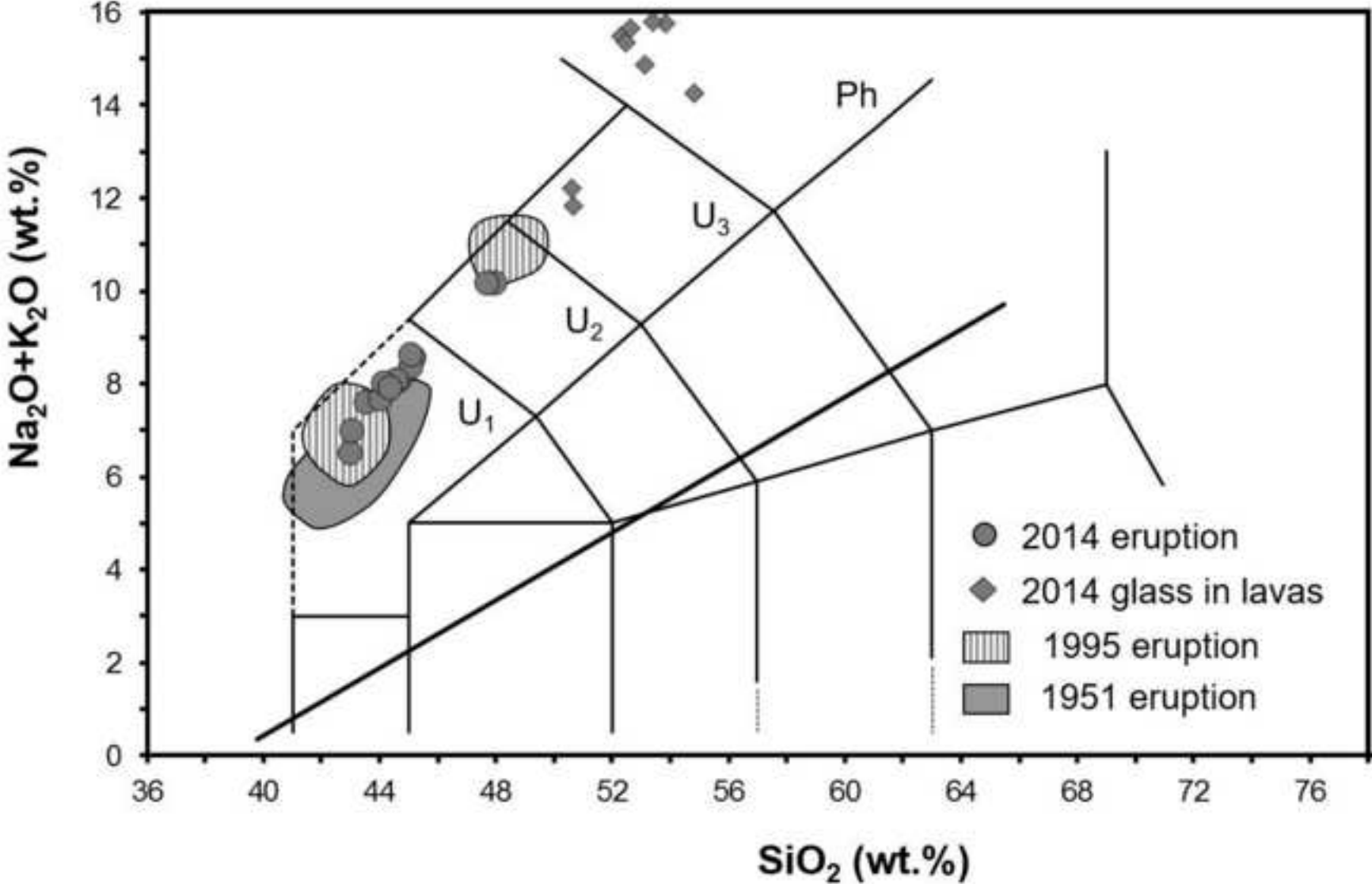




Figure 4  
[Click here to download high resolution image](#)

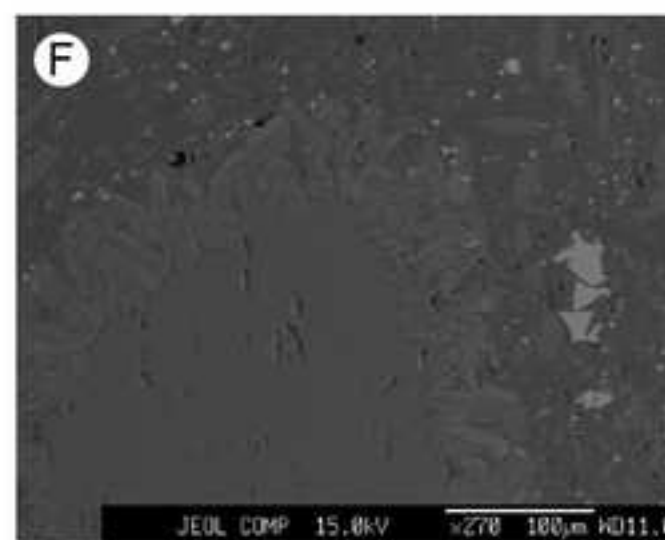
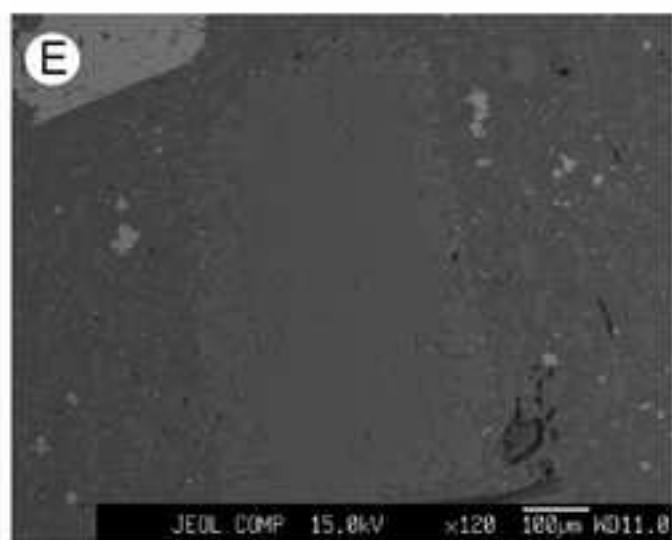
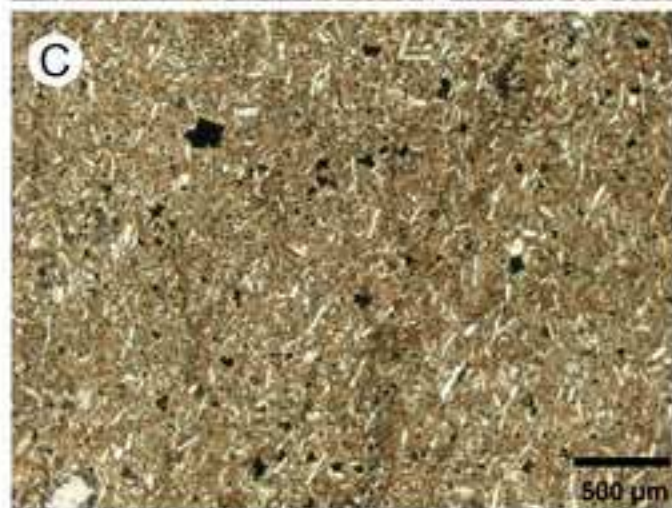
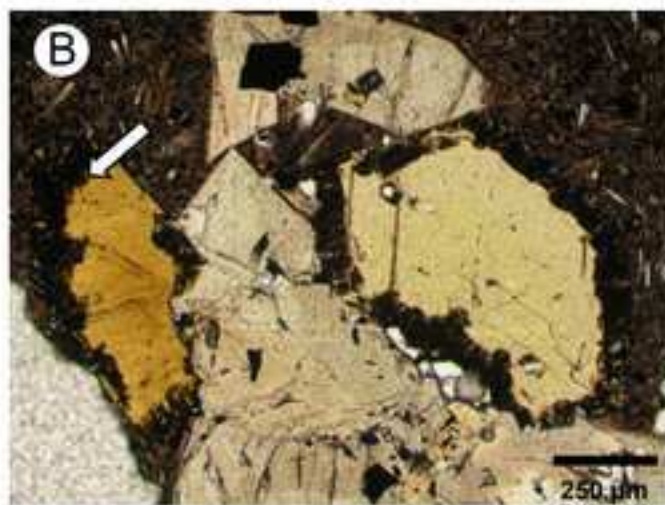
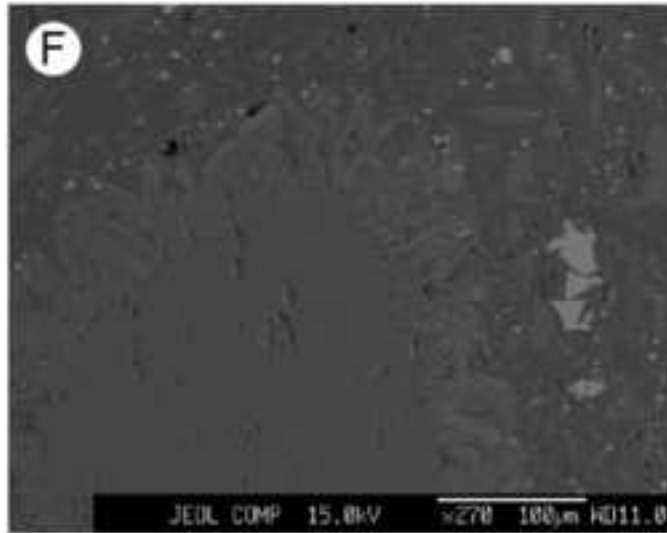
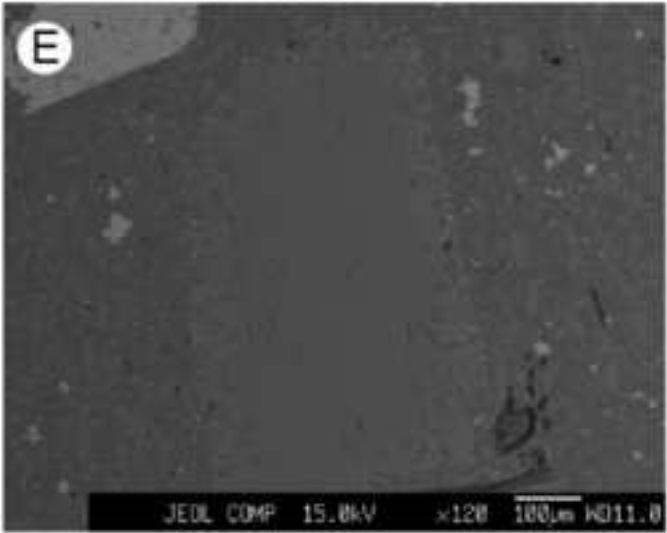
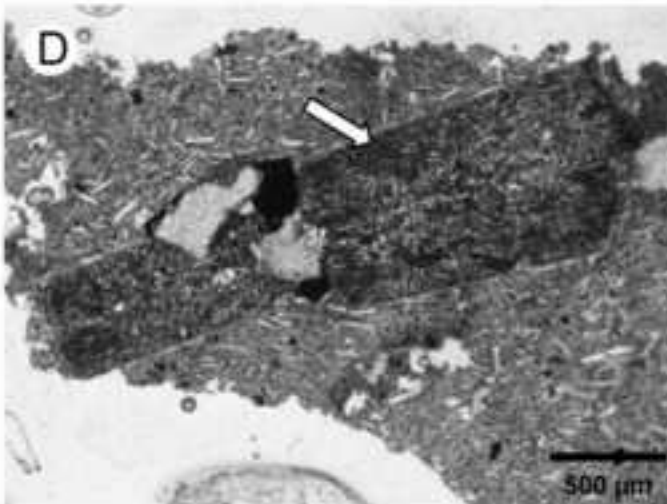
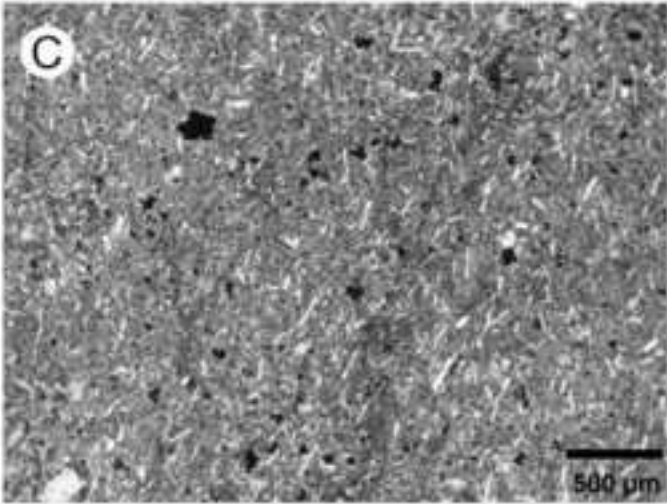
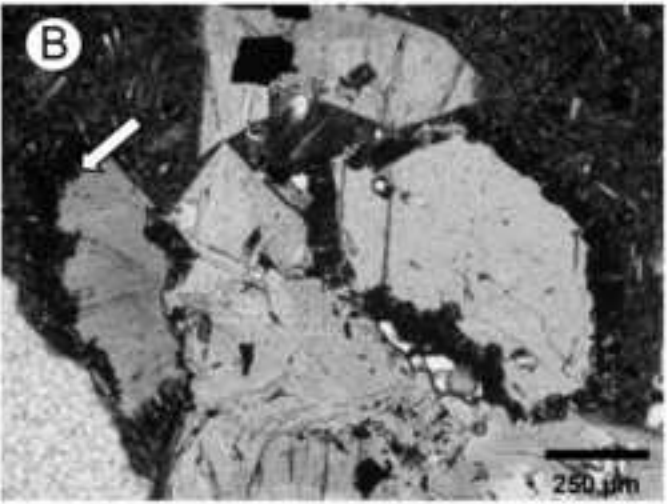
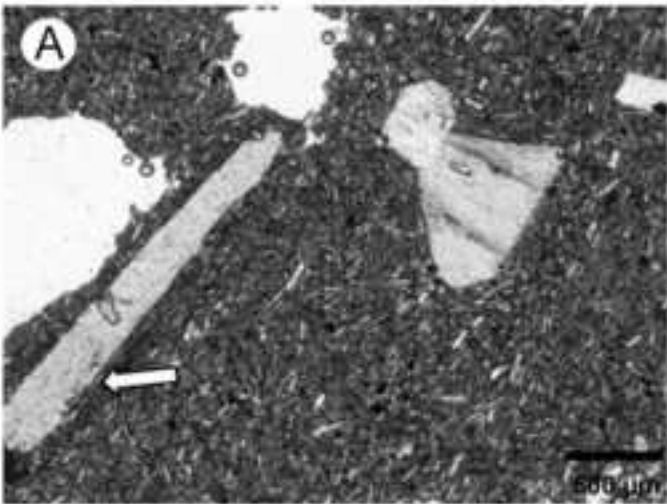


Figure 4 B&W  
[Click here to download high resolution image](#)





**Figure 5**  
[Click here to download high resolution image](#)

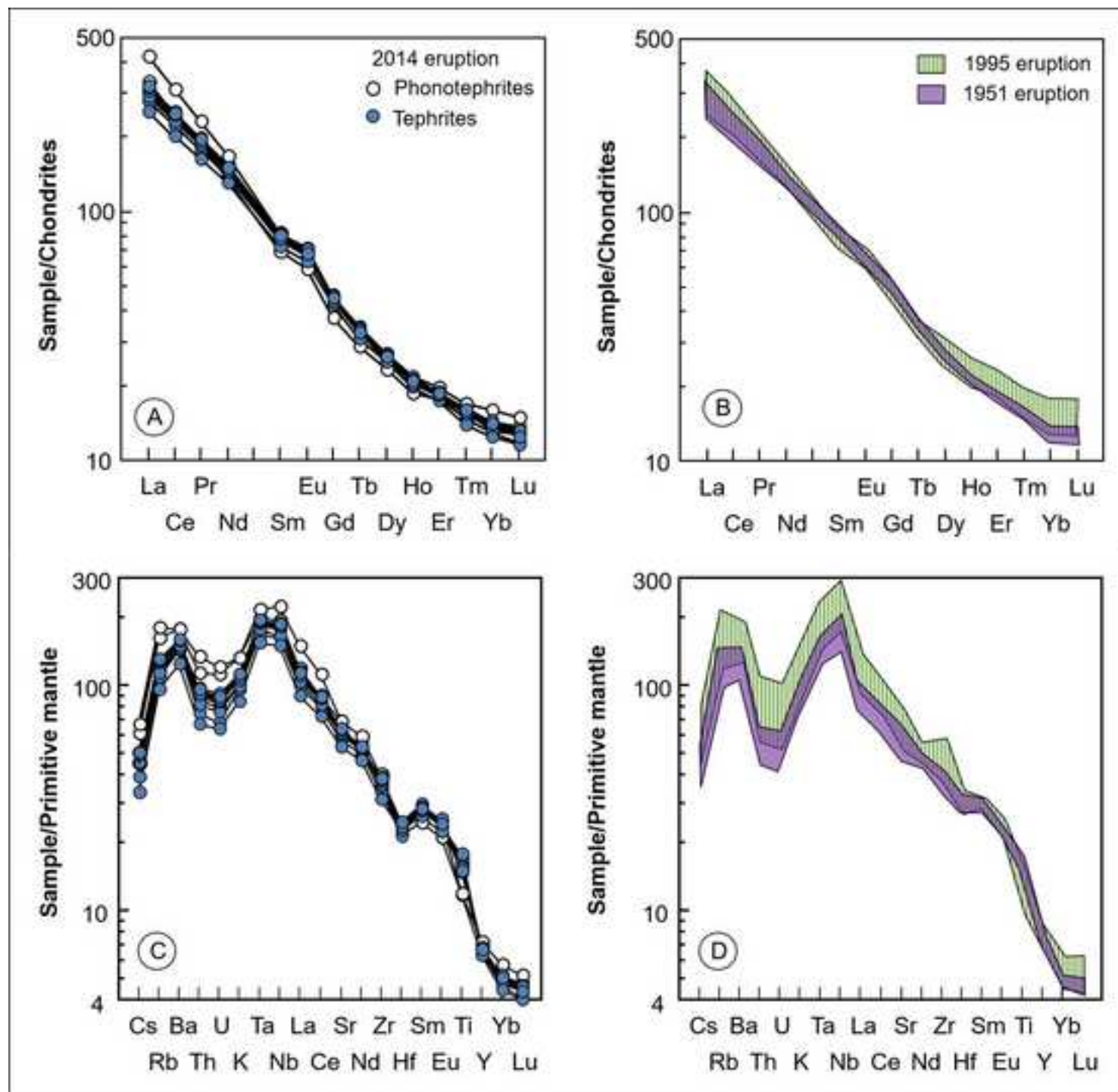


Figure 5 B&W  
[Click here to download high resolution image](#)

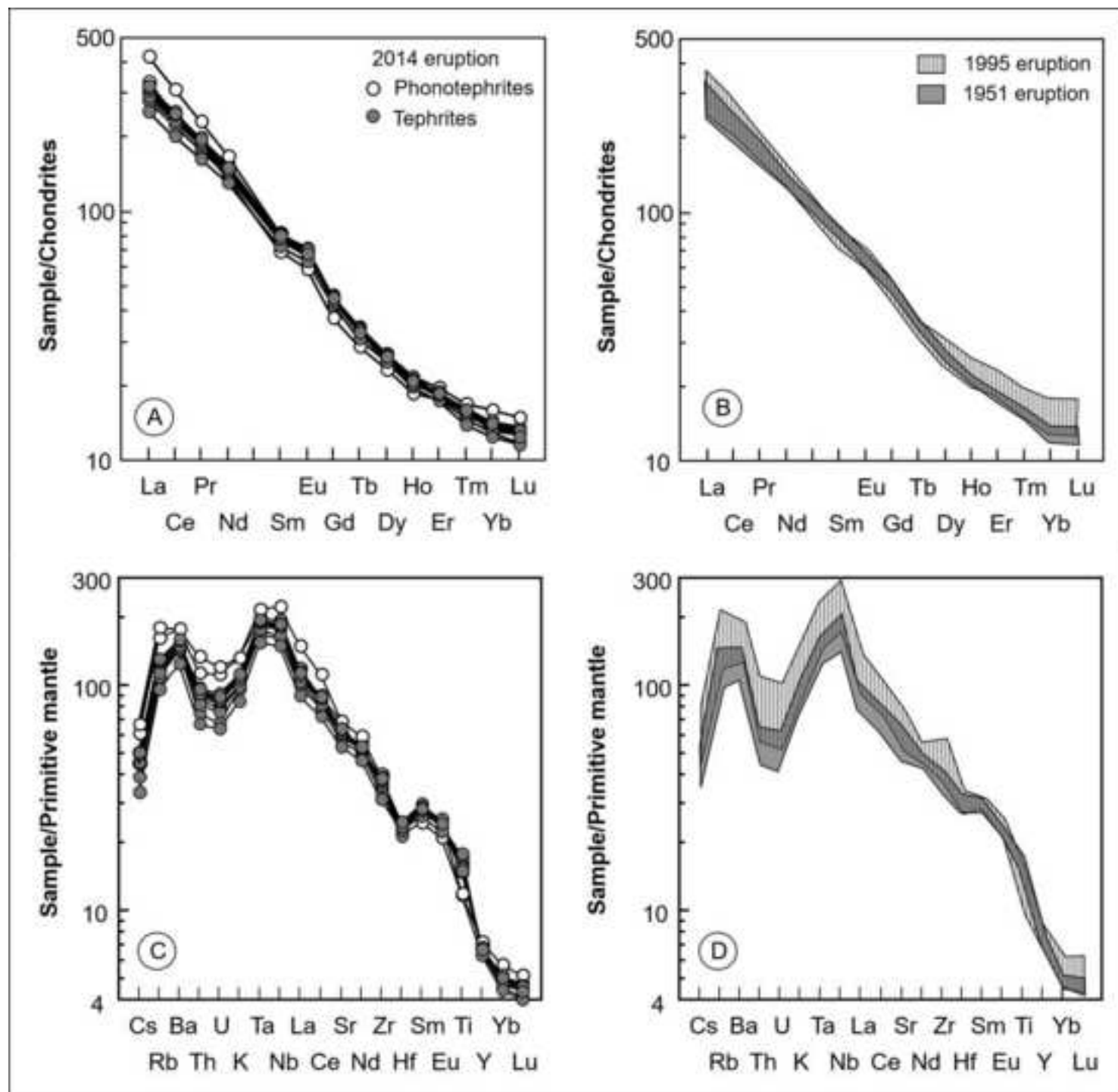


Figure 6  
[Click here to download high resolution image](#)

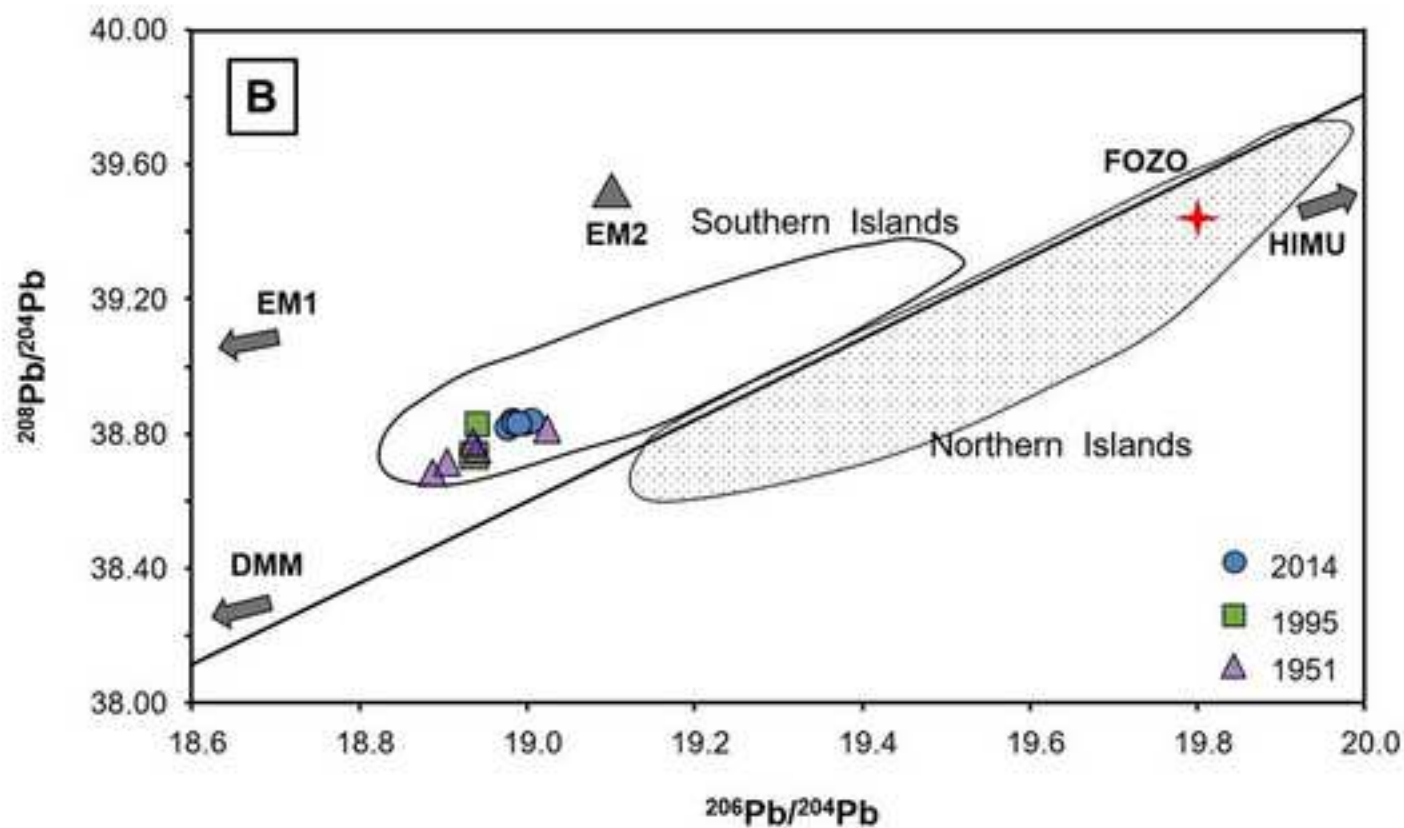
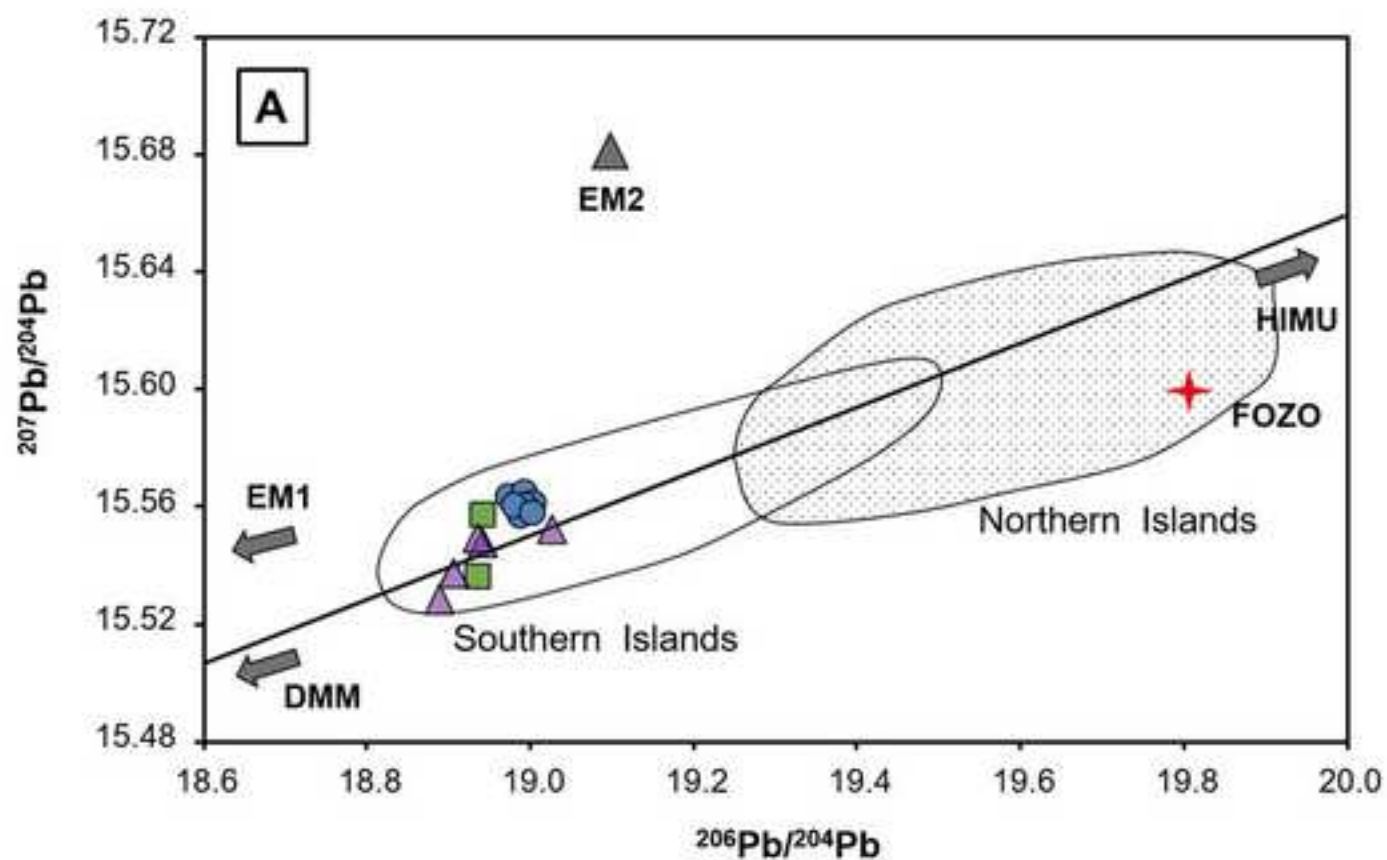


Figure 6 B&W  
[Click here to download high resolution image](#)

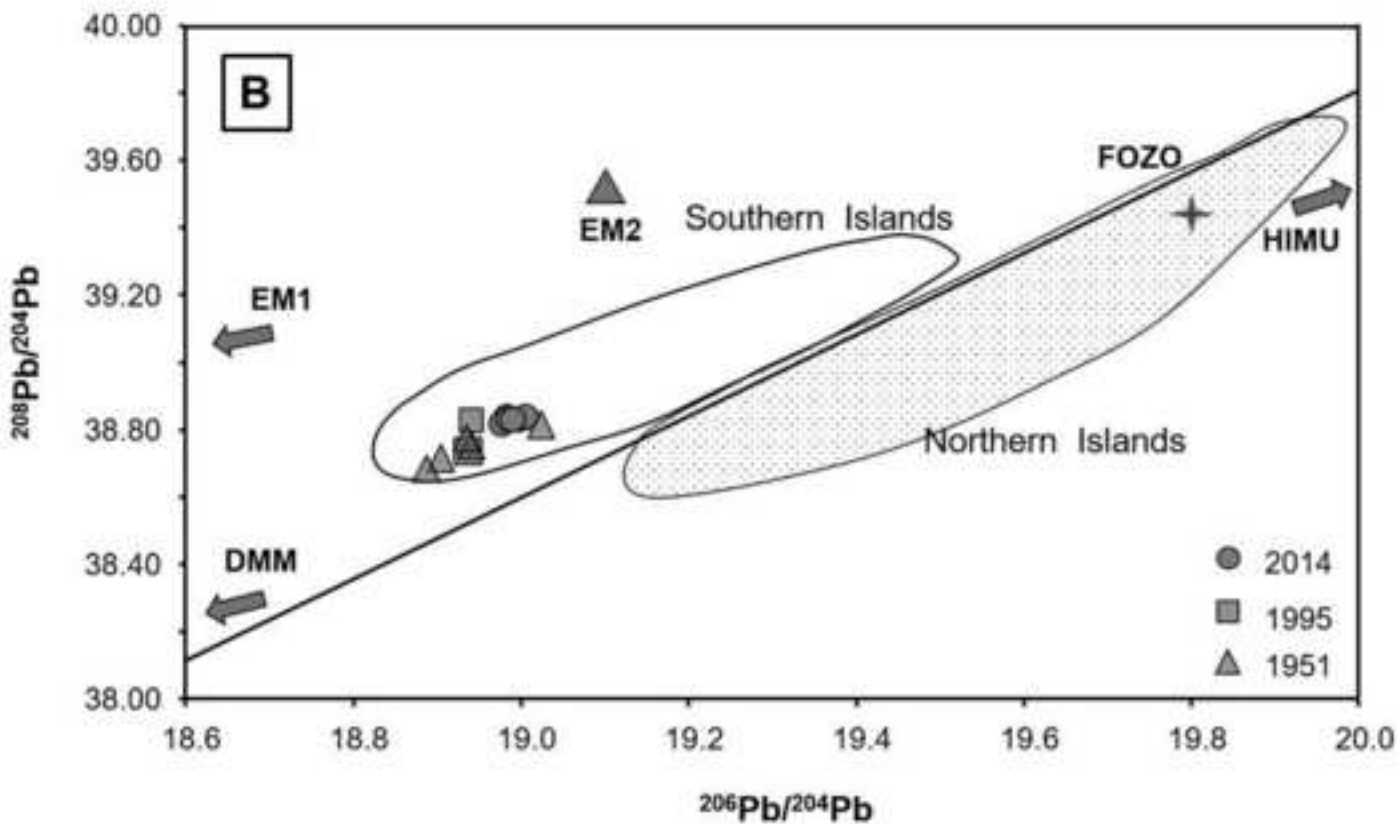
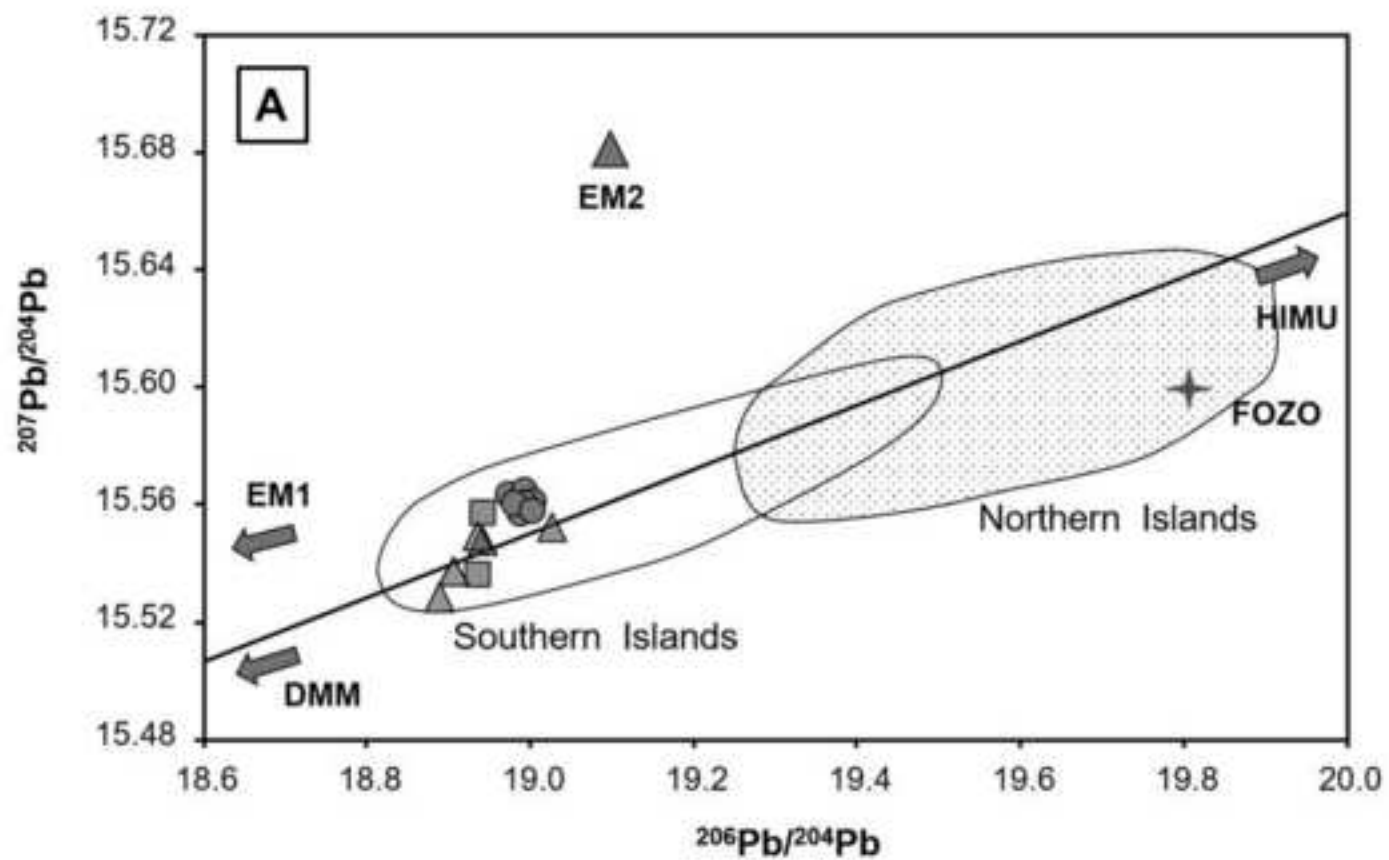


Figure 7  
[Click here to download high resolution image](#)

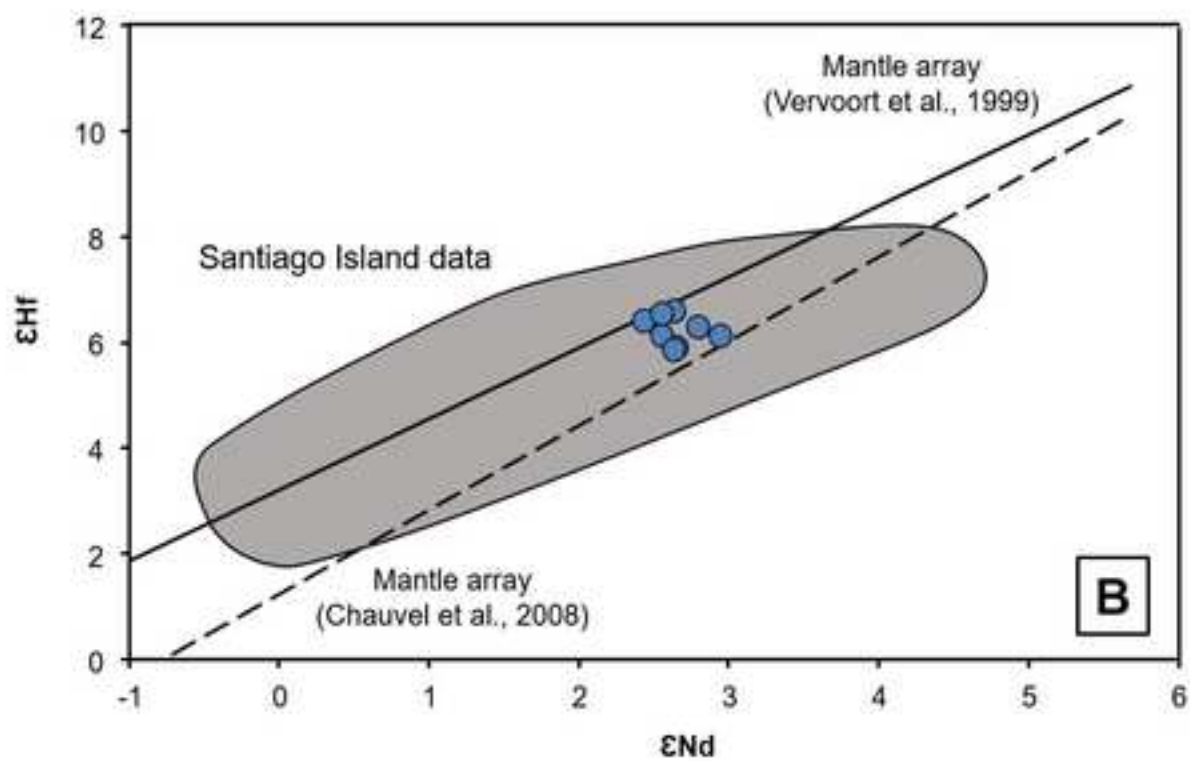
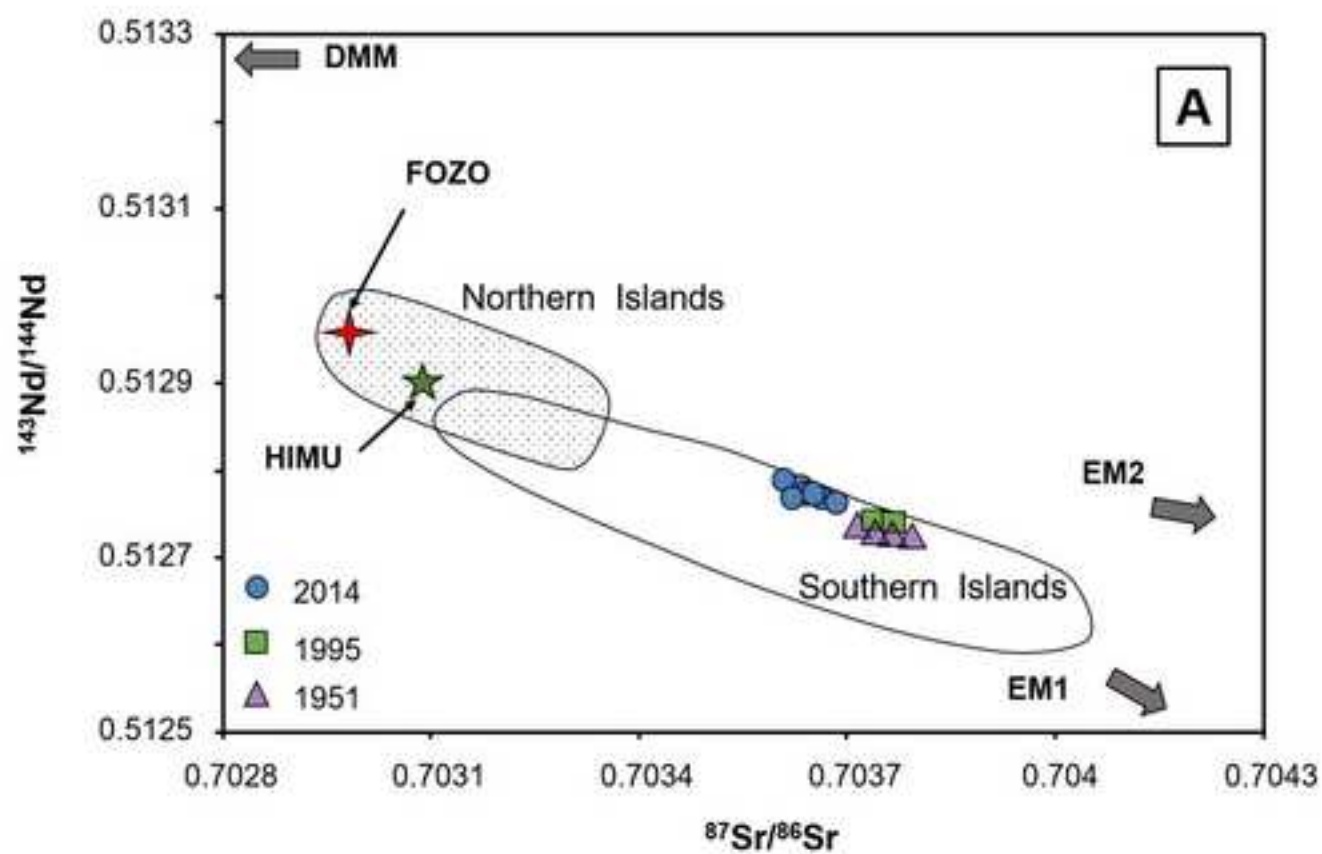




Figure 7 B&W  
[Click here to download high resolution image](#)

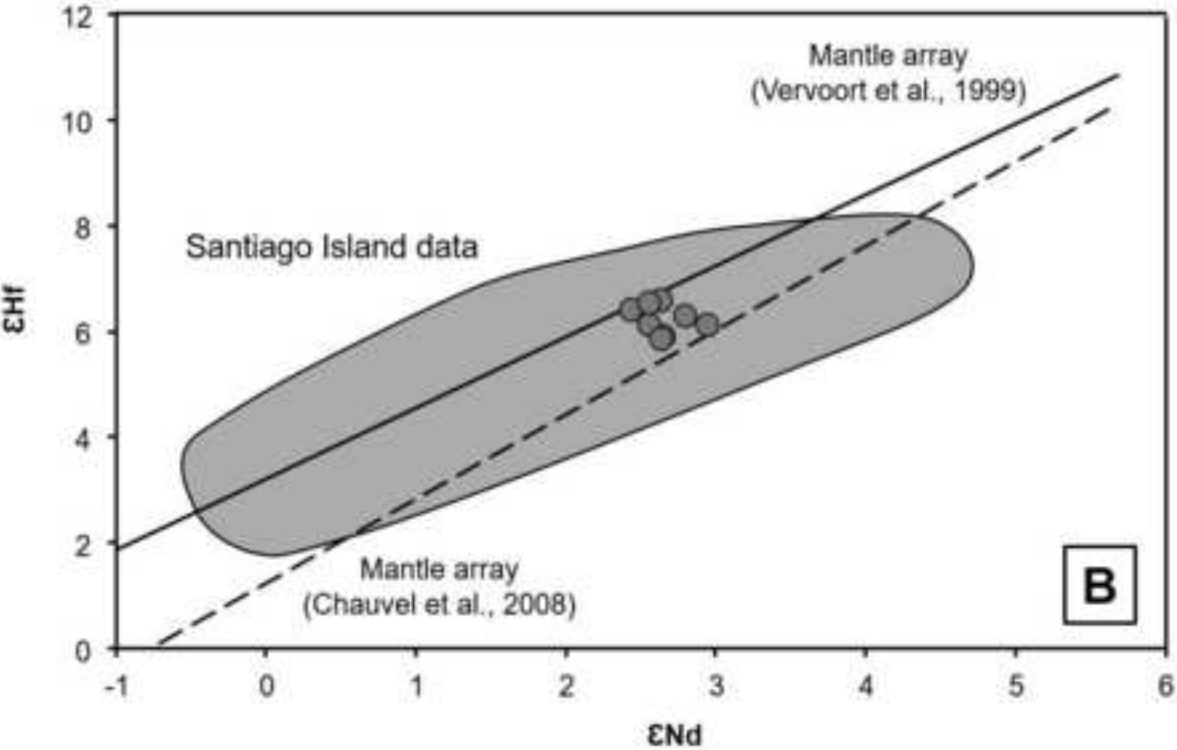
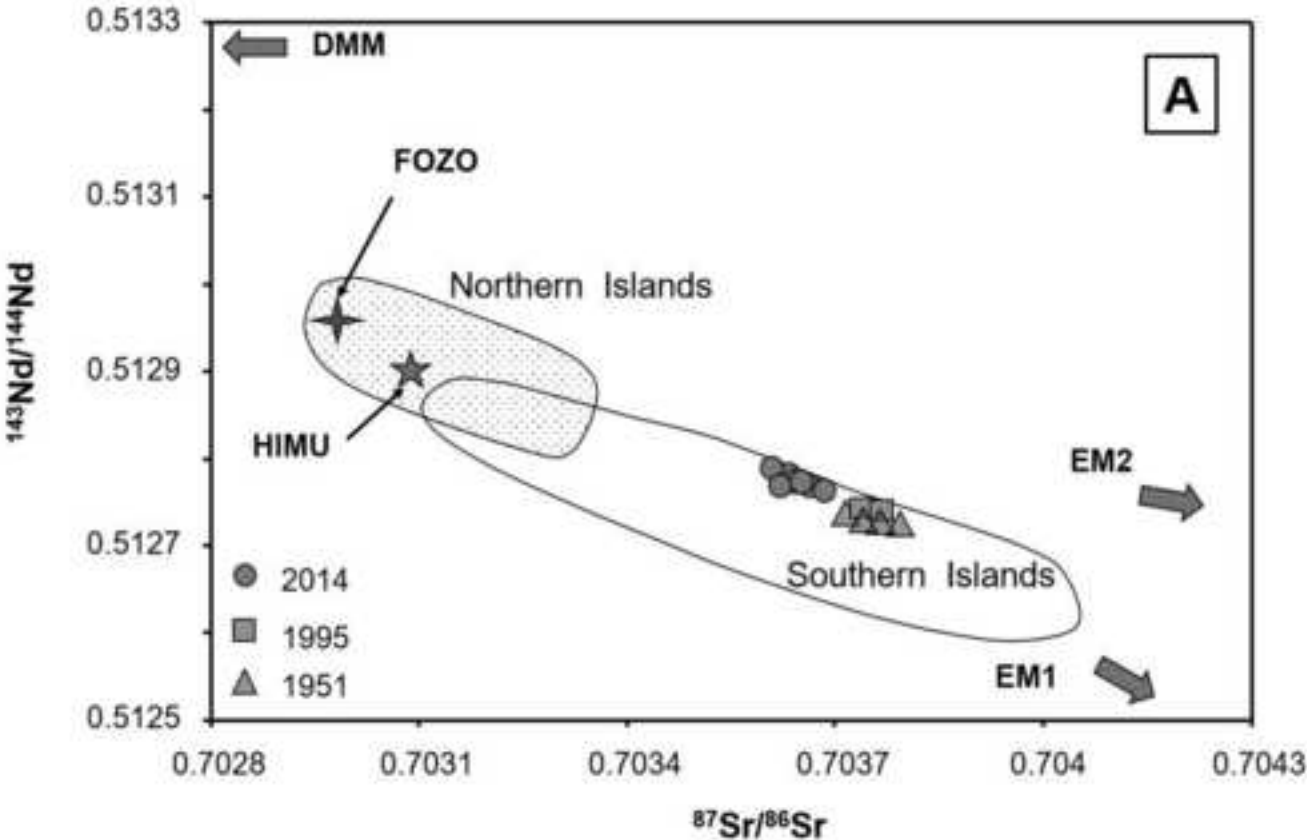




Figure 8

[Click here to download high resolution image](#)

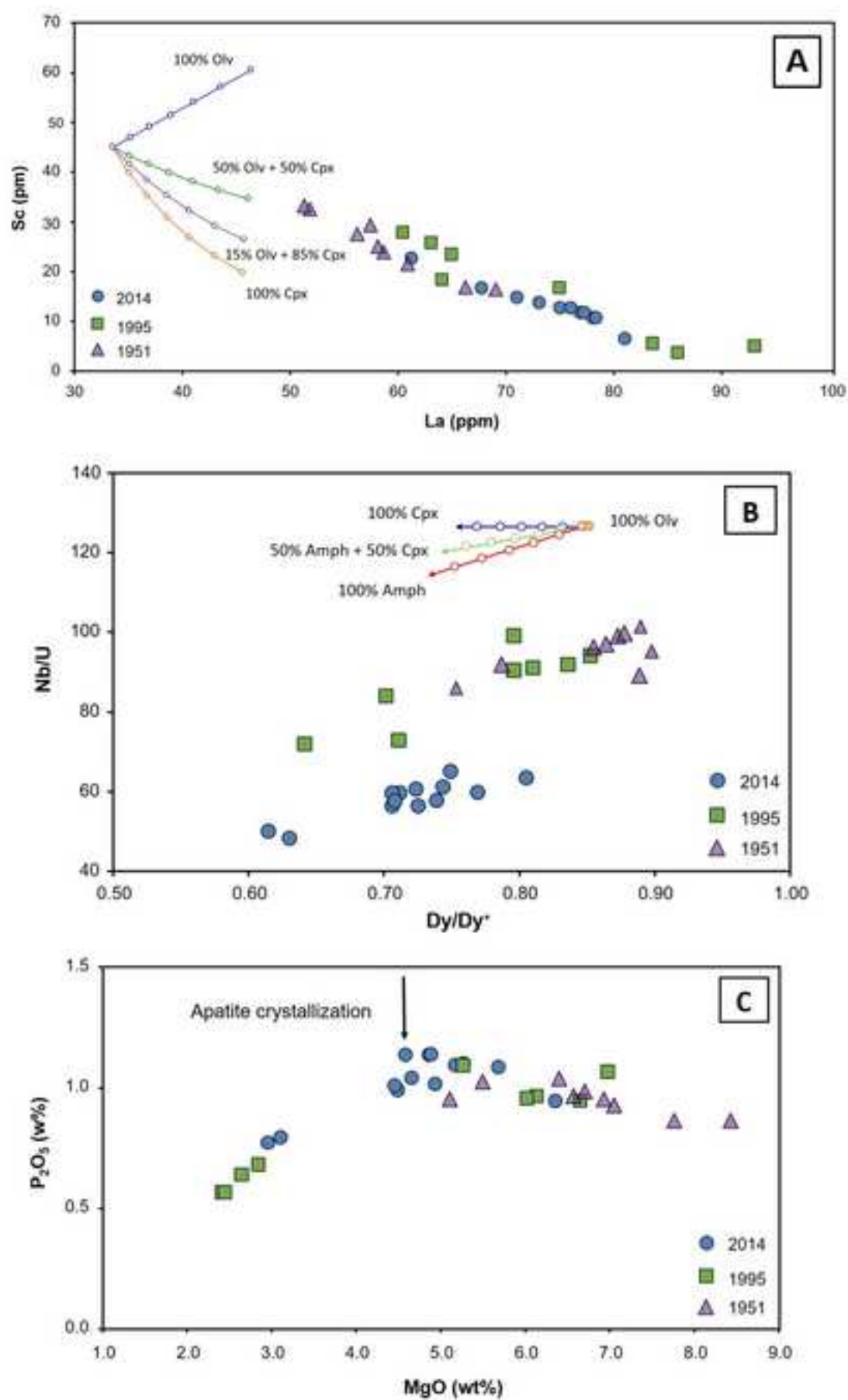


Figure 8 B&W  
[Click here to download high resolution image](#)

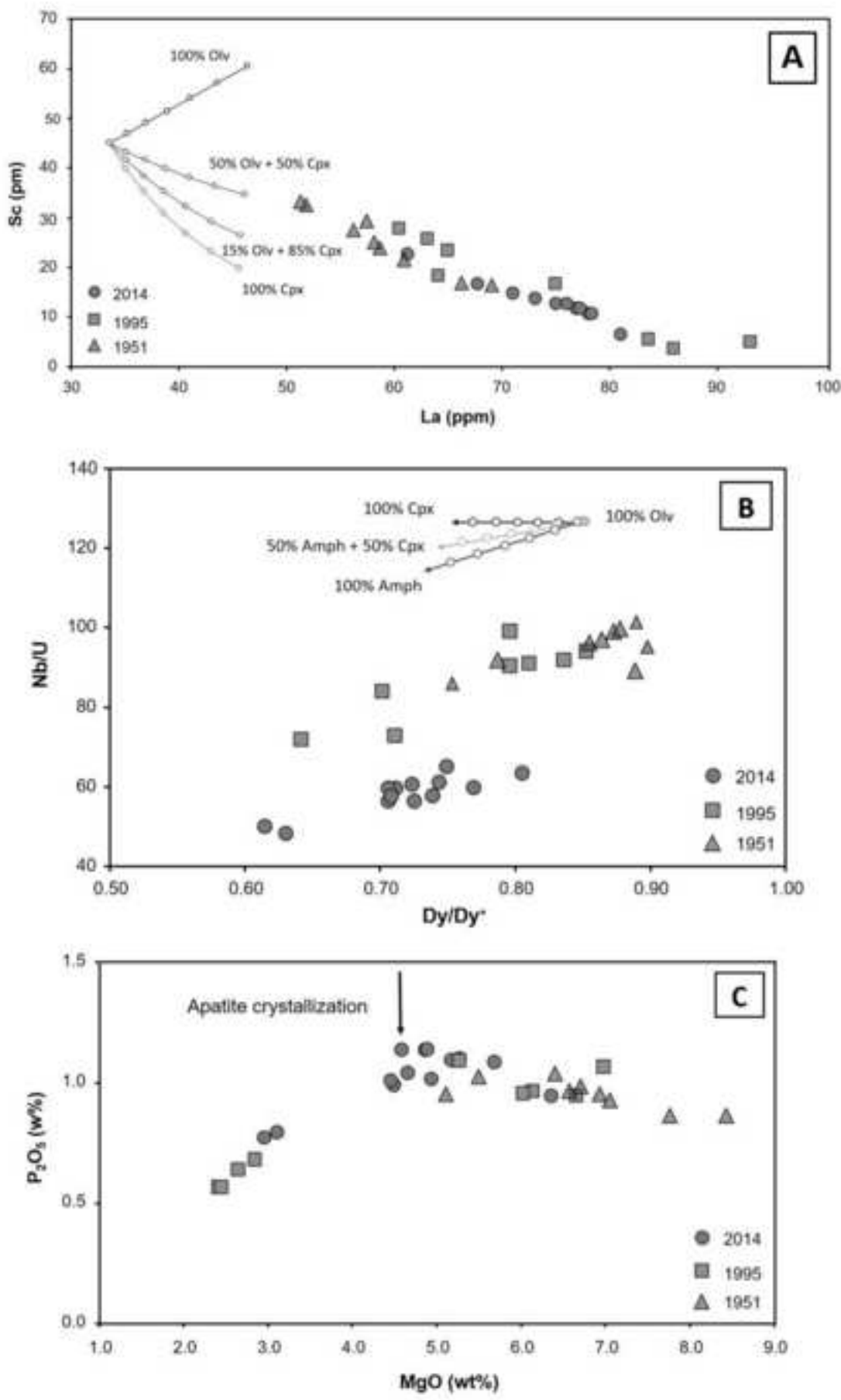


Figure 9  
[Click here to download high resolution image](#)

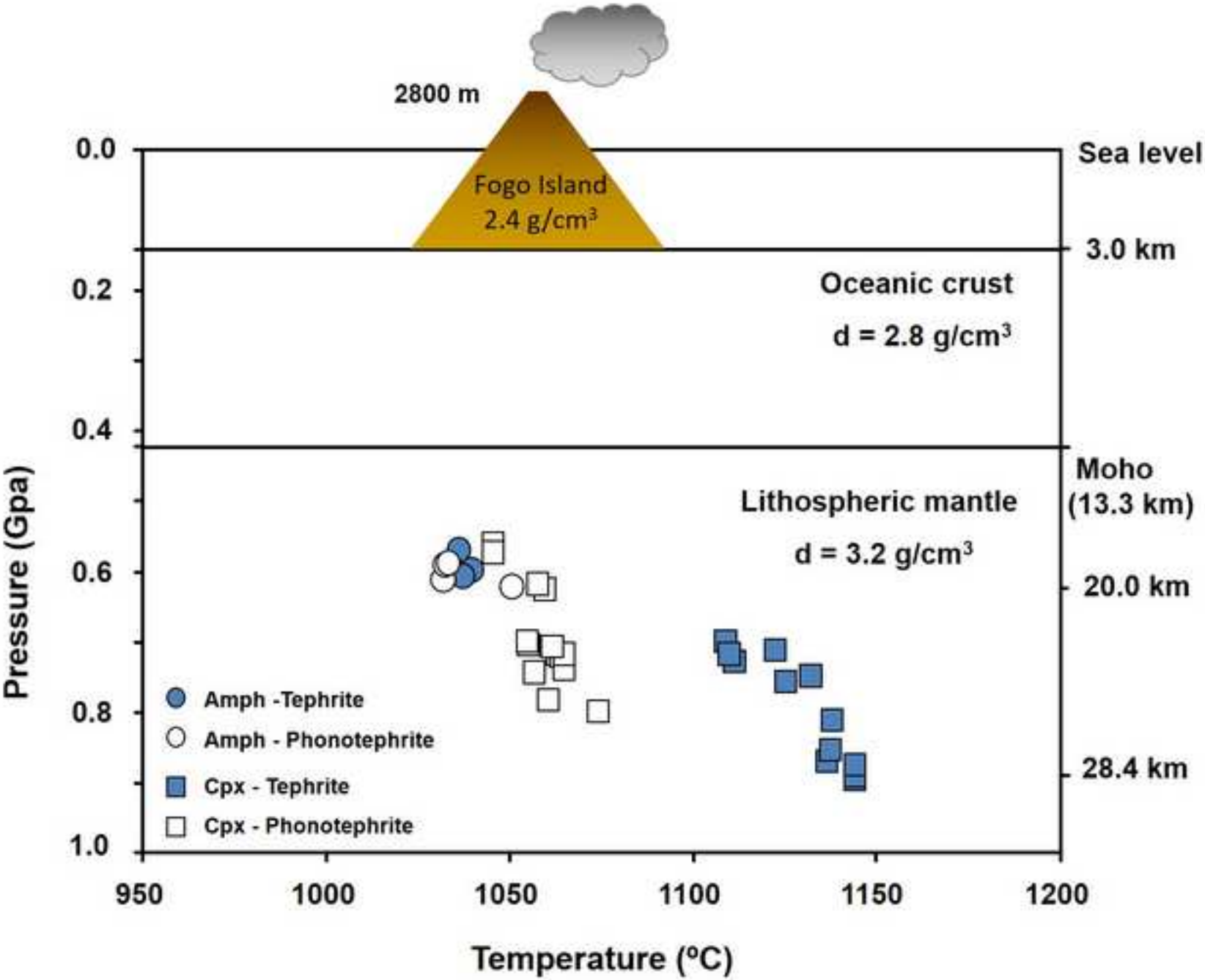


Figure 9 B&W  
[Click here to download high resolution image](#)

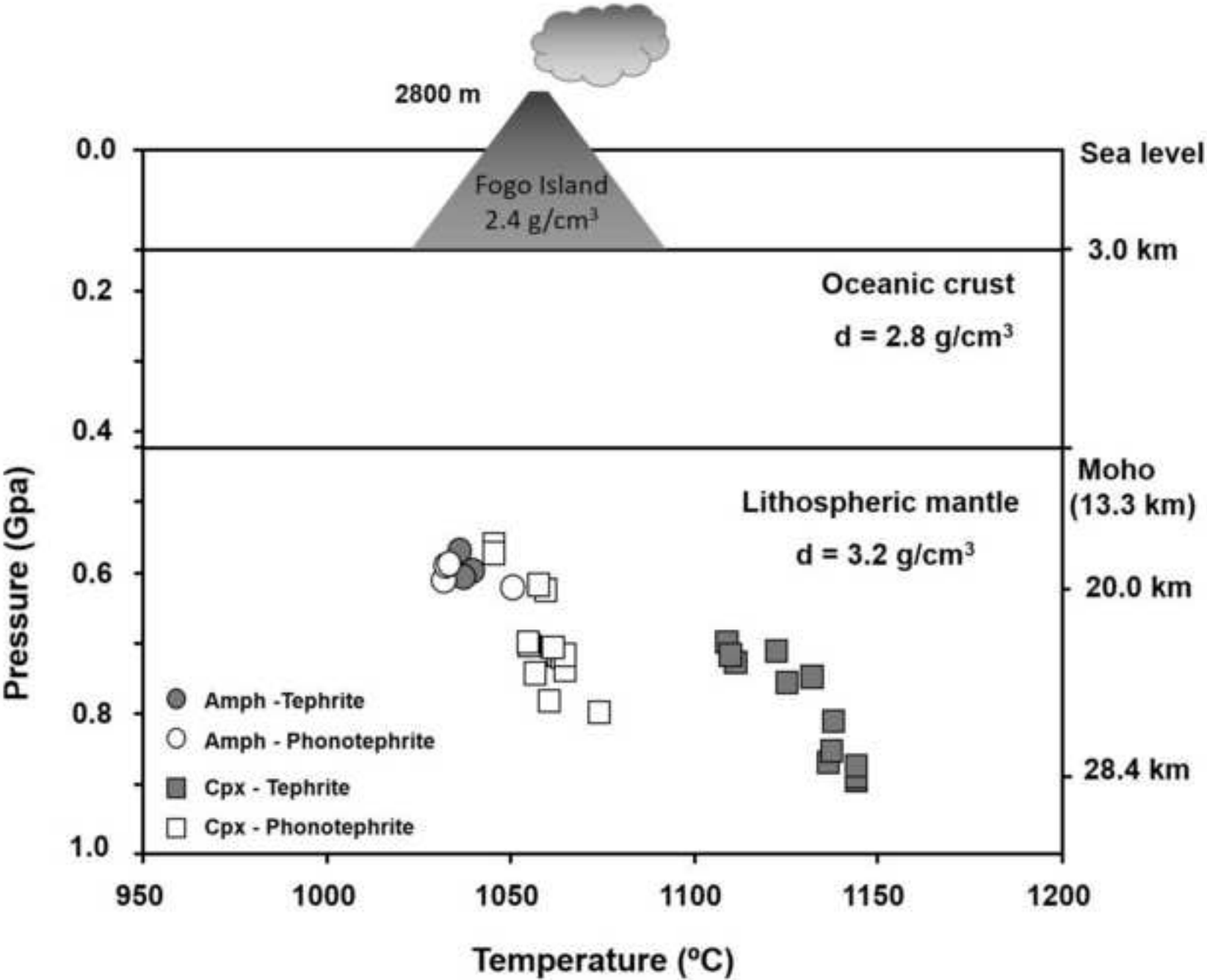


Figure 10  
[Click here to download high resolution image](#)

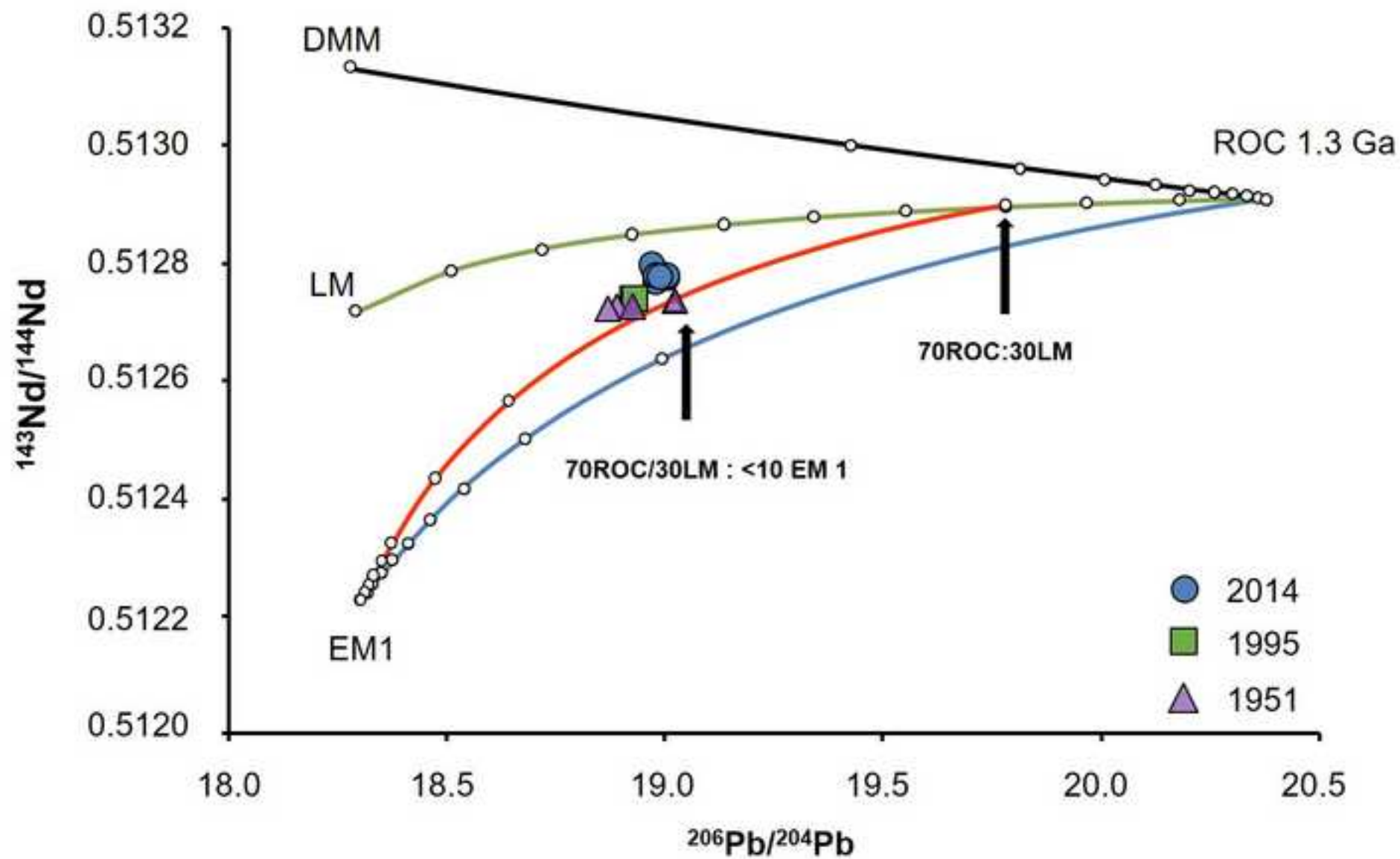


Figure 10 B&W  
[Click here to download high resolution image](#)

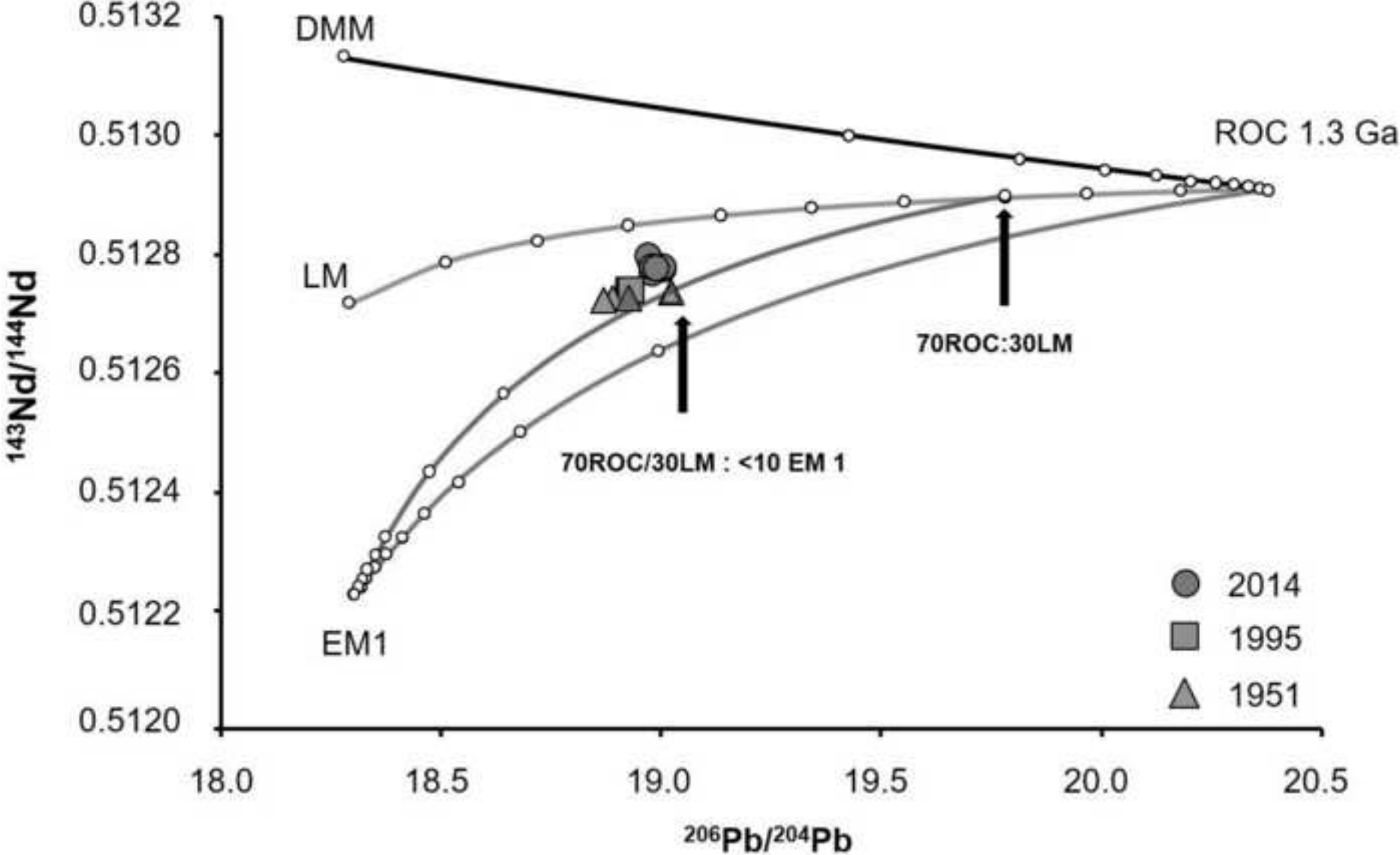


Table I: Whole rock chemical analyses of 2014 erupted lava flows and pyroclasts

Sample	F14-1	F14-2	F14-4	F14-5	F14-6	F14-7	F14-8	F14-9	F14-10	F14-11	F14-12	F14-13	F14-14
	Lava	Lava	Lava	Lava	Lava	Lava	Lava	Lava	Lava	Pyroc.	Pyroc.	Pyroc.	Pyroc.
Lithotype	Pht	Pht	Tep	Tep	Tep	Tep	Tep	Tep	Tep	Tep	Tep	Tep	Tep
SiO <sub>2</sub> (wt%)	47.99	47.74	45.19	43.54	43.03	44.70	45.10	45.07	44.03	44.62	44.16	43.10	44.40
TiO <sub>2</sub>	2.50	2.54	3.16	3.58	3.81	3.37	3.31	3.17	3.46	3.34	3.38	3.71	3.37
Al <sub>2</sub> O <sub>3</sub>	19.28	18.53	17.58	16.80	15.35	16.86	16.85	17.58	16.54	16.84	16.80	16.28	16.66
Fe <sub>2</sub> O <sub>3</sub> *	2.12	2.26	2.28	2.53	2.74	2.40	2.36	2.32	2.54	2.47	2.51	2.66	2.47
FeO*	6.06	6.46	7.61	8.44	9.12	7.99	7.86	7.73	8.48	8.24	8.36	8.88	8.22
MnO	0.21	0.22	0.21	0.22	0.21	0.22	0.22	0.22	0.22	0.22	0.22	0.21	0.22
MgO	2.93	3.08	4.47	5.25	6.33	4.91	4.63	4.43	5.15	4.55	4.83	5.66	4.87
CaO	7.96	8.21	9.95	10.95	11.98	10.47	10.30	9.83	10.82	10.51	10.62	11.43	10.74
Na <sub>2</sub> O	6.00	6.00	5.06	4.51	3.84	4.78	4.95	5.13	4.55	4.76	4.69	4.01	4.64
K <sub>2</sub> O	4.17	4.16	3.48	3.09	2.64	3.29	3.39	3.51	3.12	3.31	3.30	2.97	3.26
P <sub>2</sub> O <sub>5</sub>	0.78	0.80	1.00	1.11	0.96	1.02	1.05	1.02	1.10	1.14	1.14	1.10	1.15
LOI	-0.17	-0.18	-0.26	-0.42	-0.53	-0.4	-0.37	-0.30	-0.51	-0.09	0.65	-0.04	-0.19
Mg#	46.25	45.98	51.14	52.58	55.32	52.26	51.21	50.53	51.97	49.63	50.75	53.16	51.34
S (%)	0.012	0.008	0.007	0.006	0.009	0.009	0.008	0.009	0.008	0.023	0.012	0.023	0.022
Sc (ppm)	5	5	11	15	23	13	12	11	14	11	12	17	13
V	217	223	280	322	363	306	299	286	322	300	305	353	311
Cr	30	<20	40	60	90	50	50	60	50	70	30	30	20
Co	17	20	26	30	37	28	27	26	29	28	29	34	29
Ni	6	20	17	22	42	21	19	17	31	15	16	28	17
Rb	97	108	79	68	58	76	78	79	70	75	75	65	72
Sr	1408	1403	1256	1213	1084	1242	1280	1295	1212	1243	1194	1140	1214
Y	27.40	31.70	29.40	29.40	27.60	29.80	29.80	29.10	29.90	30.20	30.20	28.90	29.90
Zr	433	422	394	382	336	394	406	412	384	387	374	360	390
Nb	117	133	112	98.4	89	110	112	111	107	113	108	97.4	110
Cs	1.10	1.20	0.90	0.80	0.60	0.80	0.90	0.90	0.80	0.80	0.80	0.70	0.80
Ba	1198	1204	1043	973	839	1013	1050	1076	1000	1025	1013	960	1024
La	81.30	103.00	78.00	71.10	61.30	75.10	77.00	78.10	73.10	78.40	77.30	67.80	76.10
Ce	157	199	157	147	129	155	156	158	152	160	159	141	155
Pr	17.80	22.20	18.50	17.70	15.70	18.50	18.40	18.80	18.10	18.90	19.10	17.10	18.70
Nd	64.20	78.90	68.90	68.30	61.40	69.30	70.60	70.90	69.20	72.60	72.50	66.20	71.80
Sm	10.60	12.70	11.80	12.00	11.20	12.00	12.40	12.20	12.30	12.50	12.50	11.80	12.40
Eu	3.39	4.03	3.90	3.96	3.62	3.93	4.08	3.92	3.93	4.02	4.11	3.83	3.99
Gd	7.59	9.02	9.41	9.30	8.61	9.03	8.95	9.11	9.19	9.10	9.27	9.21	9.31
Tb	1.07	1.24	1.23	1.24	1.16	1.22	1.26	1.22	1.26	1.29	1.29	1.24	1.28
Dy	5.91	6.82	6.60	6.63	6.35	6.61	6.69	6.56	6.61	6.79	6.78	6.30	6.61
Ho	1.05	1.22	1.19	1.20	1.11	1.14	1.19	1.17	1.21	1.19	1.23	1.16	1.19
Er	2.90	3.25	3.08	3.11	2.86	3.06	3.04	3.07	3.01	3.05	3.10	2.99	3.09
Tm	0.38	0.43	0.39	0.41	0.35	0.41	0.40	0.41	0.40	0.41	0.42	0.38	0.40
Yb	2.30	2.64	2.33	2.16	2.03	2.35	2.39	2.30	2.23	2.27	2.34	2.13	2.28
Lu	0.33	0.37	0.33	0.32	0.29	0.32	0.33	0.31	0.31	0.31	0.34	0.29	0.31
Hf	6.50	7.40	6.90	6.90	6.80	7.00	7.00	7.30	7.30	7.00	6.40	6.80	7.10
Ta	7.85	8.70	7.65	7.04	6.13	7.49	7.61	7.75	7.32	7.63	7.59	6.70	7.50
Th	9.38	11.20	8.09	6.83	5.62	7.58	7.59	7.95	7.15	7.54	7.54	6.24	7.32
U	2.41	2.64	1.98	1.64	1.40	1.84	1.87	1.92	1.74	1.95	1.91	1.49	1.81

(\*) Fe<sub>2</sub>O<sub>3</sub>/FeO ratio calculated from the analysed Fe<sub>2</sub>O<sub>3</sub><sup>T</sup> by the method of Middlemost (1989).





Table II: Isotope analyses for selected samples

	<sup>87</sup> Sr/ <sup>86</sup> Sr	<sup>143</sup> Nd/ <sup>144</sup> Nd	<sup>176</sup> Hf/ <sup>177</sup> Hf	<sup>206</sup> Pb/ <sup>204</sup> Pb	<sup>207</sup> Pb/ <sup>204</sup> Pb	<sup>208</sup> Pb/ <sup>204</sup> Pb	ε <sub>Nd</sub>	ε <sub>Hf</sub>	Δ7/4	Δ8/4
F14-1	0.703655 ± 15	0.512774 ± 7	0.282940 ± 5	18.9901 ± 08	15.5642 ± 7	38.8462 ± 19	2.65	5.93	1.47	26.01
F14-2	0.703669 ± 12	0.512769 ± 7	0.282946 ± 5	18.9993 ± 09	15.5625 ± 8	38.8509 ± 23	2.55	6.15	1.20	25.38
F14-5	0.703689 ± 10	0.512762 ± 8	0.282954 ± 4	18.9811 ± 10	15.5588 ± 9	38.8470 ± 24	2.43	6.42	1.03	27.19
F14-6	0.703638 ± 09	0.512781 ± 7	0.282951 ± 5	18.9766 ± 10	15.5618 ± 9	38.8578 ± 21	2.79	6.33	1.37	28.80
F14-7	0.703613 ± 09	0.512789 ± 8	0.282946 ± 5	18.9717 ± 10	15.5632 ± 9	38.8341 ± 23	2.94	6.15	1.57	27.03
F14-10	0.703647 ± 10	0.512772 ± 7	0.282959 ± 5	18.9799 ± 07	15.5611 ± 7	38.8467 ± 15	2.62	6.62	1.27	27.30
F14-11	0.703656 ± 10	0.512773 ± 7	0.282938 ± 4	19.0008 ± 10	15.5609 ± 8	38.8553 ± 22	2.63	5.88	1.03	25.63
F14-14	0.703626 ± 09	0.512769 ± 6	0.282958 ± 5	18.9859 ± 09	15.5590 ± 7	38.8480 ± 18	2.55	6.57	0.99	26.70









